

***In vivo* and *In vitro* Metabolic Studies of Anabolic Steroids**

Inaugural-Dissertation
to obtain the academic degree
Doctor rerum naturalium (Dr. rer. nat.)

submitted to the Department of Biology, Chemistry, Pharmacy
of Freie Universität Berlin

by
Lingyu Liu
2023

Research of the present study was conducted from 2018 until 2023 under supervision of Prof. Dr. Maria Kristina Parr at the Institute of Pharmacy of the Freie Universität Berlin.

1st Reviewer: Prof. Dr. Maria Kristina Parr

2nd Reviewer: Prof. Dr. Matthias Bureik

Date of Defense: 29.02.2024

Acknowledgements

First of all, I would like to thank my supervisor Prof. Dr. Maria Kristina Parr, for the opportunity to work on the interesting topics, freedom in my work, and advice during difficult times.

I would like to thank Prof. Dr. Matthias Bureik, for the encouragement and the valuable suggestions in my research. I am glad to have you in my thesis jury.

I would like to thank Dr. Annekathrin Martina Keiler, Dr. Alexander Froschauer, and Prof. Dr. Oliver Zierau for the nice collaboration on the interesting research topics.

I would like to thank Prof. Dr. Francesco Botrè and Dr. Xavier de la Torre for the wonderful GC-QTOF-MS data, and thank Dr. Nils Schlörer for helping me with the NMR analysis.

Thanks to Prof. Dr. Burkhard Kleuser for allowing me to work in his lab and providing cell sources and thanks to his research group, especially Dr. Christian Zoschke and Ms. Carola Kapfer, for their patient technical guidance.

Thanks to Dr. Felix Bredendiek for aiding in LC-QTOF-MS/MS analysis, Dr. Steffen Loke for the patient guidance of chemical synthesis, and Ms. Maxi Wenzel for the technique support.

I would like to thank all former and current members of the group of Prof. Parr, especially Fan, Yanan, Ginevra, Jakob, and Yan, for your kind help and the great times spent together.

I would like to thank China Scholarship Council for the financial support of my PhD study.

I am very grateful to all the friends I met in Berlin. Thank you for the wonderful years we spent together and all the precious memories.

Last but not least, I would like to express my gratitude to my parents and my sister, for their unconditional love and endless support. Even if they are thousands of miles away, their company always warms my heart in difficult moments.

Table of Contents

I	Abbreviations	V
1	Introduction.....	1
1.1	Doping in Sports.....	1
1.2	Steroids	2
1.2.1	Human Steroid Hormones and Steroidogenesis	2
1.2.2	Endogenous Androgens	6
1.2.3	Exogenous Androgens	7
1.3	Steroid Analysis in Doping Control	11
1.4	<i>In vitro</i> and <i>In vivo</i> Models for Metabolism Studies.....	13
1.4.1	Isolated Recombinant Enzymes.....	14
1.4.2	Human Skin Cell Model.....	15
1.4.3	Fish Embryo Model	15
2	Aims.....	17
3	Materials and Methods	19
3.1	Materials	19
3.2	Methods	22
3.2.1	Synthesis of Reference Materials	22
3.2.2	Isolated Recombinant Enzyme Incubations	26
3.2.3	<i>In vitro</i> Incubations in Human Skin Cells.....	27
3.2.4	<i>In vivo</i> Incubations in Fish Embryo Model.....	28
3.2.5	GC-EI-MS Analysis.....	29
3.2.6	GC-EI-QTOF-MS Analysis	29
3.2.7	LC-ESI-QTOF-MS Analysis.....	29
3.2.8	HPLC Purification	30
3.2.9	Nuclear Magnetic Resonance	31
4	Results and Discussion	32
4.1	Synthesis of Reference Materials.....	32
4.1.1	Synthesis of 3 α /3 β ,4 α ,5 α -THCLT (13a, 13b) and 3 α /3 β ,4 α ,5 α - THCLMT (14a, 14b).....	32
4.1.2	Synthesis of 3 α /3 β -DHCLT (17a, 17b) and 3 α /3 β -DHCLMT (18a, 18b)	38
4.2	Isolated Recombinant Enzyme Incubations.....	40
4.3	<i>In vitro</i> Biotransformation of Androgens by Human Fibroblasts and Keratinocytes	47
4.3.1	Metabolite Detection.....	47
4.3.2	Comparison of Metabolic Pathways	50
4.3.3	Metabolic Characteristics in Human Fibroblasts and Keratinocytes..	52

4.4	<i>In vivo</i> Biotransformation in Fish Embryo Model	53
4.4.1	Evaluation of Medaka Embryo Model through Metabolite Analysis for MD	53
4.4.2	Biotransformation of [¹³ C ₃]-Testosterone and Methyltestosterone in Medaka Embryo Model.....	62
5	Summary and Outlook.....	67
6	Zusammenfassung und Ausblick	70
7	References.....	73
8	List of Figures.....	91
9	List of Tables	100
10	Annex	105
11	Independence Declaration.....	132

I Abbreviations

17 α -OHP	17 α -Hydroxy-pregn-4-ene-3,20-dione
17 α -OHPREG	3 β ,17 α -Dihydroxy-pregn-5-ene-20-one
3 α ,4 α ,5 α -THCLT	4 α -Chloro-5 α -androstane-3 α ,17 β -diol
3 α ,4 α ,5 α -THCLMT	4 α -Chloro-17 α -methyl-5 α -androstane-3 α ,17 β -diol
3 α ,5 α -THMD	17 α -Methyl-5 α -androst-1-ene-3 α ,17 β -diol
3 α ,5 β -THMD	17 α -Methyl-5 β -androst-1-ene-3 α ,17 β -diol
3 α -DHCLT	4-Chloroandrost-4-ene-3 α ,17 β -diol
3 α -DHCLMT	4-Chloro-17 α -methylandrost-4-ene-3 α ,17 β -diol
3 β ,4 α ,5 α -THCLT	4 α -Chloro-5 α -androstane-3 β ,17 β -diol
3 β ,4 α ,5 α -THCLMT	4 α -Chloro-17 α -methyl-5 α -androstane-3 β ,17 β -diol
3 β ,5 α -THMD	17 α -Methyl-5 α -androst-1-ene-3 β ,17 β -diol
3 β ,5 β -THMD	17 α -Methyl-5 β -androst-1-ene-3 β ,17 β -diol
3 β -DHCLT	4-Chloroandrost-4-ene-3 β ,17 β -diol
3 β -DHCLMT	4-Chloro-17 α -methylandrost-4-ene-3 β ,17 β -diol
3 β -HSD	3 β -Hydroxysteroid dehydrogenase/ Δ^{5-4} isomerase
5 α Adiol	Androstanediol (5 α -Androstane-3 α ,17 β -diol)
5 α -DHMD	17 β -Hydroxy-17 α -methyl-5 α -androst-1-ene-3-one
5 β -DHMD	17 β -Hydroxy-17 α -methyl-5 β -androst-1-ene-3-one
5 α -DHT	17 β -Hydroxy-5 α -androstan-3-one
5 β -DHT	17 β -Hydroxy-5 β -androstan-3-one
5 β -MSL	5 β -Mestanolone (17 β -Hydroxy-17 α -methyl-5 β -androstane-3-one)
Δ^5 -diol	5-Androstenediol (Androst-5-ene-3 β ,17 β -diol)
AAF	Adverse Analytical Finding
AAS	Anabolic Androgenic Steroids
AdR	Adrenodoxin reductase
Adx	Adrenodoxin
AED	Androstenedione (Androst-4-ene-3,17-dione)
AKR	Aldo-Keto Reductase
ASOIF	Association of Summer Olympic International Federations
CLT	Clostebol (4-Chloro-17 β -hydroxyandrost-4-ene-3-one)

CLMT	Methylclostebol (4-Chloro-17 β -hydroxy-17 α -methylandrosta-4-ene-3-one, CLMT)
Code	World Anti-Doping Code
CPR	Cytochrome P450 reductase
CYP	Cytochrome P450
DHCMT	Dehydrochloromethyltestosterone (4-Chloro-17 β -hydroxy-17 α -methyl-androsta-1,4-dien-3-one)
DHEA	Dehydroepiandrosterone (3 β -Hydroxyandrosta-5-ene-17-one)
DHEA-d ₆	Dehydroepiandrosterone-2,2,3,4,4,6-d ₆
DMP	Dess-Martin periodinane
dpf	Day post fertilization
E1	Estrone (3-Hydroxyestra-1,3,5(10)-trien-17-one)
E2	Estradiol (Estra-1,3,5(10)-triene-3,17 β -diol)
EA	Epiandrosterone (3 β -Hydroxy-5 α -androsta-17-one)
EIC	Extracted ion chromatogram
Etio	Etiocholanolone (3 α -Hydroxy-5 β -androsta-17-one)
FLFII	Female leukophore-free
GC-EI-MS	Gas Chromatography coupled by Electron Ionization to Single Quadrupole-Mass Spectrometry
GC-EI-QTOF-MS	Gas Chromatography coupled by Electron Ionization to Quadrupole Time-of-Flight-Mass Spectrometry
GC-MS(/MS)	Gas Chromatography (Tandem) Mass Spectrometry
HSD	Hydroxysteroid dehydrogenase
ISTD	Internal standard
IOC	International Olympic Committee
ISL	International Standard for Laboratories of WADA
LC-ESI-QTOF-MS	High-Performance Liquid Chromatography coupled by Electrospray Ionization to Quadrupole Time-of-Flight-Mass Spectrometry
LC-ESI-MS	High-Performance Liquid Chromatography coupled by Electrospray Ionization to Mass Spectrometry
LC-MS(/MS)	Liquid Chromatography (Tandem) Mass Spectrometry
MD	Metandienone (17 β -Hydroxy-17 α -methylandrosta-1,4-dien-3-one)

MSL	Mestanolone (17 β -Hydroxy-17 α -methyl-5 α -androstan-3-one)
MSTFA	N-Methyl-N-(trimethylsilyl)-trifluoroacetamide
MT	17 α -Methyltestosterone (17 β -Hydroxy-17 α -methylandrostan-4-ene-3-one)
NMR	Nuclear Magnetic Resonance Spectroscopy
NUS	Non-uniform sampling
OH-MD	Hydroxy-metandienone
PREG	Pregnenolone (3 β -Hydroxy-pregn-5-ene-20-one)
P4	Progesterone (Pregn-4-ene-3,20-dione)
rt	Room temperature
RT	Retention time
SDR	Short-Chain Dehydrogenase Reductase
SRD5A	Steroid 5 α -Reductase
T	Testosterone (17 β -Hydroxyandrostan-4-ene-3-one)
T-d ₃	Testosterone-16, 16, 17-d ₃
TD	Technical Documents
THMT	Tetrahydromethyltestosterone
TMS	Trimethylsilyl
UGT	Uridine Diphosphoglucuronosyl-Transferase
WADA	World Anti-Doping Agency

1 Introduction

1.1 Doping in Sports

The term “doping” commonly refers to the use of prohibited performance-enhancing substances in competitive sports. The history of doping behavior can be traced back to ancient times, where Greek athletes were known to experiment with special diets and stimulants to gain an advantage in sports [1]. In the modern age, the problem of drug misuse in sports was first tackled by the International Olympic Committee (IOC) in the 1960s, and the Medical Commission was established in 1967 to address the medical and ethical aspects of doping in sports. With the purpose of harmonizing the international antidoping efforts, the World Anti-Doping Agency (WADA) was founded in 1999 [2, 3].

The three main elements in World Anti-Doping Program are: (1) The World Anti-Doping Code (Code), (2) International Standards and Technical Documents (TD), and (3) Models of Best Practice and Guidelines. The Code provides the fundamental and universal document in human sports doping control, which harmonizes anti-doping policies, rules and regulations within sport organizations and among public authorities around the world. The Code gives a comprehensive definition of “doping”, which is “the occurrence of one or more of the anti-doping rule violations set forth in Article 2.1 through Article 2.11 of the Code” [4]. The definition can be mainly specified as the presence of prohibited substances in a specimen; and the use or attempted use of a prohibited substance or a method [4, 5]. By establishing a universal standard, the Code aims to ensure fair and clean competition, protect the health and rights of athletes, and preserve the integrity of sport [4].

The International Standards are responsible for harmonizing the technical and operation parts within anti-doping programs among anti-doping organizations [4]. As a mandatory International Standard, the Prohibited List is updated annually [6]. It “indicates what substances and methods are prohibited in sport and when”. This list is subdivided by categories, identifying which substances and methods are prohibited at all times (in- and out-of-competition), in the competition only, as well as in some cases, just in particular sports [6]. The substances and methods covered in the prohibited list are shown in **Table 1**, in which sections S1, S4, S5, and S9 comprise steroids. This thesis focuses on the metabolism of anabolic androgenic steroids (AAS), also known as anabolic steroids, which belong to the section S1. More details concerning AAS will be discussed

in chapter 1.2. As defined in the Code [7], a report identifying “the presence of a prohibited substance or its metabolites or markers or evidence of the use of a prohibited method” in a sample is called adverse analytical finding (AAF).

Table 1: Groups of the Prohibited List 2023 of WADA

	Prohibited at All Times	Prohibited in Competition	Prohibited in Particular Sports
Substances	S0 Non-approved substances	S6 Stimulants	P1 Beta-blockers
	S1 Anabolic agents	S7 Narcotics	
	S2 Peptide hormones, growth factors, related substances, and mimetics	S8 Cannabinoids	
	S3 Beta-2 agonists	S9 Glucocorticoids	
	S4 Hormone and metabolic modulators		
	S5 Diuretics and masking agents		
Methods	M1 Manipulation of blood and blood components		
	M2 Chemical and physical manipulation		
	M3 Gene and cell doping		

1.2 Steroids

1.2.1 Human Steroid Hormones and Steroidogenesis

Steroid hormones are small lipophilic organic molecules that play a substantial role in maintaining proper physiological functioning within the body [8]. They can be broadly categorized into two main classes: corticosteroids and sex steroids. Corticosteroids, including mineralocorticoids and glucocorticoids, are involved in maintaining water and electrolyte balance (mineralocorticoids) and regulating metabolism, immune responses, and stress responses (glucocorticoids). Sex steroids, such as progestogens, estrogens, and androgens, are essential for sexual differentiation, reproduction, and the development of secondary sexual characteristics [9, 10]. The core structure of steroids is called gonane, whose structure consists of 17 carbon atoms connected within four rings labeled as A, B, C, and D. Among these, rings A, B, and C are cyclohexane rings, while ring D is cyclopentane [11]. The backbone of endogenous corticosteroids and progestogens is a pregnane structure with 21 carbon atoms. Endogenous androgens share a core structure known as androstane, which consists of 19 carbon atoms. Estrogens, on the other hand, have an estrane backbone with a C18 structure. The three backbones for the main classes of steroids are shown in **Figure 1**.

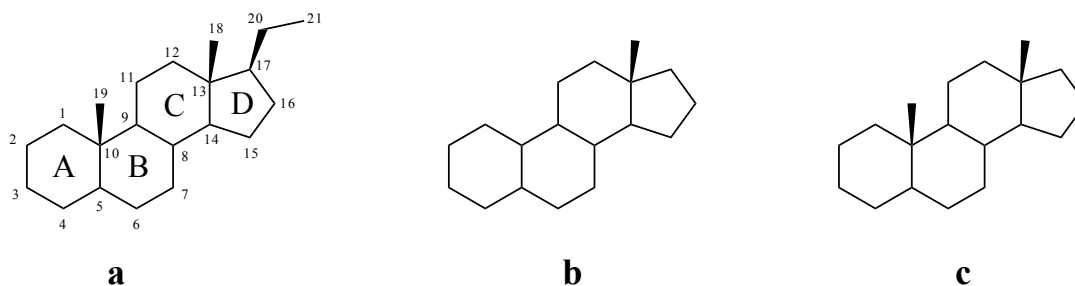


Figure 1: Backbones of (a): pregnane with exemplary numbering of carbon atoms (C1-C19) and rings (A-D), (b): estrane, (c): androstane

The major enzymes responsible for steroidogenesis include cytochrome P450 enzymes (CYPs) and hydroxysteroid dehydrogenases (HSDs) [12].

CYPs are a superfamily of enzymes containing a heme cofactor and, therefore, are hemoproteins. They can catalyze a variety of reactions, such as hydroxylation, *N*-, *O*- and *S*-dealkylation, sulfoxidation, epoxidation, deamination, dehalogenation, peroxidation, and *N*-oxide reduction [13, 14]. In this way, they contribute to the transformation of lipophilic drugs into more hydrophilic drug metabolites [15]. In humans, there are 57 functional P450s [14, 16]. Most of the human CYPs, e.g. CYP1A2, CYP2B6, CYP2A6, CYP2C8, CYP2C9, CYP2E1, CYP2D6, and CYP3A4, are primarily located in the liver and have been studied intensively due to their importance in drug metabolism [17].

CYPs are primarily located either on the cytoplasmic side of the endoplasmic reticulum or on the matrix side of the inner mitochondrial membrane [18]. In order to catalyze redox reactions, CYPs rely on electron transfer proteins that transfer electrons from the cofactor nicotinamide adenine dinucleotide phosphate (NADPH) to the heme iron atom of the CYP. In the endoplasmic reticulum, there is a single electron transfer partner, cytochrome P450 reductase (CPR), whereas in mitochondria, there is a short electron transfer chain encompassing adrenodoxin (Adx) and adrenodoxin reductase (AdR) [8, 18]. The main CYP steroidogenic enzymes are mitochondrial CYP11B1 (11 β -hydroxylase) and CYP11B2 (aldosterone synthase) along with microsomal CYP17A1 (17 α -hydroxylase, 17,20-lyase), CYP19A1 (aromatase), and CYP21A2 (21-hydroxylase) [19].

HSDs belong to two major superfamilies, the short-chain dehydrogenase reductases (SDRs) and the aldo-keto reductases (AKRs). They have the ability to catalyze positional and stereospecific reactions on oxo- or hydroxy-substituents on the steroid nucleus and side chains. The HSDs can exist in pseudo-equilibrium states, allowing them to function preferentially as either NADPH-dependent ketosteroid reductases or as NAD⁺-dependent

hydroxysteroid oxidases. This is attributed to their affinity to the co-factors NADH/NAD⁺ or NADPH/NADP⁺ [20, 21]. The specific co-factor preference can vary among different HSD isoforms and tissues, resulting in differences in their catalytic activities and regulation. Human HSDs in the SDR family include 3 β -HSD (3 β -hydroxysteroid dehydrogenase/ Δ^{5-4} isomerase) (type 1 and type 2); 11 β -HSD (type 1 and type 2); and all 17 β -HSD isoforms in addition to type 5 [20, 22]. Among these, the 3 β -HSD isoenzymes are responsible for the oxidation and isomerization of Δ^5 -3 β -hydroxysteroid precursors into Δ^4 -3-ketosteroids, thus playing an essential role in the formation of active steroid hormones [23, 24]. In humans, the expression of the type I 3 β -HSD was observed in placenta and peripheral tissues, whereas the type 2 isoenzyme is predominantly expressed in the adrenal gland, ovary, and testis [23]. 17 β -HSD can catalyze either the stereospecific reduction of the 17-ketone group, producing potent ligands for the estrogen and androgen receptor, or the oxidation of the 17-hydroxyl group, thereby reducing the availability of ligands for the same receptors [22, 25].

Human HSDs in AKR family include four isoforms [26] corresponding to AKR1C1 (20 α (3 α)-HSD), AKR1C2 (type 3 3 α -HSD), AKR1C3 (type 2 3 α -HSD/type 5 17 β -HSD), and AKR1C4 (type 1 3 α -HSD) [27, 28]. In the human body, these four AKR1C enzymes are widely expressed in various tissues. RNA expression analysis indicates that AKR1C1 is highly expressed in the liver, mammary gland, and brain, while it is expressed at lower levels in the prostate, testis, adrenal gland, and uterus [29]. AKR1C2 is more widely expressed and is found in the brain, kidney, liver, lung, placenta, and testis [30, 31]. AKR1C3 is expressed in many endocrine organs such as the prostate, adrenals, breast, and uterus [32, 33], whereas AKR1C4 is expressed exclusively in the liver [30, 34]. The four isoforms exhibit both 3 α -HSD and 3 β -HSD activities to varying degrees [34], catalyzing the reduction of 3-oxo group to 3 α - or 3 β -hydroxy. The main HSDs responsible for steroidogenesis are 3 β -HSD (Δ^{5-4} isomerase) and 17 β -HSD enzymes.

The simplified biosynthetic pathway of endogenous steroids is depicted in **Figure 2**. The biosynthesis of steroid hormones starts with the conversion of cholesterol (cholest-5-en-3 β -ol) to pregnenolone (3 β -hydroxy-pregn-5-ene-20-one, PREG) through side-chain cleavage catalyzed by CYP11A1. Subsequently, progesterone (pregn-4-ene-3,20-dione, P4) is formed by 3 β -HSD from pregnenolone. CYP17A1 catalyzes the hydroxylation of pregnenolone and progesterone to result in the corresponding 17 α -hydroxysteroids (3 β ,17 α -dihydroxy-pregn-5-ene-20-one, 17 α -OHPREG; 17 α -hydroxy-pregn-4-ene-3,20-dione, 17 α -OHP). P4 and 17 α -OHP are subsequently converted by

CYP21A2 as well as either CYP11B2 or CYP11B1 to yield the mineralo- or glucocorticoids, respectively. The weak androgens dehydroepiandrosterone (3 β -hydroxyandrost-5-ene-17-one, DHEA) and androstenedione (androst-4-ene-3,17-dione, AED) are formed from the 17 α -hydroxyderivatives of pregnenolone and progesterone catalyzed by CYP17A1 via its 17,20-lyase activity. A subsequent reduction of the 17-oxo group in DHEA or AED by 17 β -HSD leads to the formation of 5-androstenediol (androst-5-ene-3 β ,17 β -diol, Δ^5 -diol) or testosterone (17 β -hydroxyandrost-4-ene-3-one, T). The conversion of androgens into estrogens is catalyzed by the aromatase (CYP19A1), resulting in the formation of estrone (3-hydroxyestra-1,3,5(10)-trien-17-one, E1) and estradiol (estra-1,3,5(10)-triene-3,17 β -diol, E2) from AED and T, respectively [8, 12, 35].

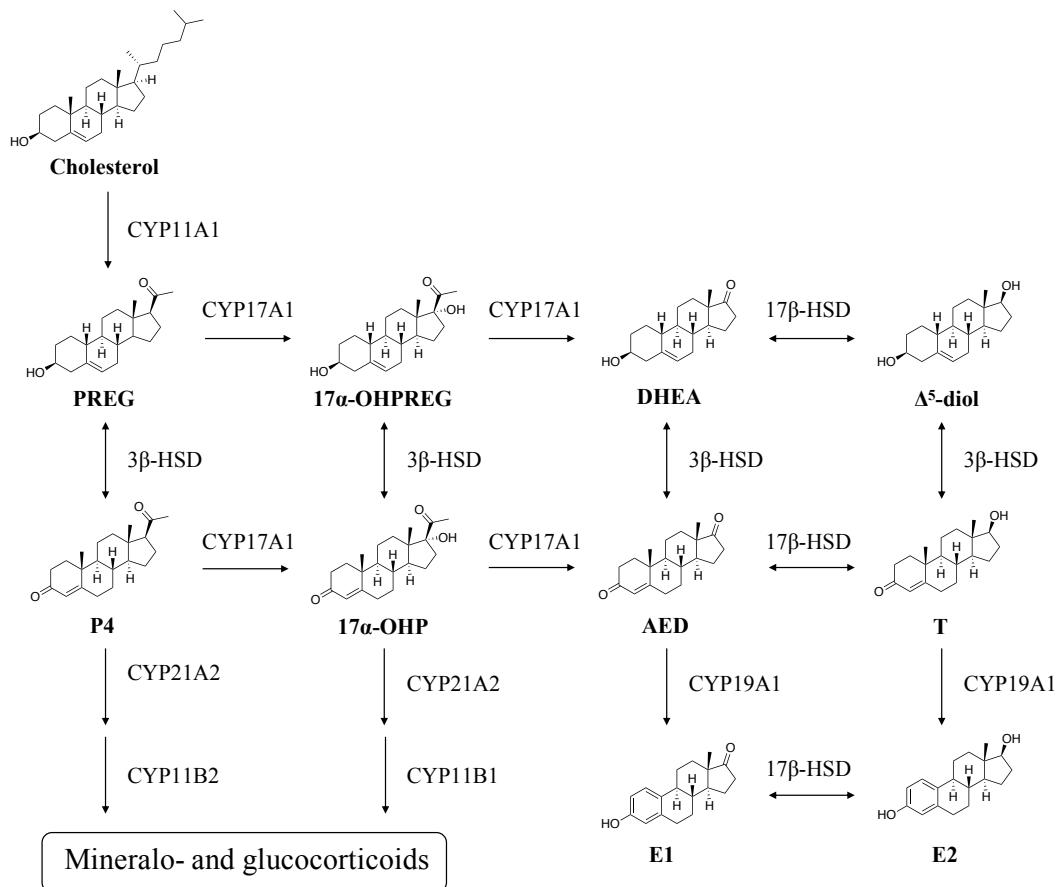


Figure 2: The simplified biosynthetic pathway of endogenous steroids starting from cholesterol. Progestogens: PREG, P4, 17 α -OHPREG, and 17 α -OHP; androgens: DHEA, AED, Δ^5 -diol and T; estrogen: E1 and E2; partially adapted from [8, 12, 35-37]

1.2.2 Endogenous Androgens

T is the principal secreted androgen and is mainly produced in the Leydig cells of the testes in males, whereas smaller amounts are synthesized by the ovaries and the adrenal glands in females [38, 39]. The metabolism of T has been extensively investigated *in vivo* and *in vitro* [38, 40-45].

In humans, T undergoes both phase I and phase II metabolism. The phase I metabolism mainly includes oxidation and reduction at positions 3 or 17, hydrogenation of 4,5-double bond, as well as hydroxylation at various positions, with different enzymes such as AKRs (AKR1Cs subfamily, AKR1D1), steroid 5 α -reductase (SRD5A) [46], and CYPs [47] being involved. AKR1D1 is the only known human steroid 5 β -reductase and is responsible for the NADPH-dependent reduction of the 4,5-double bond in steroids, yielding the corresponding 5 β -hydrogenated products [48]. This enzyme is predominantly expressed in the liver [49, 50]. In contrast, steroid 5 α -reductase catalyzes the NADPH-dependent stereospecific reduction of 4,5-double bonds in steroids, resulting in the formation of 5 α -hydrogenated products. There are three main isoforms, however, only isoforms 1 (SRD5A1) and 2 (SRD5A2) function as genuine steroid 5 α -reductases, whereas isoform 3 (SRD5A3) appears to exhibit only minimal steroidogenic 5 α reductase activity [8]. In the human body, the type I isoform is widely distributed, with high expression in the hair follicle, the sebaceous glands of the skin, and the liver, whereas the type II isoform is primarily found in androgen-dependent tissues, such as the prostate, the epididymis and the seminal vesicles [51, 52]. In phase II metabolism, T and its metabolites are mainly conjugated with glucuronic acid or sulfate in reactions catalyzed by uridine diphosphoglucuronosyl-transferases (UGTs) or sulfotransferases, respectively [38]. This thesis primarily focuses on phase I metabolism.

In human metabolism, 5 α -reductase catalyzes the formation of the potent androgen 17 β -hydroxy-5 α -androstane-3-one (5 α -DHT) from T [53], while the steroid 5 β -reductase leads to the production of the inactive 17 β -hydroxy-5 β -androstane-3-one (5 β -DHT) [42, 54]. The reduction of 3-oxo groups in 5 α -DHT and 5 β -DHT results in the formation of androstanediol (5 α -androstane-3 α ,17 β -diol, 5 α Adiol), 5 β -androstane-3 α ,17 β -diol, and 5 α -androstane-3 β ,17 β -diol. Combined with AKR1Cs as well as 5 α - and 5 β -reductases, 17 β -HSD enzymes contribute to the formation of the metabolites AED, androsterone (3 α -hydroxy-5 α -androstane-17-one), etiocholanolone (3 α -hydroxy-5 β -androstane-17-one, Etio), epiandrosterone (3 β -hydroxy-5 α -androstane-17-one, EA) [38, 55]. Several CYP enzymes (CYP3A4, 3A5, 2B6, 2C8, 2C19, and 3A7) are responsible for T hydroxylation

at positions 1, 2, 6, 11, 15, or 16 [47, 56, 57]. Moreover, additional metabolites originating from dehydrogenation of C6-7 have been observed; this reaction might also be catalyzed by CYP3A4 [58, 59]. However, the excretion of hydroxylated metabolites into human urine is found to be extremely low [38]. The positions of potential phase I metabolic reactions for T are shown in **Figure 3**.

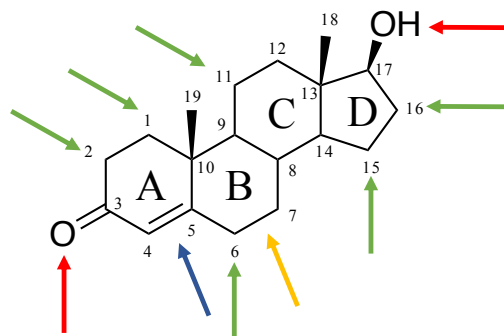


Figure 3: Possible positions of metabolism reactions for T in humans; blue: hydrogenation catalyzed by steroid 5 α - or 5 β -reductases; red: oxidations or reductions catalyzed by AKR1Cs; green: hydroxylation catalyzed by CYPs; orange: dehydrogenation

1.2.3 Exogenous Androgens

AAS are a large group of molecules including endogenous androgens, such as T, as well as synthetic compounds similar in chemical structure to T. These substances have been widely misused for muscle building and enhancement of performance in sports for decades. As described in chapter 1.1, AAS belong to substance group S1 “Anabolic Agents” of WADA’s prohibited list and have been the most frequently detected class of substances in WADA accredited laboratories since 2003 (**Figure 4**).

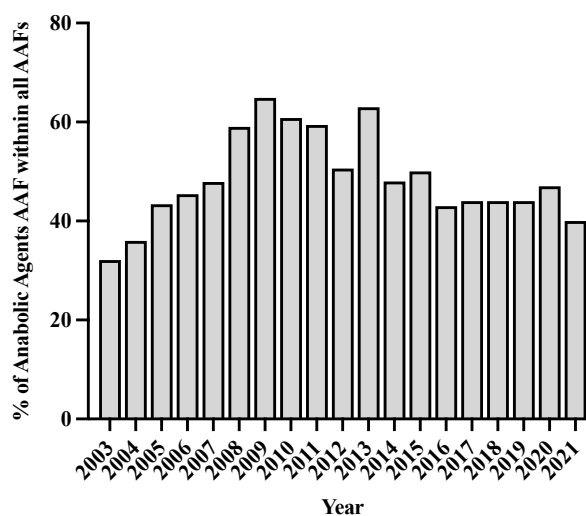


Figure 4: AAFs of AAS in relation to the total amount of AAFs of all groups between 2003 and 2021 by WADA accredited laboratories [60-78]

Similar to T, AAS possess both anabolic and androgenic properties. The androgenic actions are mainly related to the development and maintenance of primary and secondary sexual characteristics, whereas the anabolic actions include promoting protein synthesis and muscle growth, enhancing nitrogen retention, and stimulating erythropoiesis [39, 79-83].

In particular, their ability to promote muscle growth through anabolic effects is the main reason for their misuse by athletes in sports. AAS can also shorten the recovery period after intense and prolonged physical activity due to the effect on erythropoiesis. Additionally, they can stimulate an aggressive and determined attitude, which may be beneficial in sports involving physical contact with opponents [39]. Consequently, AAS are extensively used in sports that require significant muscle mass and strength, such as weightlifting, boxing, and cycling, as well as in sports where increased muscle size can enhance an athlete's speed potential, such as rugby and sprint. According to the findings by WADA in disciplines of the Association of Summer Olympic International Federations (ASOIF), weightlifting consistently reports the highest number of AAFs related to "Anabolic Agents". In addition to weightlifting, the misuse of AAS is also frequently detected in athletics, cycling, football, rugby, and boxing [60]. Moreover, the use of AAS is also popular among recreational athletes and the general population due to their ability to enhance athletic performance and physical appearance. These substances are commonly categorized as performance- and image-enhancing drugs.

However, due to their androgenic properties, the misuse of AAS can lead to significant side effects, including hepatotoxicity, cardiovascular changes, reproductive and endocrine disturbances, dermatological, and psychiatric effects. Specifically, AAS misuse in men may cause infertility, azoospermia, testicular atrophy, and gynecomastia, whereas women may experience excessive body hair growth, menstrual irregularity, and virilization [39, 79]. Additionally, the misuse of AAS in adolescents may reduce body strength due to premature epiphyseal closure of the growth plates in the long bones [84].

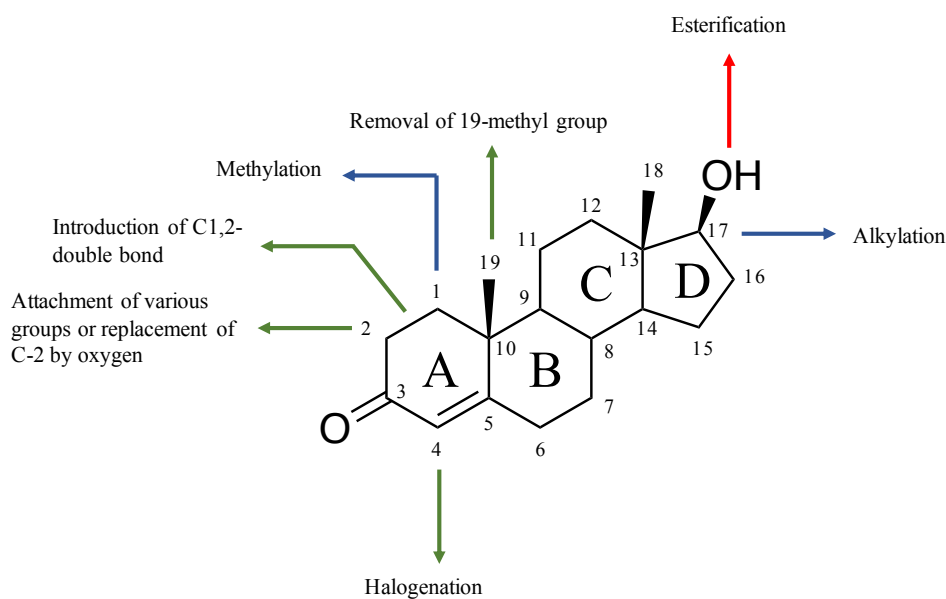


Figure 5: Main chemical modifications of AAS derived from T. Red arrow: the first type enables depot activity; blue arrows: the second type confers oral activity; green arrows: the third type hinders the aromatization and reduces 5 α -reduction

With the aim of enhancing anabolic effects, maximizing bioavailability, optimizing pharmacokinetics, and preventing estrogenic side effects, most of the exogenous AAS are synthesized via structural modifications of T [9, 81, 85, 86]. These chemical modifications are mainly classified into three types based on the potential effects (**Figure 5**). The first type is esterification of the 17 β -hydroxy group, which improves the suitability of T for intramuscular or oral administration and provides a sustained-release effect. Methylation of position C-1 and alkylation of position C-17 produce the second type, which prevents the deactivation by first-pass metabolism in the liver and confers better oral activity to the steroids [39, 87]. The third type involves reducing the metabolism of AAS, including hindering aromatization or reducing 5 α -reduction, which can be achieved through dehydrogenation of C1-2, coupling of various groups at C-2, replacement of C-2 with an oxygen atom, removal of the 19-methyl group, and halogenation on position 4 [82, 88, 89]. Despite numerous attempts to achieve selectivity for anabolic effects over androgenic effects, these efforts have not been successful. All anabolic steroids exhibit a certain degree of androgenic activity.

In this work, the focus was mainly on five exogeneous AAS (**Figure 6**): 17 α -methyltestosterone (17 β -hydroxy-17 α -methylandro-4-ene-3-one, MT), metandienone (17 β -hydroxy-17 α -methylandro-1,4-dien-3-one, MD), clostebol (4-chloro-17 β -hydroxyandro-4-ene-3-one, CLT), methylclostebol (4-chloro-17 β -hydroxy-17 α -methylandro-4-ene-3-one, CLMT), and dehydrochloromethyltestosterone (4-chloro-

17 β -hydroxy-17 α -methyl-androsta-1,4-dien-3-one, DHCMT). All structures are derived from T through specific modifications, including the addition of a 17 α -methyl group, formation of a 1,2-double bond, and introduction of a 4-chloro substituent. All five steroid compounds are included in WADA's Prohibited List [6]. MD has been one of the most commonly detected anabolic steroids (**Figure 7**), especially after the year 2006, when a newly introduced metabolite improved detection [90]. DHCMT has been misused for doping in 1980s by East German athletes [91], with the number of AAFs reaching its peak in 2013. Although not as widely misused as MD and DHCMT, MT and CLT have been consistently detected in doping control since 2003. CLMT was explicitly added to the prohibited list only in 2020 [6].

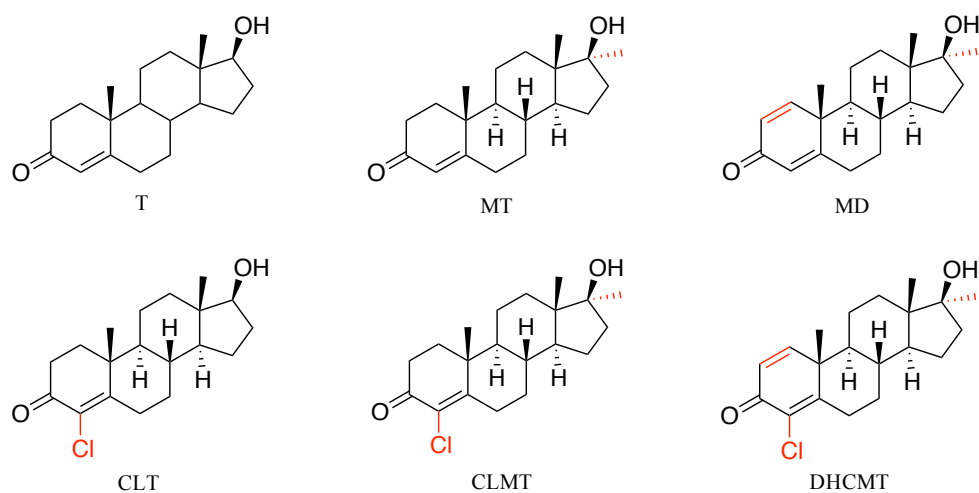


Figure 6: Chemical structures of T, MT, MD, CLT, CLMT, and DHCMT

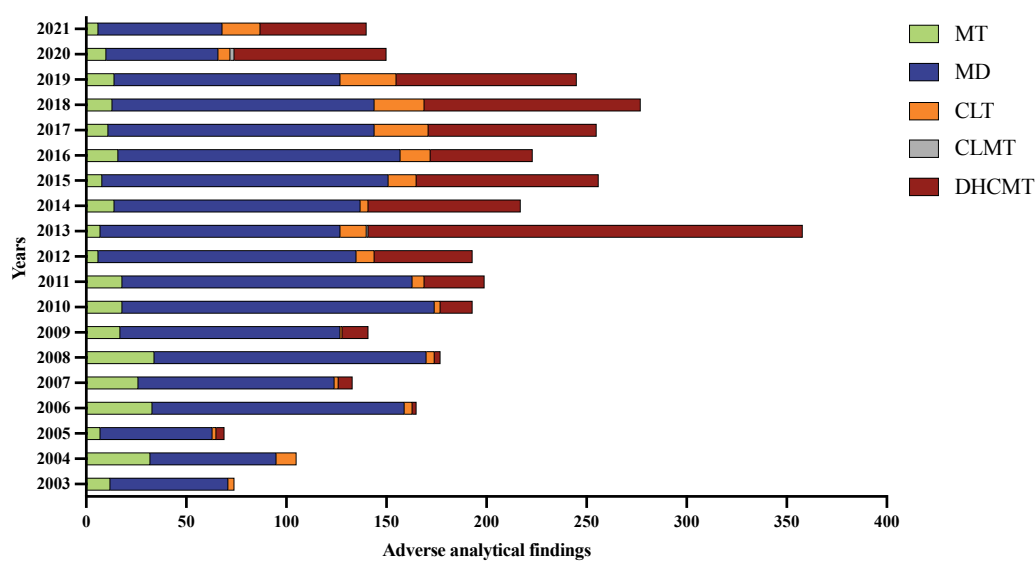


Figure 7: AAFs of MT, MD, CLT, CLMT, and DHCMT between 2003 and 2021 [60-78]

In general, the metabolism of exogenous AAS follows similar principles to that of endogenous AAS, such as T (as described in chapter 1.2.2), undergoing phase I and phase II metabolism in the human body. This serves to inactivate the drugs and facilitate their elimination from the body. In human phase I metabolism of the five focused AAS, they may all undergo A-ring reduction, 3-keto reduction, 5 α -reduction, as well as hydroxylation in various positions (positions 6, 11, 12, 16, 18, or 20 in MD; positions 2, 4, 6, or 20 in MT; positions 6, 11, or 16 in CLT; positions 6, 12, 16, or 20 in DHCMT). Additionally, hydrogenation of 1,2-double bonds can occur in MD and DHCMT, while oxidation of C6-7 can take place in the metabolism of MD and MT. 17-Epimerization and D-ring rearrangement have been commonly observed in the metabolism of 17 α -methyl steroids, such as MD, MT, and DHCMT [92-94]. Notably, both reactions are involved with the urinary degradation of 17 β -sulfate metabolites with a 17 α -methyl group. The removal of the 17 β -sulfate group results in the formation of a stabilized cation, subsequently undergoing various eliminations or substitutions. As a result, different compounds are generated, such as D-ring rearrangement products, 18-nor-17,17-dimethyl analogs, as well as the corresponding 17-epimer [95, 96].

AAS have also been used in clinical practice since the 1940s [97]. Apart from androgen replacement therapy, AAS also play a role in the treatment of short stature, hereditary angioedema, chronic kidney disease, osteoporosis in postmenopausal women, inoperable breast cancer, the human immunodeficiency virus (HIV)/ acquired immunodeficiency syndrome (AIDS)-associated wasting syndrome, sarcopenia, and for diseases characterized by a negative nitrogen balance [97-100]. Currently, only a limited number of AAS have been approved for therapeutic use by regulatory authorities for specific medical conditions. For example, T preparations are commonly used to treat hypogonadism in men and are also approved for the treatment of perimenopause and menopause symptoms in women [101, 102]. Additionally, CLT is also therapeutically applied to improve wound healing or treat skin lesions [103].

1.3 Steroid Analysis in Doping Control

The International Standard for Laboratories (ISL) is a mandatory International Standard within the World Anti-Doping Program. It aims to ensure that WADA-accredited laboratories provide valid test results based on reliable evidence and to promote consistency in the analysis of samples. The TD complement the ISL by outlining specific technical requirements or procedural issues [104].

The analysis and detection of prohibited compounds in doping control is performed by WADA-accredited laboratories according to the TD [105]. Most of these analyses are conducted using urine specimens as the matrix. Currently, the routine screening of AAS and their metabolites includes the analysis of the unconjugated excreted fraction and of the conjugated fraction (glucuronides or sulfates) [106-108].

The analysis of the unconjugated fraction is usually performed after enzymatic hydrolysis using β -glucuronidase. After liquid-liquid extraction or solid phase extraction of the deconjugated steroids from the matrix, the extracts are analyzed directly by liquid chromatography (tandem) mass spectrometry (LC-MS(/MS)) or by gas chromatography (tandem) mass spectrometry (GC-MS(/MS)) after derivatization. Compared to LC-MS(/MS), GC-MS(/MS) is the more commonly used technique for AAS control, as the majority of AAS and their metabolites are poorly ionized in LC-MS/MS [5, 36].

The derivatization technique for steroids introduced by Donike laid the foundation for comprehensive steroid profiling in doping control [109, 110] and has become a routine method for trace-level analysis of steroids to improve chromatographic as well as mass spectrometric properties of analytes in GC-MS analysis [111]. The derivatization is generally performed using two different derivatization methods prior to GC separation, resulting in the formation of per-TMS (derivatization with catalyst) or mono/bis-TMS (derivatization without catalyst) derivatives [19, 57]. Per-TMS derivatization can be achieved through the mixture of *N*-methyl-*N*-trimethylsilyltrifluoroacetamide (MSTFA) with ammonium iodide (NH₄I) and ethanethiol or dithioerythritol. This process results in the generation of the highly reactive trimethyliodosilane (TMIS), which forms *in situ* through the reaction of iodide with MSTFA. The hydroxy and oxo groups in steroids are converted into corresponding TMS ethers and enol-ethers, respectively, which enhances the sensitivity of the analytes [36, 112]. In contrast, derivatization using MSTFA without catalyst yields only TMS ethers of sterically unhindered hydroxy groups [19, 57].

The silylation of steroid derivatives increases their volatility and thermal stability, thus ensuring robust detection by GC-MS [113]. Additionally, the reduction in polarity achieved through silylation allows for better chromatographic behavior by minimizing undesirable nonspecific column adsorption and therefore improves the chromatography results [114].

In recent years, methods based on LC-MS(/MS) have been more and more applied in the direct determination of intact phase II metabolites of AAS, such as glucuronides or sulfate conjugates [115-117]. In comparison to GC-MS(/MS) methods that involve

deconjugation of analytes, direct analysis of phase II metabolites by LC-MS(/MS) enables easier sample preparation procedures, as no hydrolysis is performed and an additional derivatization step is not necessarily needed [88].

1.4 *In vitro* and *In vivo* Models for Metabolism Studies

Due to their widespread use in enhancing athletic performance and medical therapy, the metabolism of AAS has been extensively investigated for decades via both *in vivo* and *in vitro* studies. Most anabolic steroids undergo extensive metabolic transformations and are rarely excreted unchanged in humans [118]. In doping-control studies, the determination of the prohibited compounds is achieved by detecting appropriate markers. These markers can be either the parent compound itself, and/or one or more of its metabolites [58]. Moreover, although a number of compounds have been extensively studied, such as MD, there is continued interest in identifying new metabolites that have the potential to extend the detection window in anti-doping control studies. Therefore, metabolic studies of AAS are crucial for enhancing doping detection and also for result interpretation in further investigations of AAS metabolism.

In metabolic research on anabolic steroids, various models are used to study their metabolism and effects. Human administration is considered the most relevant approach as it directly reflects human physiology and response, enabling the evaluation of complex interactions and factors. However, ethical considerations can impose limitations on conducting studies involving human subjects. The WADA research ethics policy mandates that all projects submitted for funding undergo an appropriate and adequate ethics review according to international standards [119]. The ISL, specifically the Code of Ethics (Annex A), explicitly states that “The Laboratories and ABP Laboratories shall follow the Helsinki Declaration and any applicable national standards as they relate to the involvement of human subjects in research” [104].

However, due to the considerations regarding the potential risks and impacts on participants, laboratories may face difficulties in obtaining ethics approval. The Helsinki Declaration developed by The World Medical Association is widely recognized as a crucial ethical guideline for medical research involving human subjects, whereas anti-doping research differs from traditional medical research in various aspects, including its objectives, assessment of risks and benefits, identification of vulnerable populations, and pre-trial scientific requirements [120]. For example, as doping athletes are continuously motivated to use novel substances to evade the existing laws (legal and sports), research

involving non-approved substances with limited safety information is inevitable to develop methods for detection [121]. However, this makes it more challenging for researchers to obtain ethical approval.

In addition, animal models can also be an alternative choice for *in vivo* studies, such as rodents (mice, rats), dogs or pigs. These models allow for reproducing physiological conditions and provide insight into the systemic response to anabolic steroids. However, animal testing is strictly regulated in the European Union, and any experimental procedures involving the treatment of animals require approval from the responsible governing animal welfare authority. With the aim of improving the treatment of research animals while advancing the quality of scientific and medical research and testing, the principle of 3Rs (replacement, reduction, and refinement) was originally introduced by Russell and Burch in 1959 [122]. These principles promote the use of alternative methods to animal testing whenever possible, the reduction of the number of animals used, and the refinement of experimental procedures to minimize any potential suffering or distress [122].

This chapter provides essential background information on various possibilities to perform metabolic studies with a special focus on *in vitro* and *in vivo* methods relevant to this work, including the *in vivo* fish embryo model and *in vitro* human skin cell model used for investigating the metabolism of anabolic steroids.

1.4.1 Isolated Recombinant Enzymes

Metabolic studies using isolated recombinant enzymes are straightforward, allow for the investigation of specific metabolic pathways and provide valuable insights into the function and regulation of enzymes involved in metabolism.

In general, the commercially available recombinant enzymes are pure enough to ensure a controlled and well-defined reaction for studying the enzymes' function and allow researchers to focus solely on their catalytic activity without interference from other cellular components. The kinetic studies in isolated enzymes can provide valuable information about substrate specificity, affinity, and reaction rates. This helps in understanding the enzymes' role in specific metabolic pathways and their contribution to various physiological processes. Moreover, compared to *in vivo* studies or whole-cell biotransformation, human liver microsomes, organoids, isolated cells, etc., the enzyme incubation assay is more convenient to handle and the results can be obtained faster.

In this work, isolated recombinant enzymes from the AKR1C subfamily were used to investigate the catalytic mechanism involved in the stereoselectivity of 3-keto reduction. This may provide the knowledge required to interpret the metabolic pathways occurring in the human body.

1.4.2 Human Skin Cell Model

As the largest organ in the human body, the main function of the skin is to protect the body from pathogens and prevent water loss. Due to its unique properties, the skin is an ideal target for the application of cosmetic and pharmaceutical products. In particular, it allows for various modes of drug administration, including epidermal, dermal, and transdermal routes, which can help to minimize the risk of adverse effects associated with systemic application. Moreover, targeting the skin can bypass the hepatic first-pass effect, thereby enhancing the efficacy of certain medications [123]. Several androgen preparations designed for transdermal application are available in the therapeutic drug market.

The human skin is composed of three main layers: epidermis, dermis, and hypodermis (also known as subcutaneous tissue). Keratinocytes and fibroblasts are the main cellular components of the epidermis and dermis, respectively, and their metabolic activities are crucial for the proper function of the skin. More specifically, keratinocytes are involved in the formation of the skin barrier and the regulation of immune responses in the cutaneous environment. They are commonly used in assessing skin metabolism due to their abundance and accessibility in human tissue samples. Fibroblasts are responsible for producing and maintaining the extracellular matrix, which provides structural support to the skin and contributes to its elasticity and strength [124]. *In vitro* skin cell models enable controlled investigation of specific metabolic processes, providing valuable insights into the distinctive characteristics of steroid metabolism in the skin and holding the potential to contribute to the screening of topically applied compounds for doping purposes.

It has been previously established that human keratinocytes and fibroblasts exhibit enzyme activities of 5α -reductase, 3α -HSD, and 17β -HSD [123, 125], which play a crucial role in the phase I metabolism of AAS.

1.4.3 Fish Embryo Model

Fish have gained increasing attention in recent years as valuable models for biotransformation studies, especially zebrafish (*Danio rerio*), as in large parts genome

organization and physiology are comparable between humans and teleosts [126]. The zebrafish water tank model was even tested as an alternative model for metabolism studies of doping-related compounds. This is attributed to the small size, rapid development, transparent embryos, and particularly genetic similarities of zebrafish to humans. The sequencing of the zebrafish genome has revealed that approximately 70% of human genes have a corresponding ortholog in zebrafish [127, 128]. According to the EU Directive 2010/63/EU on the protection of animals used for scientific purposes, the earliest life stages of animals, such as fish embryos, are not defined as protected and do not fall under the regulatory frameworks for animal experimentation. Therefore, no specific approval is required for conducting experiments with fish embryos before hatching [129-131]. Like zebrafish, Japanese medaka (*Oryzias latipes*) is also one of the commonly used fish models in biomedical research. There are 104 conserved syntenic segments shared between medaka and humans, which involve at least three orthologous gene pairs in the dataset [132].

Sex-specific models can provide valuable insights into sex-dependent effects on steroid metabolism. In mammals, the sex-determining gene *Sry*, located on the Y chromosome, plays a crucial role in initiating the development of the male phenotype [133]. Females typically have two identical sex chromosomes (XX), whereas males possess two different sex chromosomes (XY). In contrast to mammals, the sex determination in many fish species, including the medaka, is labile and can be determined either chromosomally or by environmental factors [134]. Monosex populations, offspring with only one sex, can be produced by experimentally produced YY or XX males interbreeding with normal females [133]. This provides opportunities for investigations sex-dependent metabolic studies. Moreover, in the female leukophore-free (FLFII) strain, the sex of male embryos can be identified early and non-destructively by observing the presence of male-associated leucophores using fluorescence microscopy (48-72 hours post fertilization) [135].

2 Aims

Given the extensive metabolic reactions that may occur following the administration of AAS and the continued emergence of new designer steroids, a comprehensive understanding of steroid metabolism is crucial for the development of effective detection methods in doping control research. Appropriate models are necessary for metabolic studies, which can provide insights into the investigations of metabolic pathways that may occur in the human body during the excretion of the doping compounds. The aim of this work is to investigate the metabolism of AAS using various metabolic models, including isolated recombinant enzymes, human skin cells, and medaka fish embryos, which may contribute to the enhancement of detection of misused AAS in doping control analysis.

The sequence of the A-ring reduction in MD has been extensively investigated in previous research based on the excreted metabolites [93, 136, 137]. Enzyme reactions with members of the AKR1s subfamily (AKR1C2, AKR1C3, AKR1C4, and AKR1D1) allow for the investigation of specific reduction reactions within the A-ring. This helps to propose a rational order of reduction and provides valuable insights into the characterization of stereoselective metabolism catalyzed by AKR1Cs and AKR1D1.

AAS like T and CLT, in addition to being misused as doping agents, are also employed for therapeutic purposes, such as in the topical treatment of hypogonadism [101] and various skin diseases [103]. Transdermal administration is an effective route of drug delivery due to its convenient, controlled, and patient-friendly nature. However, in contrast to the extensive investigations of metabolic studies in the liver, limited knowledge is available for cutaneous metabolism. Therefore, the metabolic studies of AAS in human skin cells hold significance not only for doping control research but also for drug development processes. To gain a comprehensive insight into anabolic steroid metabolism in human skin cell models (keratinocytes or fibroblasts), six structurally related AAS compounds, T, MD, MT, CLT, DHCMT, and CLMT were selected as model substances.

Although *in vitro* models are valuable for understanding metabolic pathways and are relatively easy to manipulate, they may have limitations in terms of the range of reactions that occur within a specific model. Common models used for *in vivo* biotransformation studies, such as rodents, dogs or pigs, as well as the most straightforward way, human

administration, all face ethical concerns. In this study, MD was used as a model substance to assess whether the medaka embryo model is an alternative non-animal test model to study human-like metabolism. Moreover, to further investigate the phase I metabolic patterns of AAS in the medaka embryo model, 2,3,4-¹³C₃-Testosterone ([¹³C₃]-T) and MT were used as substrates.

These investigations allow for the identification of potential biomarkers or metabolites and may contribute to the development of more sensitive and specific detection methods, as well as to the pharmacokinetic and pharmacodynamic evaluation of new drugs in development. Moreover, the metabolic knowledge gained from known compounds can also contribute to the interpretation of analytical results obtained from designer drugs and aid in targeting doping athletes.

3 Materials and Methods

3.1 Materials

Table 2: Steroids and reference materials

17 β -Hydroxy-5 α -androstan-3-one	Steraloids (Newport, RI, USA)
17 β -Hydroxy-5 β -androstan-3-one	Steraloids (Newport, RI, USA)
17 β -Hydroxy-17 α -methyl-5 α -androstan-3-one	Tokyo Chemical Industry Co., Ltd (Tokyo, Japan)
17 β -Hydroxy-17 α -methyl-5 β -androst-1-ene-3-one	In house synthesized
17 α -Methyltestosterone	Tokyo Chemical Industry Co., Ltd (Tokyo, Japan); Sigma Aldrich (Taufkirchen, Germany)
17 α -Methyl-5 α -androstane-3 α ,17 β -diol	National Measurement Institute (North Ryde, Australia)
17 α -Methyl-5 α -androstane-3 β ,17 β -diol	In house synthesized
17 α -Methyl-5 β -androstane-3 α ,17 β -diol	National Measurement Institute (North Ryde, Australia)
17 α -Methyl-5 β -androstane-3 β ,17 β -diol	In house synthesized
4-Chloro-3 α -hydroxy-androst-4-ene-17-one	Australian National Measurement Institute (North Ryde, Australia)
5 α -Androstane-3 α ,17 β -diol	Steraloids (Newport, RI, USA) or TCI (Tokyo, Japan)
6 β -Hydroxy-metandienone	In house synthesized
Androst-4-ene-3,17-dione	Steraloids (Newport, RI, USA) or TCI (Tokyo, Japan)
Clostebol	Steraloids (Wilton, USA)
Dehydrochloromethyltestosterone	Cohnchem Scientific Co., Ltd (Derby, UK)
Etiocholanolone	Steraloids (Newport, RI, USA)
Metandienone	LGC Standards (Wesel, Germany)
Methylclostebol	in house synthesized
Testosterone	Sigma Aldrich (Taufkirchen, Germany)
Testosterone-16, 16, 17-d ₃	Sigma Aldrich (Taufkirchen, Germany)
Testosterone-[d ₃] glucuronide	TRC (North York, USA)
2,3,4- ¹³ C ₃ -Testosterone	Sigma Aldrich (Taufkirchen, Germany)

Table 3: Solvents, reagents, and materials

Acetone	VWR (Dresden, Germany)
Acetonitrile (LC-MS grade)	Fisher (Schwerte, Germany)
Acetonitrile (HPLC grade)	VWR (Dresden, Germany)
Ammonium iodide	Sigma Aldrich (Taufkirchen, Germany)
Acetic acid glacial	VWR (Darmstadt, Germany)
Dess-Martin periodinane	Sigma Aldrich (Taufkirchen, Germany)
Dichloromethane	Fisher Scientific (Loughborough, United Kingdom)
Dulbecco's modified Eagle's medium high glucose (DMEM)	Sigma Aldrich (St. Louis, MO, USA)
Dulbecco's phosphate buffered saline (DPBS)	Sigma Aldrich (St. Louis, MO, USA)
Epilife medium	Thermo Fisher Scientific Life Technologies GmbH (Darmstadt, Germany)
Ethanethiol	Sigma Aldrich (Taufkirchen, Germany)
Ethanol absolut	ChemSolute (Renningen, Germany)
Ethyl acetate	VWR (Dresden, Germany)
Fetal bovine serum (FBS)	Sigma-Aldrich (St. Louis, MO, USA)
Formic acid (LC-MS grade)	Sigma Aldrich (Taufkirchen, Germany)
Formic acid (p.a.)	Merck (Darmstadt, Germany)
Helium	Air liquide (Düsseldorf, Germany)
Human keratinocyte growth supplement (HKGS, 100X)	Thermo Fisher Scientific Life Technologies GmbH (Darmstadt, Germany)
Human recombinant enzyme AKR1C2	Cusabio (Houston, TX, USA)
Human recombinant enzyme AKR1C3	Novus Biologicals Europe (Abingdon, United Kingdom)
Human recombinant enzyme AKR1C4	MyBioSource (San Diego, CA, USA)
Human recombinant enzyme AKR1D1	MyBioSource (San Diego, CA, USA)
Hydrochloric acid	Fisher (Schwerte, Germany)
Hydrogen peroxide 30 %	Sigma Aldrich (Taufkirchen, Germany)
L-Glutamine	Sigma-Aldrich (St. Louis, MO, USA)

Methanol (HPLC-grade)	Fisher Scientific (Loughborough, United Kingdom)
Methanol (MS quality)	Fisher (Schwerte, Germany)
Methanol (p.a.)	VWR (Dresden, Germany)
MilliQ water	Millipore S.p.A., Milano, Italy
NADPH regenerating system solution A and solution B	Corning Gentest (Woburn, MA, USA)
<i>n</i> -Hexane	VWR (Darmstadt, Germany)
β -Glucuronidase from <i>Escherichia coli</i> (>140 U/mL)	Roche Diagnostics (Mannheim, Germany)
<i>N</i> -Methyl- <i>N</i> -trimethylsilyl-trifluoroacetamide (MSTFA)	Chemische Fabrik Karl Bucher (Waldstetten, Germany)
Nitrogen	Air liquide (Düsseldorf, Germany)
Penicillin/streptomycin	Sigma-Aldrich (St. Louis, MO, USA)
Phosphate buffered saline (PBS, 0.5 M, pH 7.4)	Corning Gentest (Woburn MA, USA)
Potassium carbonate	Merck (Darmstadt, Germany)
Potassium dihydrogen phosphate	Merck (Darmstadt, Germany)
Potassium hydroxide	Ferak Berlin GmbH (Berlin, Germany)
Potassium hydrogencarbonate	Sigma Aldrich (Taufkirchen, Germany)
Sodium borohydride	Merck (Darmstadt, Germany)
Sodium chloride	Sigma Aldrich (Taufkirchen, Germany)
Sodium hydrogen carbonate	Merck (Darmstadt, Germany)
Sodium hydroxide	Sigma Aldrich (Taufkirchen, Germany)
Sodium sulfate	Merck (Darmstadt, Germany)
Sulfuric acid 96 %	Merck (Darmstadt, Germany)
<i>t</i> -Butyl methyl ether (TBME)	Carl Roth (Darmstadt, Germany)
Trypsin-EDTA solution	Sigma-Aldrich (St. Louis, MO, USA)
Zinc powder (< 45 μ m)	Merck (Darmstadt, Germany)

3.2 Methods

3.2.1 Synthesis of Reference Materials

Due to the structural similarities, the reference compounds 4 α -chloro-5 α -androstane-3 ξ ,17 β -diols (3 α ,4 α ,5 α -THCLT, **13a**; 3 β ,4 α ,5 α -THCLT, **13b**) and 4-chloroandrost-4-ene-3 ξ ,17 β -diols (3 α -DHCLT, **17a**; 3 β -DHCLT, **17b**) for CLT metabolites as well as 4 α -chloro-17 α -methyl-5 α -androstane-3 ξ ,17 β -diols (3 α ,4 α ,5 α -THCLMT, **14a**; 3 β ,4 α ,5 α -THCLMT, **14b**) and 4-chloro-17 α -methylandrost-4-ene-3 ξ ,17 β -diols (3 α -DHCLMT, **18a**; 3 β -DHCLMT, **18b**) for CLMT metabolites were synthesized through identical reaction steps but with different starting materials. The methods used for the synthesis were adapted from da Silva *et al.*, Kratena *et al.*, and Schänzer and Donike [118, 138, 139]. The synthesis of compounds **17a**, **17b**, **18a**, and **18b** is illustrated in **Figure 8**. The chemical structures of compounds involved in the synthesis are shown in **Table 43** in Annex.

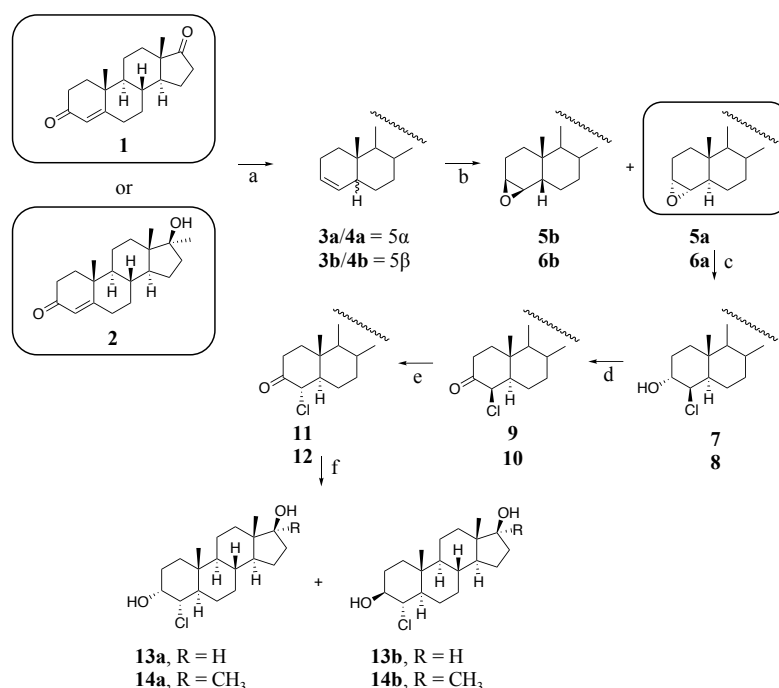


Figure 8: Reaction scheme for 4 α -chloro-5 α -androstane-3 ξ ,17 β -diol (**13a**, **13b**) and 4 α -chloro-17 α -methyl-5 α -androstane-3 ξ ,17 β -diol (**14a**, **14b**) steroids: (a) Zn, AcOH, reflux; (b) H₂O₂, HCO₂H, CH₂Cl₂, rt, 6 h; (c) conc. HCl, CHCl₃, rt, 30 min; (d) DMP, CH₂Cl₂, rt, 1 h; (e) KOH, MeOH, rt; (f) NaBH₄, rt, 1 h. This figure is adapted from my published paper [140]

Synthesis of 3 α ,4 α ,5 α -THCLT (**13a**) and 3 β ,4 α ,5 α -THCLT (**13b**)

To a boiling solution of AED (**1**; 2 g, 6.98 mmol) in glacial acetic acid (120 mL), 12.0 g of zinc dust were added in portions over 10 min, after which the reaction was complete. The suspension was filtered, the retentate was washed with glacial acetic acid

and the combined filtrates were evaporated to dryness. Afterwards, the residue was re-dissolved in water (400 mL) and extracted with diethyl ether (3 X 400 mL). The organic layers were washed with 10% aq. NaHCO₃ (3 X 400 mL) and water (3 X 400 mL), dried over Na₂SO₄ and evaporated to dryness to give a white crystalline solid (1.77 g) composed of an isomeric mixture of 5 α - (**3a**) and 5 β -androst-3-en-17-one (**3b**).

A stirred solution of the olefin mixture **3a** and **3b** (1.77 g) in dichloromethane (26 mL) was treated with 30% hydrogen peroxide (1.3 mL) and 100% formic acid (1.2 mL) for 6 hours at room temperature (rt). After dilution with methanol (260 mL) and basification with aq. NaOH (1 M), the solution was neutralized with aq. HCl (1 M). Methanol was reduced by evaporation, then the residue was diluted with water (100 mL), and finally extracted with dichloromethane (3 X 100 mL). The combined organic layers were washed with 10% aq. NaHCO₃ (2 X 100 mL) and water (100 mL), dried over Na₂SO₄ and evaporated to dryness to give 1.88 g of a mixture of epoxides (**5a**, **5b**). Afterwards, the crude product was purified by HPLC fractionation (details in chapter 3.2.8) collecting **5a** as pure compound.

Epoxide **5a** (94 mg) was dissolved in chloroform (1.7 mL). Concentrated HCl (37%, 700 μ L, 829.08 μ g, 8.41 mmol) was added dropwise and the resulting biphasic mixture was stirred vigorously. After 30 minutes, the solution was transferred to a separatory funnel and the phases were separated. The aqueous phase was diluted with water (10 mL), extracted with CH₂Cl₂ (3 X 15 mL) and the pooled organic phases were washed with saturated NaHCO₃ solution (2 X 20 mL) and brine (saturated NaCl solution, 20 mL). The extracts were dried over Na₂SO₄ and evaporated to dryness to give 105.4 mg of crude product (**7**).

The crude product **7** (105.4 mg) was dissolved in CH₂Cl₂ (3.5 mL). To this solution, Dess–Martin periodinane (DMP, 185.5 mg) was added in portions over 10 min. After 1 h, the reaction was quenched by adding an aqueous Na₂S₂O₃ solution and saturated NaHCO₃. The biphasic system was separated. The aqueous phase was diluted with water (10 mL) and extracted with CH₂Cl₂ (3 X 20 mL). The combined organic phases were washed with water and dried over Na₂SO₄. The crude product **9** obtained after evaporation (104.6 mg) was used in the next step without further purification. It was dissolved in methanol (10.46 mL), and a 10% aqueous solution of KOH (182 μ L) was added dropwise at rt. The solution was stirred for 5 min after the complete addition, followed by the addition of acetic acid (75 μ L) to neutralize. After evaporation, the resulting white precipitate was dissolved in water/CH₂Cl₂ (10 mL/15 mL) and after shaking, the aqueous phase was

again extracted with CH₂Cl₂ (3 X 20 mL). The pooled organic phases were washed with saturated NaHCO₃ solution (20 mL) and 20 mL of brine. Thereafter, the organic phases were dried over Na₂SO₄, yielding 94.8 mg of crude product **11**.

Substance **11** was dissolved in methanol/H₂O (3.5 mL, 9:1, v/v), and NaBH₄ was added. The solution was stirred for 60 min at ambient temperature. After methanol was evaporated, the aqueous phase was diluted with water (10 mL) and extracted with CH₂Cl₂ (3 X 25 mL). The combined organic phases were washed with water (2 X 25 mL) and dried over Na₂SO₄, yielding a mixture of crude products (**13a**, **13b**). Afterwards, the product was purified by column chromatography (silica gel 60, 460 mm x 20 mm, particle size 63 - 200 μm), using hexane/ethyl acetate (3:2, v/v) followed by HPLC fractionation (details in chapter 3.2.8).

Synthesis of 3α,4α,5α-THCLMT (**14a**) and 3β,4α,5α-THCLMT (**14b**)

To a boiling solution of MT (**2**; 2 g, 6.61 mmol) in glacial acetic acid (120 mL), zinc dust (12.0 g) was added in portions during 10 min after which the reaction was complete. The zinc suspension was filtered, the zinc was washed with glacial acetic acid and the filtrate was evaporated to dryness. The residue was diluted with water (400 mL) and extracted with diethyl ether (3 X 400 mL). The combined organic layers were washed with 10% aq. NaHCO₃ (3 X 400 mL) and water (3 X 400 mL), dried over Na₂SO₄ and evaporated to dryness to give a white crystalline solid (1.89 g) composed of an isomeric mixture of 5α-olefin (**4a**) and 5β-olefin (**4b**).

The olefin mixture **4a** and **4b** (1.89 g) was dissolved in dichloromethane (28 mL) and treated with 30% hydrogen peroxide (1.4 mL) and 100% formic acid (1.26 mL) and stirred for 6 hours at ambient temperature. After dilution with methanol (280 mL) and basification with aq. NaOH (1 M), the solution was neutralized with aq. HCl (1 M). Methanol was reduced by evaporation, then the residue was diluted with water (100 mL), and finally extracted with dichloromethane (3 X 100 mL). The extracts were washed with 10% aq. NaHCO₃ (2 X 100 mL) and water (100 mL), dried over Na₂SO₄ and evaporated to dryness to give 2.04 g of a mixture of epoxides (**6a**, **6b**). Afterwards, the crude product was purified by HPLC fractionation (details in chapter 3.2.8) to collect **6a**.

Epoxide **6a** (140 mg) was dissolved in chloroform (2.5 mL). Concentrated HCl (37%, 140 μL) was added dropwise and the resulting biphasic mixture was stirred vigorously. After 30 min the solution was transferred to a separatory funnel and the phases were

separated. The aqueous phase was diluted with water (10 mL) and extracted with CH₂Cl₂ (3 X 15 mL). The pooled organic phases were washed with saturated NaHCO₃ solution (20 mL) and brine (20 mL). The extracts were dried over Na₂SO₄ and evaporated to dryness to give 168.6 mg of crude product (**8**).

The crude product **8** (154.4 mg) was dissolved in CH₂Cl₂ (10.7 mL). To this solution, DMP (271.9 mg) was added in portions over 15 minutes. After 1 hour, the reaction was quenched with aqueous Na₂S₂O₃ solution and saturated NaHCO₃. The biphasic system was separated and the aqueous phase was diluted with water (10 mL) and extracted with CH₂Cl₂ (3 X 20 mL). The pooled organic phases were washed with water (2 X 20 mL) and dried over Na₂SO₄. The crude product after evaporation (161.0 mg) was used in the next step without further purification.

To the crude product **10** (161.0 mg) dissolved in methanol (16.1 mL), a 10% solution of KOH (279 μL) was added dropwise and the resulting mixture was stirred for 5 min. Then, the solution was neutralized with acetic acid (115 μL). After evaporation, the resulting white precipitate was dissolved in water/CH₂Cl₂ (15mL/20mL), and after shaking, the aqueous phase was again extracted with CH₂Cl₂ (5 X 20 mL). The extracts were washed with saturated NaHCO₃ solution (30 mL) and brine (30 mL). After drying over Na₂SO₄, 154.2 mg of crude product **12** were obtained.

To substance **12** dissolved in methanol/H₂O (5 mL, 9:1, v/v), NaBH₄ was added and the resulting mixture was stirred for 60 min at rt. Afterwards, methanol was evaporated, then the aqueous phase was diluted with water (10 mL) and extracted with CH₂Cl₂ (4 X 20 mL). The pooled organic phases were washed with water (2 X 25 mL) and dried over Na₂SO₄. The mixture of crude products (**14a**, **14b**) was obtained after evaporation to dryness. Afterwards, the product was purified by column chromatography (silica gel 60, 460 mm x 20 mm, particle size 63 - 200 μm), using hexane/ethyl acetate (3:2, v/v) followed by HPLC fractionation (details in chapter 3.2.8).

Synthesis of 3 α /3 β -DHCLT (17a, 17b) and 3 α /3 β -DHCLMT (18a, 18b)

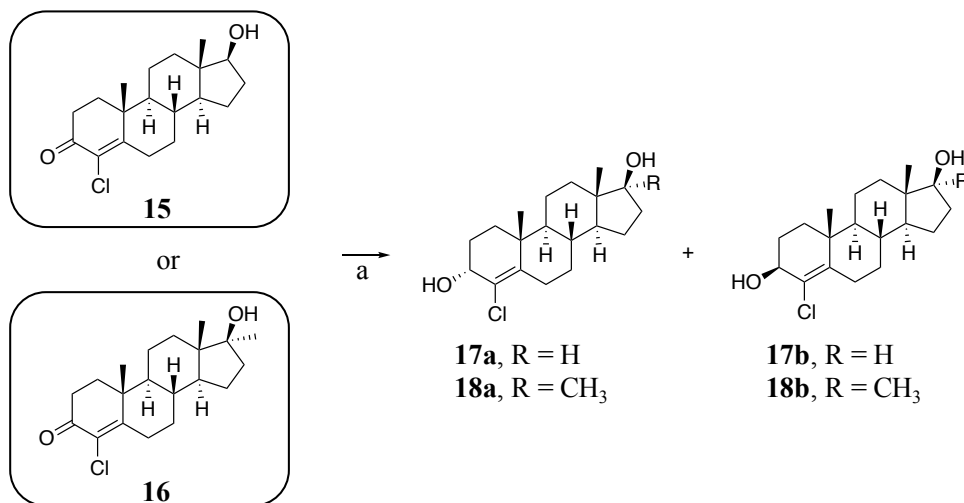


Figure 9: Reaction scheme for 4-chloroandrost-4-ene-3 ξ ,17 β -diol (17a, 17b) and 4-chloro-17 α -methylandrost-4-ene-3 ξ ,17 β -diol (18a, 18b) steroids: (a) NaBH₄, rt, 1 h. This figure is adapted from my published paper [140]

For the synthesis of the epimeric 3 α -DHCLT (17a) and 3 β -DHCLT (17b), CLT (15) (1 mg) was dissolved in methanol/H₂O (1 mL, 9:1, v/v) and NaBH₄ was added (Figure 9). The reaction mixture was stirred for 60 min at ambient temperature. After reducing methanol by evaporation, the aqueous phase was diluted with water (1 mL) and extracted with diethyl ether (2 X 2 mL). In analogy to the synthesis of compounds 17a and 17b, 1 mg of CLMT (16) was used as starting material instead of CLT (15), resulting in the formation of the two isomeric 3 α -DHCLMT (18a) and 3 β -DHCLMT (18b).

3.2.2 Isolated Recombinant Enzyme Incubations

The enzyme incubation assay started with the preparation of a reaction mixture consisting of 172 μ L of 0.1 M phosphate buffer (PBS, pH 7.4), 12.5 μ L of NADPH regenerating system solution A, 2.5 μ L of solution B, and 3 μ L of substrate solution (MD, 17 β -hydroxy-17 α -methyl-5 α -androst-1-ene-3-one (5 α -DHMD), or 17 β -hydroxy-17 α -methyl-5 β -androst-1-ene-3-one (5 β -DHMD) (1 mg/mL in methanol)). MD was incubated with AKR1D1 or AKR1C2, while 5 α -DHMD or 5 β -DHMD were incubated with AKR1C2, AKR1C3, or AKR1C4, respectively. After 5 minutes of preincubation at 37 $^{\circ}$ C, the reaction was initiated by adding the corresponding enzyme (AKR1C2, AKR1C3, AKR1C4, or AKR1D1) containing 5 μ g of protein. After incubating for 24 hours at 37 $^{\circ}$ C, the reaction was stopped by adding 200 μ L cold acetonitrile. A control sample (negative) without any enzyme was prepared for every compound, where the volume of the enzymes

was substituted by PBS 0.1 M. An internal standard (MT, 1 μ L, 1 mg/mL in methanol) was added prior to the extraction step.

After adding 1 mL of PBS (0.1 M), the extraction of the samples was performed with 2 mL of TBME. After evaporation of the organic phase, the residue was either derivatized with TMIS reagent (MSTFA/NH₄I/ethanethiol, 1000:2:3, v/w/v) by heating for 20 min at 75 °C and injected into the gas chromatography coupled by electron ionization to single quadrupole-mass spectrometry (GC-EI-MS) (details in chapter 3.2.5).

3.2.3 *In vitro* Incubations in Human Skin Cells

Human dermal fibroblasts and human keratinocytes were isolated from the foreskin (from the medically indicated circumcision of boys younger than 10 years). Cells were provided by Prof. Dr. Burkhard Kleuser's group (Dept. of Biology, Chemistry, and Pharmacy, Freie Universität Berlin, Berlin, Germany). Considering the potential variability in metabolic capabilities among different donors, human fibroblasts or keratinocytes used in this study were from three donors, respectively. Keratinocytes were cultivated in epilife medium supplemented with 1% (v/v) concentrated (100x) growth supplement (HKGS). Fibroblasts were cultivated in DMEM supplemented with 1% (v/v) L-glutamine, 1% (v/v) penicillin/streptomycin, and 7.5% (v/v) FBS. Cells (passage 2) from three different donors were grown under standard conditions (5% CO₂, 37°C) [123].

Cells were grown to confluence in the presence of 2 mL growth medium in 6-well plates and were incubated with T, MD, MT, CLT, DHCMT, or CLMT (1 μ M) for 24 h. Incubations without substrates or cells were prepared as negative controls. Media were collected and extracted by liquid-liquid extraction with 4 mL TBME twice after the addition of internal standard 1 μ L (testosterone-16, 16, 17-d₃ (T-d₃), 1 mg/mL). After centrifugation, the organic layers were combined, transferred to fresh tubes and evaporated to dryness. The combined extracts were derivatized with TMIS reagent (MSTFA/NH₄I/ethanethiol, 1000:2:3, v/w/v) by heating for 20 min at 75°C and measured by GC-EI-MS and gas chromatography coupled by electron ionization to quadrupole time-of-flight mass spectrometry (GC-EI-QTOF-MS) (details in chapter 3.2.6). The metabolites were identified by comparison of retention time (RT) and mass spectra with those of reference materials.

3.2.4 *In vivo* Incubations in Fish Embryo Model

Two independent experiments were performed with fish embryos. First, a pilot experiment was conducted to assess the correlation of metabolite production with incubation time, substrate concentration, and the sexes of embryos. To test for sex-specific effects, in addition to the embryos of mixed sexes (strain d-rR.YHNI, [133]), embryos of FLFII were used due to the fact that their genotypic sex can be identified by the presence of leucophores in male embryos after 3 days of development [141]. In this experiment, medaka embryos were exposed from the morula stage onwards for 10 days with either 10 μ M or 50 μ M MD or with 0.1% DMSO (solvent control). Subsequently, medaka embryos were incubated with 10 μ M MD for 48 h from 6 to 8 days post fertilization (dpf) due to the results obtained from the pilot experiment. The second experiment involved the incubation of medaka embryos with 10 μ M or 20 μ M [13 C₃]-T and MT for 48 h from 5 to 7 dpf. Incubations without substrates were prepared as negative controls. Moreover, to test the effect of bacteria present in the incubation system on the metabolism, medaka embryos were then exposed under sterile conditions to MT through autoclavation of the embryo-rearing medium and/or sterilization of the chorion. The embryo incubations for two independent experiments were done in Technische Universität Dresden by Leonie Hobohm and Johannes Bergleiter under the supervision of Alexander Froschauer.

For the extraction of media samples, to 1 mL of supernatant, 1 mL of phosphate buffer (pH 6.5), 50 μ L of β -glucuronidase and the internal standard (ISTD, MD incubation: 100 μ L of T-[d₃] glucuronide (10 μ g/mL); [13 C₃]-T and MT incubation, 50 μ L of T-[d₃] glucuronide (10 μ g/mL) and/or dehydroepiandrosterone-2,2,3,4,4,6-d₆ (DHEA-d₆), 10 μ g/mL) was added, the mixture was incubated for 1 h at 55 °C. After hydrolysis, 60-70 mg of solid buffer carbonate/bicarbonate was added, and liquid-liquid extraction was carried out twice with 3 mL of TBME. After centrifugation, the organic layer was combined and transferred into a clean container. After evaporation, the residue was either derivatized with TMIS reagent (MSTFA/NH₄I/ethanethiol, 1000:2:3, v/w/v) by heating for 20 min at 75 °C and injected into the GC-EI-MS (details in chapter 3.2.5), GC-QTOF-EI-MS (details in chapter 3.2.6), or reconstituted in methanol for LC-QTOF-ESI-MS/MS (details in chapter 3.2.7) analysis.

3.2.5 GC-EI-MS Analysis

The GC-EI-MS analysis of the samples was performed on an Agilent 7890A gas chromatographic system coupled to an Agilent 5975 C inert mass selective detector with the following parameters for the analysis of the intermediates and products: Agilent HP1 (17 m, 0.2 mm id, 0.11 μm), carrier gas: helium at 1 mL/min, constant flow, oven program: 183 $^{\circ}\text{C}$, +3 $^{\circ}\text{C}/\text{min}$ to 232 $^{\circ}\text{C}$, +40 $^{\circ}\text{C}/\text{min}$ to 310 $^{\circ}\text{C}$, hold for 2 min, injection volume: 2 μL , split 10:1, injection temperature: 300 $^{\circ}\text{C}$, electron ionization (EI): 70 eV, full scan mode from 40 to 750 Da.

3.2.6 GC-EI-QTOF-MS Analysis

High-resolution accurate mass analyses were performed by a gas chromatographic system coupled to a time-of-flight mass spectrometry (GC-QTOF-MS) 7890B/7250 (Agilent Technologies, Milano, Italy), equipped with an Agilent HP1 column (17 m, 0.20 mm; 0.11 μm) with helium as carrier gas (1 mL/min, constant flow). The injection was performed in split mode with a 1:10 ratio at 280 $^{\circ}\text{C}$ applying an injection volume of 2 μL . The oven temperature was programmed as 0 min 150 $^{\circ}\text{C}$, ramped with + 50 $^{\circ}\text{C}/\text{min}$ to 240 $^{\circ}\text{C}$ (0 min), + 3 $^{\circ}\text{C}/\text{min}$ to 266 $^{\circ}\text{C}$ (0 min), further + 50 $^{\circ}\text{C}/\text{min}$ to 320 $^{\circ}\text{C}$ (3 min hold). Electron ionization (EI) was performed at 70 eV with data acquisition in full scan mode (m/z 50 to 750).

3.2.7 LC-ESI-QTOF-MS Analysis

Untargeted high-resolution accurate mass analysis for the investigation of potential MD metabolites was performed on an Agilent 6550i QToF (Agilent Technologies, Santa Clara, USA) coupled to a 1290 Infinity II HPLC system (Agilent Technologies, Waldbronn, Germany). The system was equipped with an Agilent ZORBAX Eclipse Plus Phenyl-Hexyl column (3.0 \times 100 mm; 1.8 μm particle size). Column temperature was controlled and held at 30 $^{\circ}\text{C}$. Water (eluent A, $\text{H}_2\text{O}:\text{FoOH}$, 99.9:0.1, v/v) and acetonitrile (eluent B, ACN: FoOH 99.9:0.1, v/v) were used as eluents. The gradient program started with 2% eluent B increasing linear to 55% in 3 min, then to 95% in 3.5 min, 1.5 min hold and 0.2 min back to 2%. The flow rate of 0.550 mL/min resulted in a run time of 8.20 min and 1.30 min for the column equilibration. Aliquots of 1.0 μL were injected into the system.

The mass spectrometer was operated in auto MS/MS mode using positive ionization (ESI⁺). Mass range for MS spectra was between m/z 100 and m/z 1000 (2 spectra/ sec),

MS² spectra were collected between m/z 50 and m/z 1000 (3 spectra/sec). Permanently performed mass axis calibration and a high resolution ($> 10,000$) achieved high mass accuracy. Drying gas flow was set to 11 mL/min at 200 °C, sheath gas flow to 11 mL/min at 375 °C, nebulizer pressure to 35 psi (N₂), capillary voltage to 3500 V, and the nozzle voltage to 500 V.

3.2.8 HPLC Purification

The purification of the synthesized reference steroids was performed by semipreparative HPLC using an Agilent 1260 Infinity Quaternary HPLC system coupled to an Agilent Infinity 1260 diode array detector (Agilent Technologies GmbH, Waldbronn, Germany). Chromatographic separation was achieved on a Hypersil ODS C18 column (pore size: 120 Å, 250 mm length, 10 mm ID, 5 µm particle size, Thermo Scientific, Schwerte, Germany).

3 α ,4 α -Epoxy-5 α -androstan-17-one (5a) and 3 α ,4 α -Epoxy-17 α -methyl-5 α -androstan-17-one (6a)

Isocratic elution was accomplished at a flow rate of 3 mL/min using acetonitrile:water (7:3, v/v) as mobile phase. The injection volume was 0.5 mL, with a sample concentration of 10 mg/mL for a mixture of compounds **5a** and **5b**, and 9 mg/mL for a mixture of compounds **6a** and **6b**. The UV signal was monitored at 194 nm. Individual fractions containing **5a** were collected between 11.54-12.55 min, whereas fractions containing **6a** were collected between 13.64-14.69 min. The corresponding fractions of each compound were combined before evaporation.

4 α -Chloro-5 α -androstan-3 ξ ,17 β -diols (13a, 13b)

An isocratic run with solvent composition acetonitrile:water (50:50, v/v) was performed. The flow rate was 3.7 mL/min. The column temperature was set to 35 °C, and the injection volume was 0.3 mL, with a sample concentration of 500 µg/mL for product containing compound **13a**, or 2.5 mg/mL for substance containing **13b** (after pre-purification by column chromatography, details in chapter 3.2.1). The selected wavelength for UV detection was 194 nm. Individual fractions of **13a** or **13b** were collected between 16.85-18.00 min or between 15.00-16.40 min, respectively. The corresponding fractions of each compound were combined before evaporation.

4 α -Chloro-17 α -methyl-5 α -androsterane-3 ξ ,17 β -diols (14a, 14b)

The separation was performed with solvent composition water (A) and acetonitrile (B) at a flow rate of 3.7 mL/min. The following gradient pattern was used: 53% B (0 min), 89% B (24 min), 95% B (25 min), and 95% B (30 min). The injection volume was 0.5 mL, with a sample concentration of 5 mg/mL for a mixture containing **14a** and **14b** (after pre-purification by column chromatography, details in chapter 3.2.1). The UV signal was monitored at 194 nm. Individual fractions of **14a** or **14b** were collected between 12.51-13.35 min or between 11.67-12.40 min, respectively. The corresponding fractions of each compound were combined before evaporation.

3.2.9 Nuclear Magnetic Resonance

The nuclear magnetic resonance (NMR) experiments were performed on a Bruker BioSpin (Karlsruhe, Germany) Avance NEO 500 MHz spectrometer equipped with a nitrogen-cooled (prodigy BBFO) 5 mm probe or on an Avance III 600 MHz spectrometer equipped with a triple resonance QCI 5 mm cryogenic probe. 2D experiments were recorded applying non-uniform sampling (NUS) in case of COSY, edited HSQC, NOESY, and HMBC spectra. Chemical shifts are reported in δ values (ppm) relative to tetramethylsilane. Analytes were dissolved in deuterated chloroform (CDCl₃). The NMR analysis was performed by Dr. Nils Schlörer (Friedrich Schiller University Jena).

4 Results and Discussion

4.1 Synthesis of Reference Materials

4.1.1 Synthesis of 3 α /3 β ,4 α ,5 α -THCLT (13a, 13b) and 3 α /3 β ,4 α ,5 α -THCLMT (14a, 14b)

The two pairs of 4 α ,5 α -diastereomers (13a, 13b, and 14a, 14b) with fully reduced A-ring derived from CLT or CLMT were synthesized using analogous six-step reactions as described in chapter 3.2.1. According to Kratena *et al.* [139], the 3 α ,4 β ,5 α -derivatives were obtained as the main products by opening of 5 α -epoxides with hydrochloric acid. The subsequent oxidation of the 3 α -hydroxy group and the epimerization of position 4 were achieved using DMP and potassium hydroxide, respectively, to give the 4 α -chloro-5 α -androstane-3-one intermediates (11, 12) [139]. The following reduction of the 3-oxo group with NaBH₄ mainly results in the 3 β -isomers, while the 17-oxo group almost exclusively yields the 17 β -hydroxy isomer, which is in line with literature reports [118, 142]. The retention times of the per-TMS derivatives of the two pairs of 4 α ,5 α -diastereomers are given in **Table 4**. After purification, further structure confirmation was achieved by 1D and 2D-NMR analysis. Assignments are provided in **Table 5**.

Table 4: Retention times, molecular ions (M^+) at 70 eV, and mass difference to exact mass of synthesized reference compounds 13a, 13b, 14a, 14b, 17a, 17b, 18a, and 18b as per-TMS derivatives (GC-EI-QTOF-MS). This table is adapted from my published paper [140]

No.	Assignment	RT [min]	Exact mass [m/z]	Accurate mass [m/z]	$\Delta m/z$ [ppm]
13a	4 α -Chloro-5 α -androstane-3 α ,17 β -diol	5.03	470.2798	470.2777	-4.47
13b	4 α -Chloro-5 α -androstane-3 β ,17 β -diol	5.67	470.2798	470.2799	0.21
14a	4 α -Chloro-17 α -methyl-5 α -androstane-3 α ,17 β -diol	5.60	484.2954	484.2941	-2.68
14b	4 α -Chloro-17 α -methyl-5 α -androstane-3 β ,17 β -diol	6.47	484.2954	484.2947	-1.45
17a	4-Chloroandrost-4-ene-3 α ,17 β -diol	4.62	468.2641	468.2636	-1.07
17b	4-Chloroandrost-4-ene-3 β ,17 β -diol	5.20	468.2641	468.2612	-6.19
18a	4-Chloro-17 α -methylandrost-4-ene-3 α ,17 β -diol	5.16	482.2798	482.2769	-6.01
18b	4-Chloro-17 α -methylandrost-4-ene-3 β ,17 β -diol	5.88	482.2798	482.2761	-7.67

Table 5: ^1H and ^{13}C NMR chemical shifts of $3\alpha,4\alpha,5\alpha$ -THCLT (**13a**), $3\beta,4\alpha,5\alpha$ -THCLT (**13b**), $3\alpha,4\alpha,5\alpha$ -THCLMT (**14a**), and $3\beta,4\alpha,5\alpha$ -THCLMT (**14b**) in CDCl_3 , δ in ppm. This table is adapted from my published paper [140]

	$3\alpha,4\alpha,5\alpha$ -THCLT (13a)		$3\beta,4\alpha,5\alpha$ -THCLT (13b)		$3\alpha,4\alpha,5\alpha$ -THCLMT (14a)		$3\beta,4\alpha,5\alpha$ -THCLMT (14b)	
	δC	δH	δC	δH	δC	δH	δC	δH
1	31.34	$\alpha+\beta$: 1.39	35.80	α : 1.03	31.35	$\alpha+\beta$: 1.39	35.81	α : 1.03
		--		β : 1.70		--		β : 1.71
2	27.48	α : 1.86	28.65	α : 1.91	27.51	α : 1.86	28.65	α : 1.91
		β : 1.66		β : 1.50		β : 1.66		β : 1.50
3	69.94	β : 3.94	76.35	α : 3.46	69.94	β : 3.94	76.35	α : 3.46
4	69.91	β : 4.02	72.21	β : 3.70	69.91	β : 4.02	72.22	β : 3.70
5	46.14	α : 1.67	51.65	α : 1.20	46.16	α : 1.68	51.67	α : 1.21
6	24.45	α : 1.86	24.59	α : 1.98	24.50	α : 1.86	24.66	α : 1.99
		β : 1.08		β : 1.10		β : 1.08		β : 1.11
7	31.07	α : 0.79	31.08	α : 0.77	31.24	α : 0.80	31.25	α : 0.77
		β : 1.67		β : 1.69		β : 1.68		β : 1.71
8	35.20	β : 1.32	35.02	β : 1.31	36.05	β : 1.36	35.84	β : 1.35
9	54.33	α : 0.73	54.47	α : 0.63	54.25	α : 0.72	54.36	α : 0.61
10	39.32	--	38.83	--	39.33	--	38.85	--
11	20.48	α : 1.51	20.73	α : 1.49	20.54	α : 1.52	20.78	α : 1.51
		β : 1.18		β : 1.22		β : 1.19		β : 1.22
12	36.65	α : 0.98	36.65	α : 0.98	31.62	α : 1.19	31.62	α : 1.19
		β : 1.72		β : 1.73		β : 1.41		β : 1.42
13	42.88	--	42.96	--	45.43	--	45.50	--
14	50.97	α : 0.87	50.90	α : 0.86	50.63	α : 1.10	50.57	α : 1.08
15	23.32	α : 1.52	23.35	α : 1.52	23.20	α : 1.50	23.22	α : 1.50
		β : 1.18		β : 1.19		β : 1.17		β : 1.19
16	30.56	α : 1.99	30.57	α : 1.99	39.01	α : 1.66	39.02	α : 1.66
		β : 1.35		β : 1.36		β : 1.72		β : 1.73
17	81.89	α : 3.56	81.87	α : 3.56	81.69	--	81.66	--
18	11.17	0.66	11.17	0.66	14.01	0.78	14.01	0.78
19	12.46	0.78	13.21	0.79	12.46	0.80	13.21	0.80
20	--	--	--	--	25.88	1.14	25.83	1.14

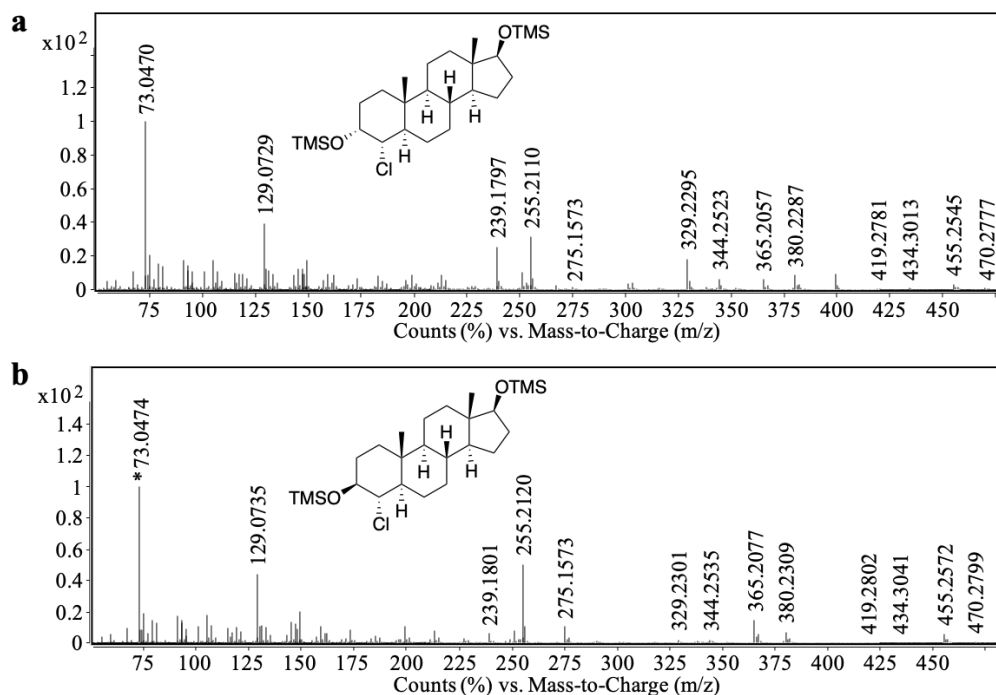


Figure 10: Normalized EI mass spectra (GC-QTOF-MS) of TMS derivatives of (a) $3\alpha,4\alpha,5\alpha$ -THCLT (**13a**, $[M]^{++}=470.2777$, mass error -4.47 ppm, RT 5.03 min), (b) $3\beta,4\alpha,5\alpha$ -THCLT (**13b**, $[M]^{++}=470.2799$, mass error 0.21 ppm, RT 5.67 min) at 70 eV. This figure is adapted from my published paper [140]

As expected, all diastereomers revealed very similar mass spectra. In the mass spectra of TMS-derivatized $3\alpha,4\alpha,5\alpha$ -THCLT (**13a**) and $3\beta,4\alpha,5\alpha$ -THCLT (**13b**) (**Figure 10**), the molecular ion m/z 470 shows a very low abundance. **Table 6** and **Table 7** show all fragments and their corresponding mass errors for compounds **13a** and **13b**, respectively, which are discussed in this section. Both spectra display ions at m/z 455, m/z 380, m/z 365, and m/z 275, corresponding to the fragments caused by losses of methyl group and/or TMSOH from the molecule. All these fragments show the typical isotopic signature of Cl-containing ions. The elimination of hydrochloric acid and TMSOH from the molecule leads to m/z 434 and m/z 344, respectively, with no Cl-isotopic pattern. Combined with the additional losses of methyl group and/or TMSOH, the fragments m/z 419, m/z 329, and m/z 239 were produced, which are less abundant in compound **13b** compared to **13a**. The abundant fragment at m/z 255 is proposed to result from the cleavage of a TMSO radical in addition to the losses of hydrochloric acid and TMSOH. The ion at m/z 129 corresponds to the typical D-ring fragment with a 17-hydroxy group [143].

Table 6: Postulated fragments, exact masses, accurate masses, mass errors ($\Delta m/z$) for 3 α ,4 α ,5 α -THCLT (**13a**) (GC-EI-QTOF-MS). This table is adapted from my published paper [140]

Postulated fragment	Exact mass [m/z]	Accurate mass [m/z]	$\Delta m/z$ [ppm]
[M] ⁺	470.2798	470.2777	-4.47
[M-CH ₃] ⁺	455.2563	455.2545	-3.95
[M-HCl] ⁺	434.3031	434.3013	-4.14
[M-CH ₃ -HCl] ⁺	419.2796	419.2781	-3.58
[M-HCl-TMSOH] ⁺	344.2530	344.2523	-2.03
[M-HCl-TMSOH-CH ₃] ⁺	329.2295	329.2295	0.00
[M-HCl-TMSOH-TMSO] ⁺	255.2107	255.2110	1.18
[M-TMSOH] ⁺	380.2297	380.2287	-2.63
[M-CH ₃ -TMSOH] ⁺	365.2062	365.2057	-1.37
[M-CH ₃ -2xTMSOH] ⁺	275.1561	275.1573	4.36
[M-HCl-2xTMSOH-CH ₃] ⁺	239.1794	239.1797	1.25
[C ₆ H ₁₃ OSi] ⁺	129.0730	129.0729	-0.77
[TMS] ⁺	73.0468	73.0470	2.74

Table 7: Postulated fragments, exact masses, accurate masses, mass errors ($\Delta m/z$) for 3 β ,4 α ,5 α -THCLT (**13b**) (GC-EI-QTOF-MS). This table is adapted from my published paper [140]

Postulated fragment	Exact mass [m/z]	Accurate mass [m/z]	$\Delta m/z$ [ppm]
[M] ⁺	470.2798	470.2799	0.21
[M-CH ₃] ⁺	455.2563	455.2572	1.98
[M-HCl] ⁺	434.3031	434.3041	2.30
[M-CH ₃ -HCl] ⁺	419.2796	419.2802	1.43
[M-HCl-TMSOH] ⁺	344.2530	344.2535	1.45
[M-HCl-TMSOH-CH ₃] ⁺	329.2295	329.2301	1.82
[M-HCl-TMSOH-TMSO] ⁺	255.2107	255.2120	5.09
[M-TMSOH] ⁺	380.2297	380.2309	3.16
[M-CH ₃ -TMSOH] ⁺	365.2062	365.2077	4.11
[M-CH ₃ -2xTMSOH] ⁺	275.1561	275.1573	4.36
[M-HCl-2xTMSOH-CH ₃] ⁺	239.1794	239.1801	2.93
[C ₆ H ₁₃ OSi] ⁺	129.0730	129.0735	3.87
[TMS] ⁺	73.0468	73.0474	8.21

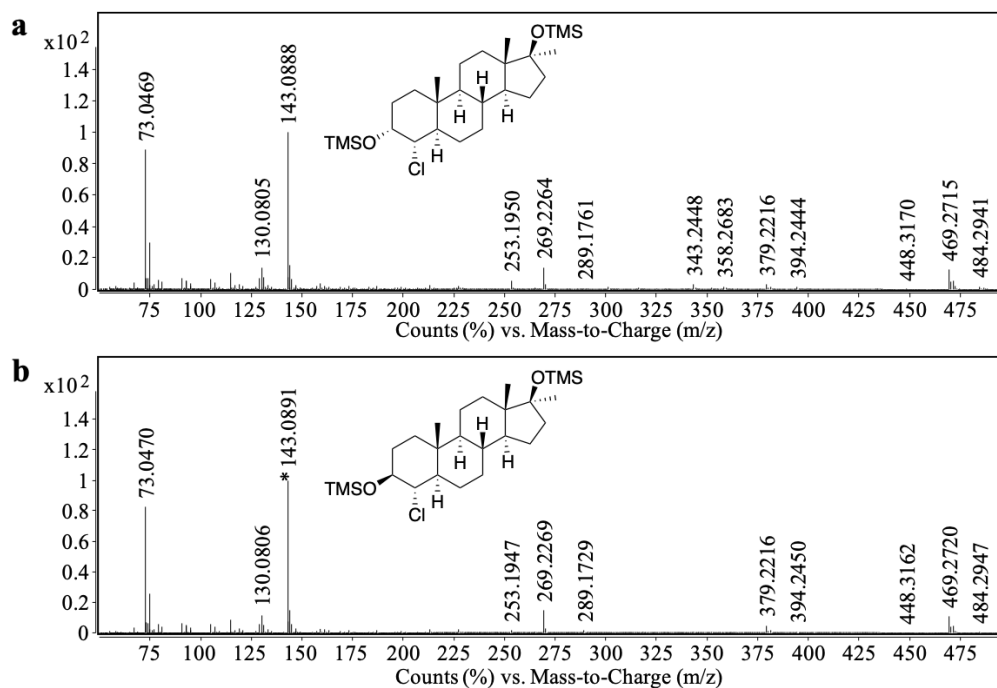


Figure 11: Normalized EI mass spectra (GC-QTOF-MS) of TMS derivatives of (a) 3 α ,4 α ,5 α -THCLMT (**14a**, $[M]^{+} = 484.2941$, mass error -2.68 ppm, RT 5.60 min), (b) 3 β ,4 α ,5 α -THCLMT (**14b**, $[M]^{+} = 484.2947$, mass error -1.45 ppm, RT 6.47 min) at 70 eV. This figure is adapted from my published paper [140]

Analogously, in the mass spectra of 4 α -chloro-17 α -methyl-5 α -androstane-3 ξ ,17 β -diols (**14a**, **14b**), a very low abundant molecular ion (m/z 484) was observed. The mass spectra of compounds **14a** and **14b** are displayed in **Figure 11**. **Table 8** and **Table 9** show all fragments and their corresponding mass errors for compounds **14a** and **14b**, respectively, which are discussed in this section. The base peak m/z 143, achieved as a D-ring fragment, is the indicator of the presence of a 17-methyl group in trimethylsilylated 17-hydroxysteroids [144]. In comparison to the mass spectra of compounds **13a** and **13b**, most of the fragments are incremented by 14 Da due to the additional methyl group in position 17 in compounds **14a** and **14b**. The losses of methyl group and TMSOH from the molecular ion lead to m/z 469 and m/z 379. The fragment m/z 394 is generated by the loss of TMSOH from the molecule. The very low abundant ions m/z 448 and m/z 358, are suggested to originate from the cleavage of hydrochloric acid and TMSOH from the molecular ion. The additional elimination of a methyl group and TMSOH yields m/z 343 and m/z 253. Similar to the fragment m/z 255 in compounds **13a** and **13b**, the corresponding fragment in compounds **14a** and **14b** incremented by 14 Da due to the presence of the 17 α -methyl group, yielding the abundant ion at m/z 269.

Table 8: Postulated fragments, exact masses, accurate masses, mass errors ($\Delta m/z$) for 3 α ,4 α ,5 α -THCLMT (**14a**) (GC-EI-QTOF-MS). This table is adapted from my published paper [140]

Postulated fragment	Exact mass [m/z]	Accurate mass [m/z]	$\Delta m/z$ [ppm]
[M] ⁺⁺	484.2954	484.2941	-2.68
[M-CH ₃] ⁺	469.2719	469.2715	-0.85
[M-HCl] ⁺⁺	448.3187	448.3170	-3.79
[M-HCl-TMSOH] ⁺⁺	358.2686	358.2683	-0.84
[M-HCl-TMSOH-CH ₃] ⁺	343.2452	343.2448	-1.17
[M-HCl-TMSOH-TMSO] ⁺	269.2264	269.2264	0.00
[M-TMSOH] ⁺⁺	394.2453	394.2444	-2.28
[M-CH ₃ -TMSOH] ⁺	379.2218	379.2216	-0.53
[M-HCl-TMSOH-CH ₃] ⁺	253.1951	253.1950	-0.39
[C ₇ H ₁₅ OSi] ⁺	143.0887	143.0888	0.70
[TMS] ⁺	73.0468	73.0469	1.37

Table 9: Postulated fragments, exact masses, accurate masses, mass errors ($\Delta m/z$) for 3 β ,4 α ,5 α -THCLMT (**14b**) (GC-EI-QTOF-MS). This table is adapted from my published paper [140]

Postulated fragment	Exact mass [m/z]	Accurate mass [m/z]	$\Delta m/z$ [ppm]
[M] ⁺	484.2954	484.2947	-1.45
[M-CH ₃] ⁺	469.2719	469.2720	0.21
[M-HCl] ⁺⁺	448.3187	448.3162	-5.58
[M-HCl-TMSOH] ⁺⁺	358.2686	358.2681	-1.40
[M-HCl-TMSOH-CH ₃] ⁺	343.2452	343.2448	-1.17
[M-HCl-TMSOH-TMSO] ⁺	269.2264	269.2269	1.86
[M-TMSOH] ⁺⁺	394.2453	394.2450	-0.76
[M-CH ₃ -TMSOH] ⁺	379.2218	379.2216	-0.53
[M-HCl-2xTMSOH-CH ₃] ⁺	253.1951	253.1947	-1.58
[C ₇ H ₁₅ OSi] ⁺	143.0887	143.0891	2.80
[TMS] ⁺	73.0468	73.0470	2.74

NMR data confirmed the structure assignments. NOE correlation of CH₃-19 with H-4 suggests that H-4 and CH₃-19 were cofacial and β -oriented, whereas the cross signal of H-5 and H-9 α in NOESY spectra confirms that H-5 and H-9 α were cofacially α -oriented [145]. The stereochemistry at C3 in compounds **13a** and **14a** was deduced from the multiplicity of H-3 (**13a**: δ H3 = 3.94 ppm, q, J = 2.9 Hz; **14a**: δ H3 = 3.94 ppm, q, J = 2.9 Hz) representing coupling constants of H-3_{eq} with H-2_{eq}, H-2_{ax}, and H-4_{ax}. This substantiated the orientation of H-3 β and established the 3 α -hydroxy configuration. In contrast, the multiplicity of H-3 in **13b** and **14b** (**13b**: δ H3 = 3.46 ppm, ddd, J =

11.6/9.3/5.3 Hz; **14b**: $\delta_{\text{H}3} = 3.46$ ppm, ddd, $J = 11.5/9.3/5.3$ Hz) showed the axial-axial coupling with H-4ax and H-2ax and the axial-equatorial coupling with H-2eq [146]. This indicates the axial orientation of H-3 α , thus confirming the 3 β -hydroxy configuration. This assignment is also confirmed by NOE correlation of H-3 α with H-1 α and H-5 α .

4.1.2 Synthesis of 3 α /3 β -DHCLT (**17a**, **17b**) and 3 α /3 β -DHCLMT (**18a**, **18b**)

The reduction of the 3-oxo-group starting from CLT or CLMT yielded corresponding diastereomers of 3-hydroxy analogs (**17a**, **17b**, **18a**, **18b**) as previously described [118]. The proposed stereochemistry of the structures was assigned according to the known stereoselectivity of the reductions with the 3 β -isomers as the major products (**17a**:**17b**, 3 α -OH:3 β -OH, 7:93; **18a**:**18b**, 3 α -OH:3 β -OH, 8:92). The assignment is also supported by the elution order; TMS derivatives of 3 β -hydroxyandrost-4-enes elute later than their 3 α analogs [142]. The retention times of the TMS derivatives of the four compounds are given in **Table 4**.

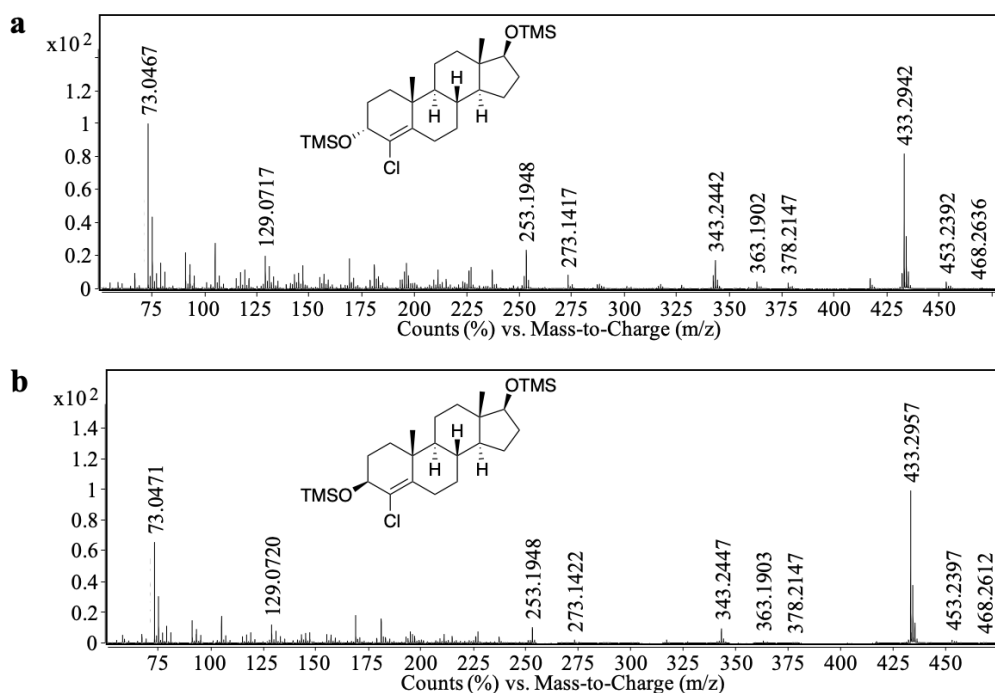


Figure 12: Normalized EI mass spectra (GC-QTOF-MS) of TMS derivatives of (a) 3 α -DHCLT (**17a**, $[M]^{+} = 468.2636$, mass error -1.07 ppm, RT 4.62 min), (b) 3 β -DHCLT (**17b**, $[M]^{+} = 468.2612$, mass error -6.19 ppm, RT 5.20 min) at 70 eV. This figure is adapted from my published paper [140]

The molecular ion of TMS-derivatized compounds **17a** and **17b** is m/z 468 (mass spectra in **Figure 12**). However, it shows a very low abundance at 70 eV. **Table 10** and **Table 20** (Annex) show all fragments and their corresponding mass errors for compounds

17a and **17b**, respectively, which are discussed in this section. The dominant fragment m/z 433 is proposed to result from the elimination of a chlorine radical [147]. With the additional losses of the TMSOH group, the ions m/z 343 and m/z 253 were generated. The elimination of methyl group and/or TMSOH group from the molecular ion resulted in the formation of the fragment ions m/z 453, m/z 378, m/z 363, m/z 273, which is substantiated by the Cl-isotopic signature.

Table 10: Postulated fragments, exact masses, accurate masses, mass errors ($\Delta m/z$) for 3 α -DHCLT (**17a**) (GC-EI-QTOF-MS). This table is adapted from my published paper [140]

Postulated fragment	Exact mass [m/z]	Accurate mass [m/z]	$\Delta m/z$ [ppm]
[M] ⁺⁺	468.2641	468.2636	-1.07
[M-CH ₃] ⁺	453.2406	453.2392	-3.09
[M-Cl] ⁺	433.2953	433.2942	-2.54
[M-Cl-TMSOH] ⁺	343.2452	343.2442	-2.91
[M-Cl-2xTMSOH] ⁺	253.1951	253.1948	-1.18
[M-TMSOH] ⁺⁺	378.2140	378.2147	1.85
[M-CH ₃ -TMSOH] ⁺	363.1905	363.1902	-0.83
[M-CH ₃ -2xTMSOH] ⁺	273.1405	273.1417	4.39
[C ₆ H ₁₃ OSi] ⁺	129.0730	129.0717	-10.07
[TMS] ⁺	73.0468	73.0467	-1.37

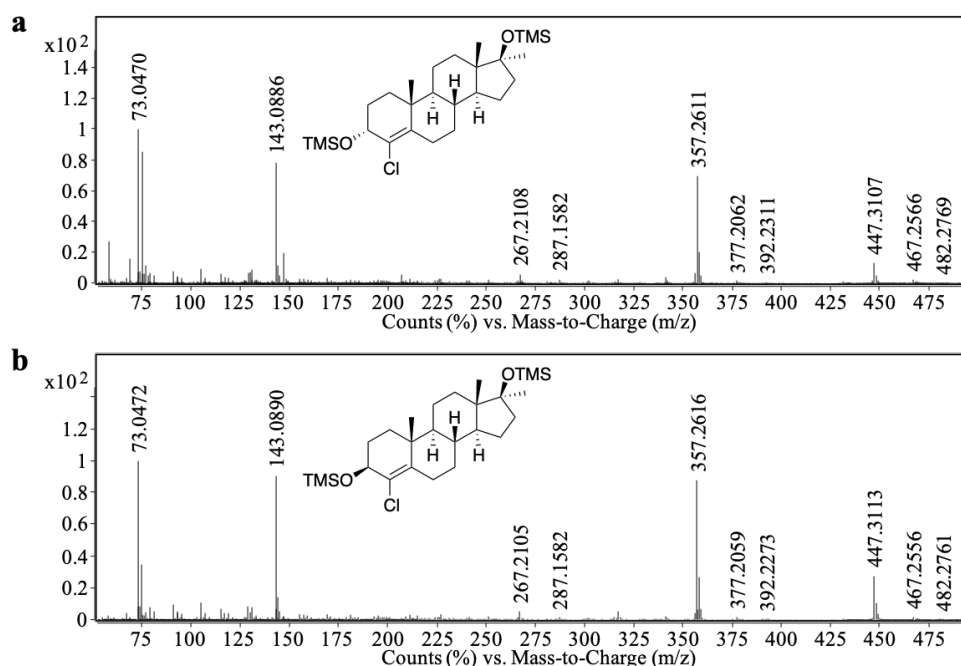


Figure 13: Normalized EI mass spectra (GC-QTOF-MS) of TMS derivatives of (a) 3 α -DHCLMT (**18a**, $[M]^{*+}=482.2769$, mass error -6.01 ppm, RT 5.16 min), and (b) 3 β -DHCLMT (**18b**, $[M]^{*+}=482.2761$, mass error -7.67 ppm, RT 5.88 min) at 70 eV. This figure is adapted from my published paper [140]

Similarly, pertrimethylsilylated compounds **18a** and **18b** also show an extremely low abundant molecular ion m/z 482 (mass spectra in **Figure 13**). **Table 11** and **Table 21** (Annex) show all fragments and their corresponding mass errors for compounds **18a** and **18b**, respectively, which are discussed in this section. The most abundant and typical fragments are m/z 447 and m/z 357, indicating the elimination of the chlorine radical and the cleavage of TMSOH, respectively. The ion at m/z 267 represents an additional loss of TMSOH. The fragments at m/z 467, m/z 392, m/z 377, and m/z 287 result from the losses of methyl group and/or TMSOH from the molecule. The ion at m/z 143 is a typical D-ring fragment for 17-hydroxylated and 17-methylated compounds [147].

Table 11: Postulated fragments, exact masses, accurate masses, mass errors ($\Delta m/z$) for 3 α -DHCLMT (**18a**) (GC-EI-QTOF-MS). This table is adapted from my published paper [140]

Postulated fragment	Exact mass [m/z]	Accurate mass [m/z]	$\Delta m/z$ [ppm]
[M] ⁺⁺	482.2798	482.2769	-6.01
[M-CH ₃] ⁺	467.2563	467.2566	0.64
[M-Cl] ⁺	447.3109	447.3107	-0.45
[M-Cl-TMSOH] ⁺	357.2608	357.2611	0.84
[M-Cl-2xTMSOH] ⁺	267.2107	267.2108	0.37
[M-TMSOH] ⁺	392.2297	392.2311	3.57
[M-CH ₃ -TMSOH] ⁺	377.2062	377.2062	0.00
[M-CH ₃ -2xTMSOH] ⁺	287.1561	287.1582	7.31
[C ₇ H ₁₅ OSi] ⁺	143.0887	143.0886	-0.70
[TMS] ⁺	73.0468	73.0470	2.74

4.2 Isolated Recombinant Enzyme Incubations

In vitro studies with isolated enzymes AKR1C2-AKR1C4 and AKR1D1 were performed to investigate the A-ring metabolism of MD as described in chapter 3.2.1. The metabolites obtained from the incubation were analyzed by GC-EI-MS and GC-EI-QTOF-MS after per-TMS derivatization (detailed method in chapter 3.2.5 and chapter 3.2.6, respectively).

The biotransformation of MD with AKR1D1 resulted in the formation of 5 β -DHMD, which was confirmed by comparison with reference material (mass spectra in **Figure 34** in Annex), whereas there are no metabolites of MD detected in the AKR1C2 incubations. The chromatogram of metabolite detected after AKR1D1 incubation with MD is shown in **Figure 14**. The postulated fragments and their corresponding mass errors for the

metabolite 5 β -DHMD are available in **Table 22** (Annex). To further investigate the metabolic mechanism of 3-oxo group reduction by AKR1Cs, the diastereomers 5 α -DHMD and 5 β -DHMD were incubated with AKR1C2, AKR1C3, and AKR1C4, respectively. Varying metabolic capacities were observed among different enzymes. The incubations of AKR1C2 and AKR1C4 showed similar metabolic profiles, in which two diastereomers resulting from the 3-oxo reduction for each substrate were detected. In contrast, biotransformation of 5 α -DHMD or 5 β -DHMD with AKR1C3 only produced one metabolite. For example, the chromatograms of metabolites detected after AKR1C4 incubation with 5 α -DHMD or 5 β -DHMD are displayed in **Figure 15**. The chromatograms of the sample extracts obtained from AKR1C2 or AKR1C3 incubations with 5 α -DHMD or 5 β -DHMD are available in **Figure 35** and **Figure 36** in Annex, respectively.

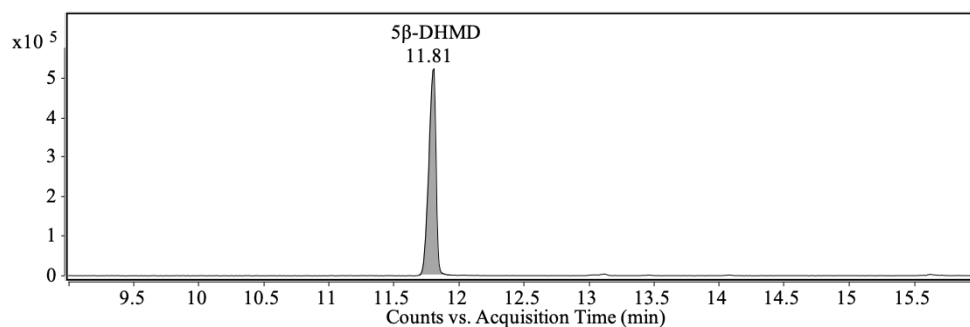


Figure 14: Extracted ion chromatogram (EIC) in GC-EI-MS (m/z 143) of a sample obtained after enzyme incubation of AKR1D1 with MD, showing 5 β -DHMD (RT 11.81 min) as per-TMS derivative

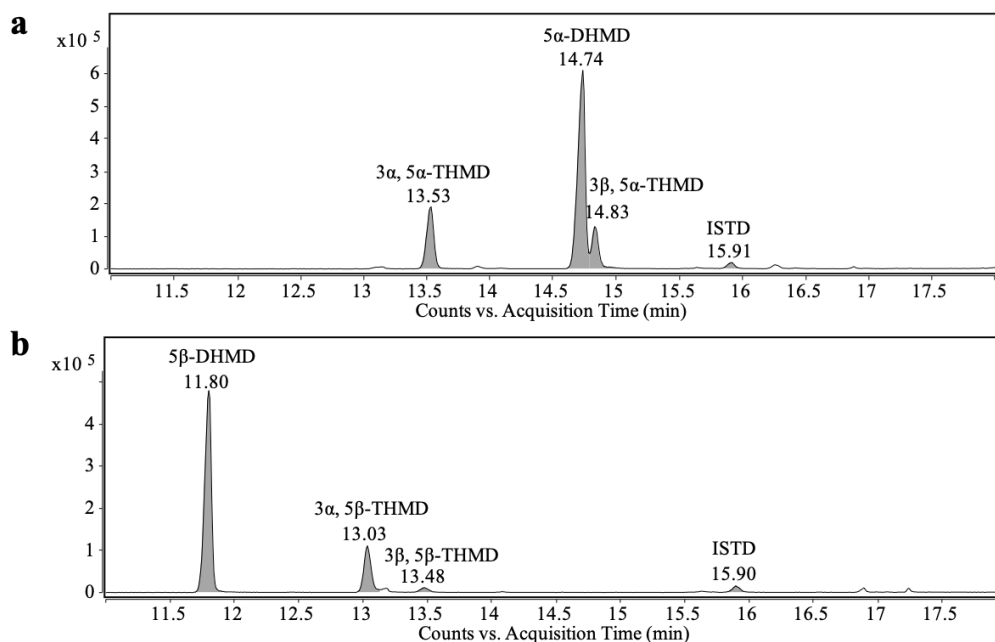


Figure 15: EICs in GC-EI-MS (m/z 143) of samples obtained after enzyme incubations of AKR14 with (a) 5 α -DHMD, showing tentatively assigned 3 α , 5 α -THMD (RT 13.53 min), 5 α -DHMD (RT 14.74 min), tentatively assigned 3 β , 5 α -THMD (RT 14.83 min), and MT (ISTD, RT 15.91 min) as per-TMS derivatives; (b) 5 β -DHMD, showing 5 β -DHMD, (RT 11.80 min), 3 α , 5 β -THMD (RT 13.03 min), tentatively assigned 3 β , 5 β -THMD (RT 13.48 min), and MT (ISTD, RT 15.90 min) as per-TMS derivatives

The metabolite detected in all 5 β -DHMD incubations, was identified as 17 α -methyl-5 β -androst-1-ene-3 α ,17 β -diol (3 α ,5 β -THMD) by the comparison of retention time and mass spectra with those of authentic material (**Figure 16** and **Figure 37** (Annex)). However, the standard references for the other isomers are not available. Due to the fact that the four metabolites exhibit highly similar mass spectra, the information obtained from fragmentation analysis based on mass spectra alone is not sufficient to infer the structures. Among the other three metabolites, 17 α -methyl-5 β -androst-1-ene-3 β ,17 β -diol (3 β ,5 β -THMD) was tentatively identified as the second metabolite resulting from 5 β -DHMD metabolism, in addition to the previously identified 3 α ,5 β -THMD. However, this metabolite was only detected in AKR1C2 and AKR1C4 incubations. To deduce the stereochemistry of the two metabolites in the 5 α -DHMD incubation, the elution order was compared with that of 5 α -androst-1-ene-3 α ,17 β -diol and 5 α -androst-1-ene-3 β ,17 β -diol reported in previous study [148]. It is assumed that they may have the same elution order due to their structural similarity. Therefore, it is proposed that 17 α -methyl-5 α -androst-1-ene-3 α ,17 β -diol (3 α ,5 α -THMD) elutes earlier than 17 α -methyl-5 α -androst-1-ene-3 β ,17 β -diol (3 β ,5 α -THMD). This assumption is supported by the fact that 3 α ,5 β -THMD and 3 β ,5 β -THMD elute in the same order as 5 β -androst-1-ene-3 α ,17 β -diol and 5 β -androst-1-ene-3 β ,17 β -diol. However, the structures still need further confirmation

with authentic reference materials. Similar to the two metabolites produced by 5 β -DHMD metabolism, the 3 α -isomer, i.e., 3 α ,5 α -THMD, was detected in all enzyme incubations with 5 α -DHMD, whereas 3 β ,5 α -THMD was only present in AKR1C2 and AKR1C4 incubations. The retention times of the per-TMS derivatives of the four diastereomers are displayed in **Table 23** (Annex).

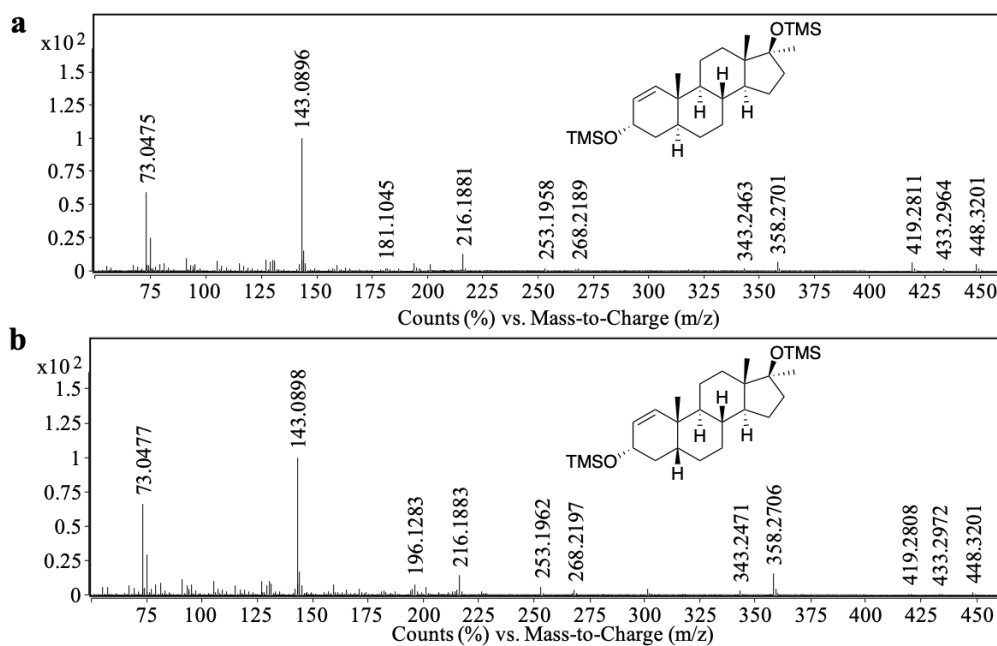


Figure 16: Normalized EI mass spectra (GC-QTOF-MS) of TMS derivatives of (a) tentatively assigned 3 α ,5 α -THMD ($[M]^{++}=448.3201$, mass error 3.12 ppm, RT 4.49 min) detected in the incubation of AKR1C4 with 5 α -DHMD, (b) 3 α ,5 β -THMD ($[M]^{++}=448.3201$, mass error 3.12 ppm, RT 4.32 min), formed by the incubation of AKR1C4 with 5 β -DHMD, at 70 eV

As mentioned above, the four diastereomers showed very similar mass spectra with only slight differences. For example, the mass spectra of 3 α ,5 α -THMD and 3 α ,5 β -THMD are displayed in **Figure 16**, while the mass spectra of 3 β ,5 α -THMD and 3 β ,5 β -THMD are available in **Figure 38** and **Figure 39** in Annex. **Table 12**, **Table 24** (Annex), **Table 13**, and **Table 25** (Annex) show all fragments and their corresponding mass errors for 3 α ,5 α -THMD, 3 β ,5 α -THMD, 3 α ,5 β -THMD, and 3 β ,5 β -THMD, respectively, which are discussed in this section. In the mass spectra of the four TMS-derivatized compounds with the molecular ion m/z 448, they all show ions at m/z 433 ($[M-CH_3]^+$), m/z 358 ($[M-TMSOH]^{++}$), m/z 343 ($[M-CH_3-TMSOH]^+$), m/z 268 ($[M-2xTMSOH]^{++}$), and m/z 253 ($[M-CH_3-2xTMSOH]^+$), indicating the fragments resulting from the losses of $\bullet CH_3$ and/or TMSOH from the molecule. The ions at m/z 143 and m/z 130 are the typical fragments of 17-methyl steroids, resulting from D-ring cleavage [112]. The fragment m/z 196 in the mass spectra of 5 β -isomers (3 α ,5 β -THMD and 3 β ,5 β -THMD) can be allocated to the A/B

ring, corresponding to the fragment m/z 194 in 5 β -DHMD that is common to steroids with a 1-ene-3-oxo structure [149]. However, this fragment was absent in the mass spectra of 5 α -isomers (3 α ,5 α -THMD and 3 β ,5 α -THMD). Instead, the fragment m/z 181 can also be assigned to the fragment of the enolized A-ring.

Table 12: Postulated fragments, mass errors ($\Delta m/z$) for the metabolite tentatively assigned as 3 α ,5 α -THMD, formed by the incubation of AKR1C4 with 5 α -DHMD (GC-ESI-QTOF-MS)

Postulated fragment	Exact mass [m/z]	Accurate mass [m/z]	$\Delta m/z$ [ppm]
[M] ⁺	448.3187	448.3201	3.12
[M-CH ₃] ⁺	433.2953	433.2964	2.54
[M-TMSOH] ⁺	358.2686	358.2701	4.19
[M-CH ₃ -TMSOH] ⁺	343.2452	343.2463	3.20
[M-2xTMSOH] ⁺	268.2186	268.2189	1.12
[M-CH ₃ -2xTMSOH] ⁺	253.1951	253.1958	2.76
[C ₁₀ H ₁₇ OSi] ⁺	181.1043	181.1045	1.10
[C ₇ H ₁₅ OSi] ⁺	143.0887	143.0896	6.29
[TMS] ⁺	73.0468	73.0475	9.58

Table 13: Postulated fragments, exact masses, accurate masses, mass errors ($\Delta m/z$) for the metabolite 3 α ,5 β -THMD, formed by the incubation of AKR1C4 with 5 β -DHMD (GC-ESI-QTOF-MS)

Postulated fragment	Exact mass [m/z]	Accurate mass [m/z]	$\Delta m/z$ [ppm]
[M] ⁺	448.3187	448.3201	3.12
[M-CH ₃] ⁺	433.2953	433.2972	4.39
[M-TMSOH] ⁺	358.2686	358.2706	5.58
[M-CH ₃ -TMSOH] ⁺	343.2452	343.2471	5.54
[M-2xTMSOH] ⁺	268.2186	268.2197	4.10
[M-CH ₃ -2xTMSOH] ⁺	253.1951	253.1962	4.34
[C ₁₁ H ₂₀ OSi] ⁺	196.1278	196.1283	2.55
[C ₇ H ₁₅ OSi] ⁺	143.0887	143.0898	7.69
[TMS] ⁺	73.0468	73.0477	12.32

According to previous studies, 5 β -metabolites are the predominant metabolites of MD in humans. This may be attributed to the presence of the 1,2-double bond, which was considered to inhibit the activity of 5 α -reductase [5, 150]. In this study, the conversion of MD into 5 β -reduced metabolite (i.e., 5 β -DHMD) catalyzed by AKR1D1 showed a very high efficiency, almost all of MD was successfully reduced by AKR1D1.

The AKR1C subfamily members exhibit varying degrees of preference for 3α -HSD and 3β -HSD activities [34]. As stressed by Steckelbroeck *et al.*, when using 5α -DHT as a substrate for 3-oxo reduction, AKR1C1 primarily functions as a 3β -HSD with subsidiary 3α -HSD activity. AKR1C2 acts as a highly efficient and almost exclusive 3α -HSD. AKR1C3 exhibits weak $3\alpha/3\beta$ -HSD activity, and AKR1C4 is considered to be an efficient 3α -HSD with subsidiary 3β -HSD activity [34]. However, the results obtained from the incubations seem to indicate a different preference to some extent. The relative peak area (peak area of the substance in correlation to the complete peak area of all detected substances (substrate and metabolites for each incubation)) after correction with the internal standard (MT) was used to compare the results, as shown in **Figure 17**. The biotransformations of the two substrates 5α - or 5β -DHMD by the three isoforms exhibited similar patterns. However, these three isoforms showed different preferences for 3α - and 3β -HSD activity. AKR1C2 and AKR1C4 exhibited both 3α -HSD and 3β -HSD activities for these two substrates, whereas AKR1C3 exclusively showed 3α -HSD activity.

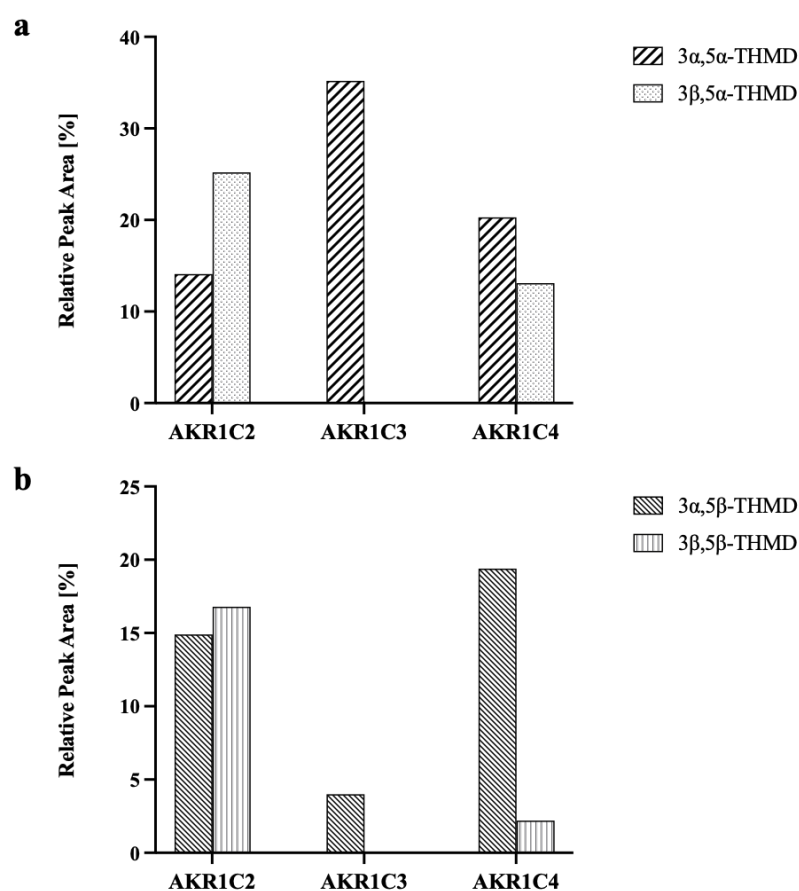


Figure 17: The peak area (relative to the internal standard (MT; EIC m/z 143)) of metabolites detected in the incubation of AKR1C2-AKR1C4 enzymes with (a) 5α -DHMD (EIC m/z 143), (b) 5β -DHMD (EIC m/z 143); the relative peak area is the peak area of the substances in correlation to the complete peak area of all detected substances (substrate and metabolites for each incubation), in GC-EI-MS analysis

The sequence of the A-ring reduction in 1,4-dien-3-one steroids has been discussed before based on the metabolites detected from human administration studies [93, 136, 137]. It has been proposed that the reduction of the A-ring in MD starts from hydrogenation of the 4,5-double bond, followed by reduction of the 3-oxo group. The last step is hydrogenation of the 1,2-double bond.

The absence of metabolites in the MD incubation with AKR1C2 suggests that 3-oxo group reduction may not occur in the presence of both C1,2-double bond and C4,5-double bond. In contrast, the occurrence of 3-oxo reduction in 5 α - and 5 β -DHMD indicates that it can occur in the presence of C1,2-double bond but after hydrogenation of C4,5-double bond. It has been reported that the reduction of A-ring in steroids with a 4-ene-3-one structure initiates from reduction of C4,5-double bond, implying that 3-oxo group reduction can only occur in the absence of C4,5-double bond [28]. Furthermore, as stressed by Loke *et al.*, if the C1,2-double bond was reduced before the C4,5-double bond, 5 α -metabolites would be detected as urinary metabolite of MD. However, according to previous studies, this is not the case [93]. Yet, the order of 3-oxo reduction and hydrogenation of C1,2-double bond remains uncertain. The presence of 5 β -reduced metabolite (i.e., 5 β -DHMD) only suggests that hydrogenation of C4,5-double bond can occur before that of C1,2-double bond, which is supported to some extent by the absence of metabolites with 4-ene-3-one or only 3-oxo structures in previous studies [93]. Therefore, the results obtained from this study partially support the sequence of A-ring reduction that aligns with previous postulations [93, 136, 137]. The proposed sequence of A-ring reduction is displayed in **Figure 18**.

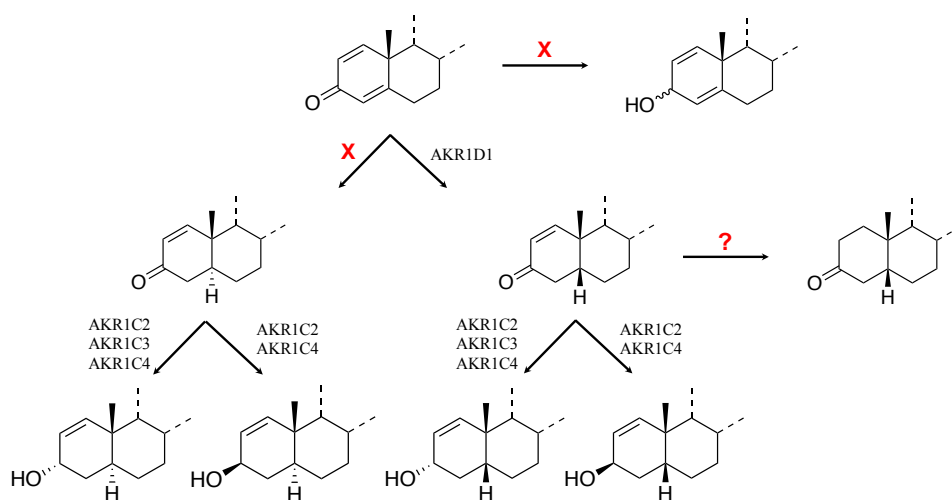


Figure 18: Proposed sequence of A-ring reduction

4.3 *In vitro* Biotransformation of Androgens by Human Fibroblasts and Keratinocytes

4.3.1 Metabolite Detection

Growth media samples following the exposure of human fibroblasts and keratinocytes with T, MD, MT, CLT, DHCMT, and CLMT were analyzed by GC-EI-MS and GC-EI-QTOF-MS after per-TMS derivatization. The metabolites were identified by the comparison of retention times and mass spectra with either commercially available authentic materials or in-house synthesized references. The incubation of human fibroblasts and keratinocytes with anabolic steroids shares a very similar metabolic pattern, although the abundance of metabolites produced by each cell type varied to some extent. This will be discussed in chapter 4.3.3. After the incubation, only reduced metabolites and oxidized metabolites were detected in the sample extracts, with reduced metabolites dominating. However, no metabolites were detected from MD and DHCMT.

In sample extracts from T incubation, 5α -DHT and 5α Adiol were identified by the comparison of the retention time and mass spectra with those of reference materials (**Figure 40** and **Figure 41** in Annex). **Table 26** and **Table 27** in Annex display the postulated fragments and their corresponding mass errors for these two metabolites. However, 5α Adiol was only observed in some of the T incubation samples. As an example, **Figure 19** shows a typical chromatogram of the samples obtained after incubation of T with keratinocytes. Both metabolites have been reported in previous research conducted in human skin cells [125, 151, 152]. The result is consistent with previous findings in keratinocytes and fibroblasts that were isolated from breast or genital skin, where T can be principally converted to the potent derivative 5α -DHT [151, 153].

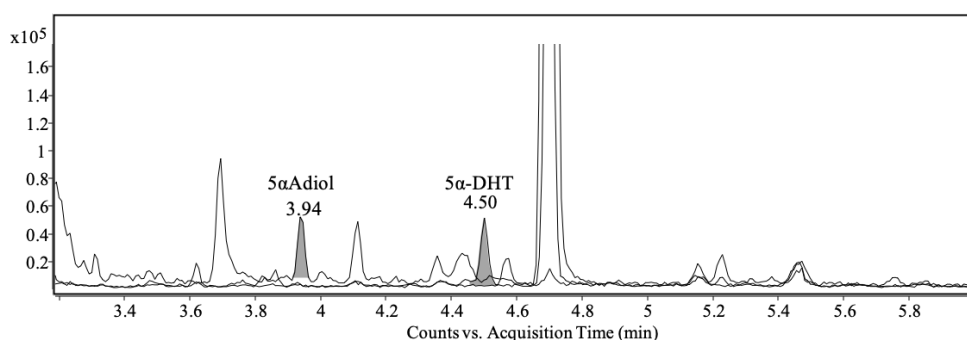


Figure 19: Overlay of EICs of samples obtained after incubation of human keratinocytes with T, showing metabolites 5α Adiol (RT 3.94 min; EIC m/z 241.1951 ± 0.5000) and 5α -DHT (RT 4.50 min; EIC m/z 434.3031 ± 0.5000) as per-TMS derivatives. This figure is adapted from my published paper [140]

Similar to T incubation, the 5 α -reduced metabolite, 17 β -hydroxy-17 α -methyl-5 α -androstane-3-one (mestanolone, MSL), was detected in MT incubation and confirmed by comparison with the reference material (**Figure 42** in Annex). **Table 28** (Annex) displays the postulated fragments and their corresponding mass errors for the metabolite MSL. **Figure 20** shows the GC-EI-MS chromatogram of the sample extracts after MT incubation. This metabolite was not reported as a metabolite after MT administration before [93, 94, 118, 137, 154-158]. However, no skin cell incubation or transdermal administration of MT was performed. Moreover, the two main urinary metabolites of MT in humans [118], 17 α -methyl-5 α -androstane-3 α ,17 β -diol (3 α 5 α -tetrahydromethyltestosterone, 3 α 5 α -THMT) and 17 α -methyl-5 β -androstane-3 α ,17 β -diol (3 α 5 β -THMT), were absent from the sample extracts. The observed differences are likely due to the rapid reduction of the 3-oxo group after the 4,5-double bond reduction in the human body compared to the skin cell incubation [38]. Despite the presence of 3 α -HSD enzymes has been reported in human skin cells [123, 125], their activities in skin cells are lower compared to the liver, where these enzymes are predominantly expressed [29-34]. Therefore, it is possible that the amount of the fully reduced metabolites may be too low to be detected.

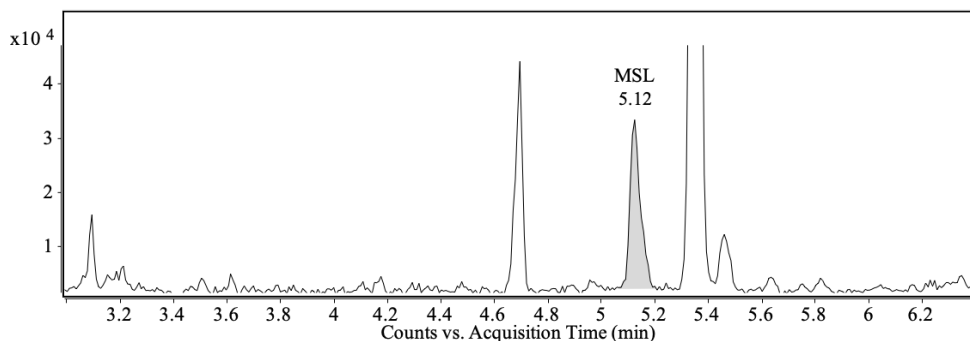


Figure 20: EIC of metabolites detected after incubation of human keratinocytes with MT (EIC m/z 448.3187 \pm 0.5000), showing metabolite MSL (RT 5.12 min) as per-TMS derivative. This figure is adapted from my published paper [140]

After CLT incubation 3 α -DHCLT, 3 β -DHCLT, 3 α ,4 α ,5 α -THCLT and 3 β ,4 α ,5 α -THCLT were identified by comparison with synthesized references. The mass spectra of these four metabolites are available in **Figure 43**, **Figure 44**, **Figure 45**, and **Figure 46** in Annex. The postulated fragments and their corresponding mass errors are available in **Table 29**, **Table 30**, **Table 31**, and **Table 32** in Annex. The typical chromatogram of the sample extracts after CLT incubation is displayed in **Figure 21**. An additional signal was assigned to 4-chloro-3 α -hydroxyandrost-4-ene-17-one by comparison with the

commercially available reference (**Figure 47** in Annex). **Table 33** (Annex) shows the postulated fragments and their corresponding mass errors. However, it was not traceable in all samples due to its very low abundance. This compound was found as the main metabolite of CLT after human oral administration and transdermal administration [103, 118]. The metabolite 3α -DHCLT was first reported as a metabolite of CLT in cattle in 1994 [159]. A metabolite with a fully reduced A-ring was first reported in cattle after intramuscular administration of CLT acetate, but its stereochemical structure was not clearly determined [160]. Later, excretion studies identified 4ξ -chloro- 5ξ -androstane- $3\xi,17\beta$ -diol- 3ξ -sulfate as a phase II metabolite in human urine [161]. However, the stereochemical structure remained undefined due to the lack of authentic material. By transfer of the findings reported in here, reasonable assignments will be possible and structure confirmation of the urinary metabolites will be achieved in future studies. In contrast to the findings of de la Torre *et al.* through human transdermal administration [103], where 5β -reduced metabolites were predominant, only 5α -metabolites were detected in this study.

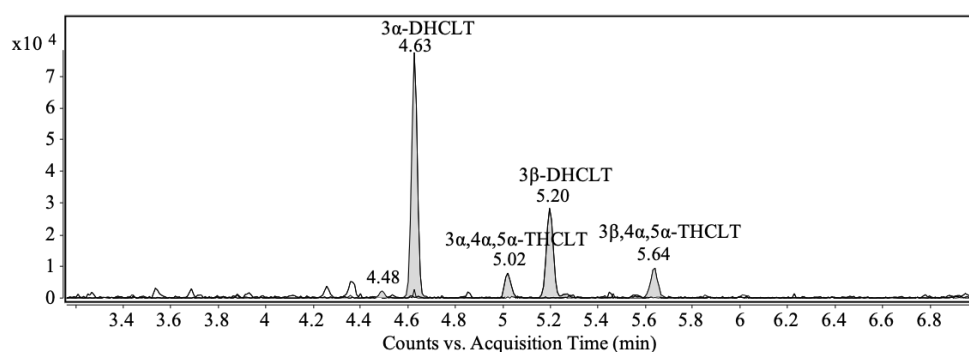


Figure 21: Overlay of EICs of metabolites detected after incubation of human keratinocytes with CLT, showing metabolites 4-chloro- 3α -hydroxy-androst-4-ene-17-one (RT 4.48 min; EIC m/z 466.2485 ± 0.5000), 3α -DHCLT (RT 4.63 min; EIC m/z 433.2953 ± 0.5000), $3\alpha,4\alpha,5\alpha$ -THCLT (RT 5.02 min; EIC m/z 455.2563 ± 0.5000), 3β -DHCLT (RT 5.20 min; EIC m/z 433.2953 ± 0.5000), and $3\beta,4\alpha,5\alpha$ -THCLT (RT 5.64 min; EIC m/z 455.2563 ± 0.5000) as *per*-TMS derivatives. This figure is adapted from my published paper [140]

Analogous to CLT, 3α -DHCLMT, 3β -DHCLMT, $3\alpha,4\alpha,5\alpha$ -THCLMT, and $3\beta,4\alpha,5\alpha$ -THCLMT were detected in CLMT incubation, and confirmed by comparison with synthesized references. The mass spectra of these four metabolites are available in **Figure 48**, **Figure 49**, **Figure 50**, and **Figure 51** in Annex. The postulated fragments and their corresponding mass errors are available in **Table 34**, **Table 35**, **Table 36**, and **Table 37** in Annex. The typical chromatogram of sample extracts of CLMT incubation is shown in **Figure 22**. Limited data is available regarding the metabolism of CLMT, with

only a few studies with microbiota [162, 163] and one *in vivo* study in uPA^{+/+}-SCID chimeric mouse [164]. Although CLMT has been misused in the early 1970s by East German athletes, information on the metabolic studies is limited [165]. 4-Chloro-17 α -methylandroster-4-ene-3 ξ ,17 β -diol, the active substance in the supplement Promagnon, was reported as a metabolite in uPA^{+/+}-SCID chimeric mouse urine after CLMT administration [164]. No fully reduced metabolites (i.e., THCLMT) have been reported before.

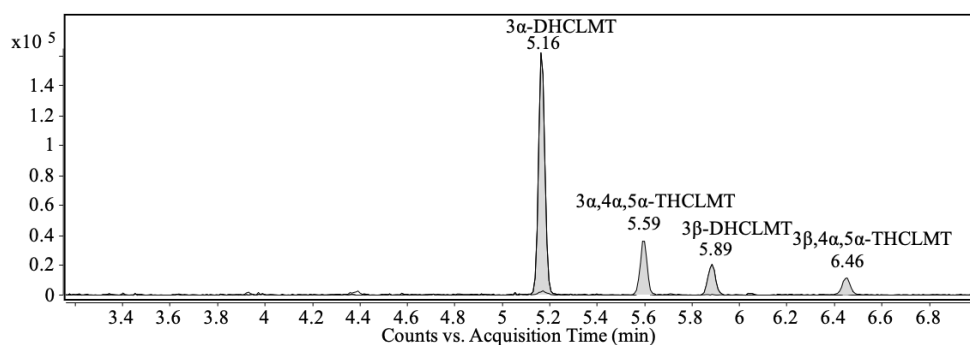


Figure 22: Overlay of EICs of metabolites detected after incubation of human keratinocytes with CLMT, showing metabolites 3 α -DHCLMT (RT 5.16 min; EIC m/z 357.2608 \pm 0.5000), 3 $\alpha,4\alpha,5\alpha$ -THCLMT (RT 5.59 min; EIC m/z 469.2719 \pm 0.5000), 3 β -DHCLMT (RT 5.89 min; EIC m/z 357.2608 \pm 0.5000), and 3 $\beta,4\alpha,5\alpha$ -THCLMT (RT 6.46 min; EIC m/z 469.2719 \pm 0.5000) as per-TMS derivatives. This figure is adapted from my published paper [140]

4.3.2 Comparison of Metabolic Pathways

According to the results obtained in this study, it was observed that the sequences of A-ring reduction among these six steroids in human skin cells are different based on the characteristics of chemical structures.

As stressed in previous studies, the 4-ene-3-one steroids typically follow the order starting with reduction of the 4,5-double bond followed by reduction of the 3-oxo group [28]. Moreover, as discussed in chapter 4.2, steroids with a 1,4-dien-3-one structure seem to follow the same sequence as 4-ene-3-one steroids, with the 1,2-double bond undergoing additional reduction at the last step of the A-ring reduction [93, 137]. This finding is also partially supported by the studies conducted with isolated recombinant AKR1C2-4 enzymes, where the 3-oxo reduction did not take place in MD, whereas it occurred in 5 α - and 5 β -DHMD. This indicates that the presence of C4,5-double bond may hinder the 3-oxo reduction.

The metabolism of T, MD, and MT in this study is consistent with the proposed metabolic sequence. 5 α -DHT and MSL were produced from T and MT incubation, respectively, through the 5 α -reduction catalyzed by steroid-5 α -reductase [166]. This is

subsequently followed by reduction of the 3-oxo group in 5 α -DHT by 3 α -HSD resulting in 5 α Adiol (**Figure 23**).

In contrast to T and MT, no metabolites were detected in the incubation of MD with either keratinocytes or fibroblasts. This may be attributed to the fact that the first step of A-ring reduction, i.e., the reduction of the C4,5-double bond, did not take place in MD incubation as in T and MT incubations. It has been proposed that the presence of a 1,2-double bond inhibits the activity of 5 α -reductase [5, 150]. This assumption is strongly supported by the absence of 5 α -metabolites after oral administration of MD [93]. Moreover, the absence of 5 β -reduced metabolites in all sample extracts substantiates a limited or negligible role of 5 β -reductase in the metabolism by human skin cells. This is in line with the previous findings in human skin models. The expression of 5 α -reductase (SRD5A1 and SRD5A2) has been reported in both human foreskin keratinocytes and fibroblasts [123, 125]. In contrast, the 5 β -reductase (AKR1D1) is most abundantly expressed in the liver [49, 50] and has not been reported in human skin cells. Therefore, no further A-ring reduction occurs in MD in the presence of the C4,5 double bond, resulting in no detectable metabolites in MD incubations.

Conversely, the compounds with a chlorine group at position 4, CLT and CLMT, undergo a different metabolic sequence compared to T and MT. As described by Schänzer *et al.*, the chlorine atom at C-4 might inhibit 5 α - and 5 β -reductase to some degree [118]. The production of the metabolites 3 α /3 β -DHCLT and 3 α /3 β -DHCLMT from CLT and CLMT, respectively, implies that the 3-oxo group can be reduced in the presence of the C4,5-double bond, which is in line with the statements by Schänzer *et al.* [5, 118]. It is proposed that the subsequent reduction of the 4,5-double bond leads to corresponding fully reduced metabolites 3 α /3 β ,4 α ,5 α -THCLT and 3 α /3 β ,4 α ,5 α -THCLMT (**Figure 23**).

According to the sequence proposed by Loke *et al.*, the 5 α -reduction may take place after the reduction of the 1,2-double bond in DHCMT, followed by the reduction of the 3-oxo group [167], whereas the 5 β -reduction can occur in the presence of 1,2-double bond. However, the specific enzyme responsible for catalyzing 1,2-double bond reduction in humans remains unclear, and the data obtained in the study reported in here underline that there is no evidence to support its expression in human skin cells. In the presence of C1,2-double bond, hydrogenation of the 4,5-double bond catalyzed by 5 α -reductase did not occur in DHCMT incubations, as also observed in MD incubations. Consequently, this hindered the reduction of the 3-oxo group, resulting in no metabolites detected in DHCMT incubations.

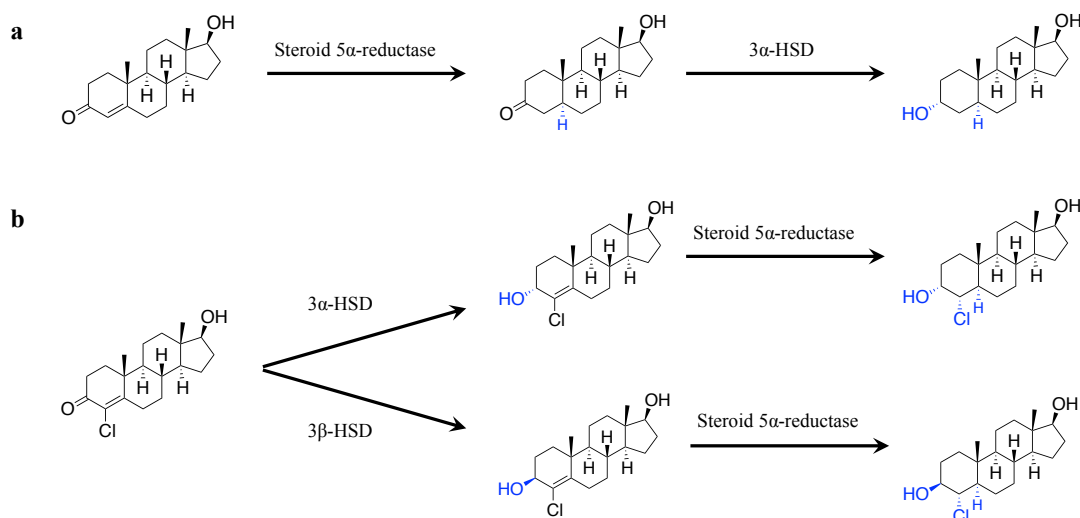


Figure 23: Proposed A-ring reduction sequence of (a) T and (b) CLT

4.3.3 Metabolic Characteristics in Human Fibroblasts and Keratinocytes

Fibroblasts or keratinocytes used in this study were from three donors, respectively. The metabolites produced by cells from different donors exhibited similar metabolite patterns, albeit with slight differences in their quantities. Furthermore, it seems that the two types of cells showed different metabolic capabilities based on the chemical structures. The difference observed between fibroblasts and keratinocytes may be due to the varying levels of enzyme expression. For example, it has been reported that the mRNA expression of SRD5A1 was found in both foreskin keratinocytes and fibroblasts, while SRD5A2 was only detectable in fibroblasts [123, 125]. Based on the results, the metabolic conversion levels of compounds with a chlorine group at position 4 appear to be slightly higher in keratinocytes. With the exception of compound 3β,4α,5α-THCLT, the relative peak area of metabolites 3α-DHCLT, 3β-DHCLT, 3α,4α,5α-THCLT, 3α-DHCLMT, 3β-DHCLMT, 3α,4α,5α-THCLMT, and 3β,4α,5α-THCLMT detected in keratinocyte incubation was 4.8-, 1.8-, 2.1-, 12.1-, 4.9-, 3.2-, and 2.3-fold higher than in fibroblasts, respectively (**Figure 24**). In contrast, compounds lacking the chlorine group tend to produce a higher level of metabolites in fibroblasts. More specifically, the relative peak area of metabolites 5α-DHT and MSL detected in fibroblast incubation was found to be 3.0- and 5.4-fold higher than in keratinocytes, respectively.

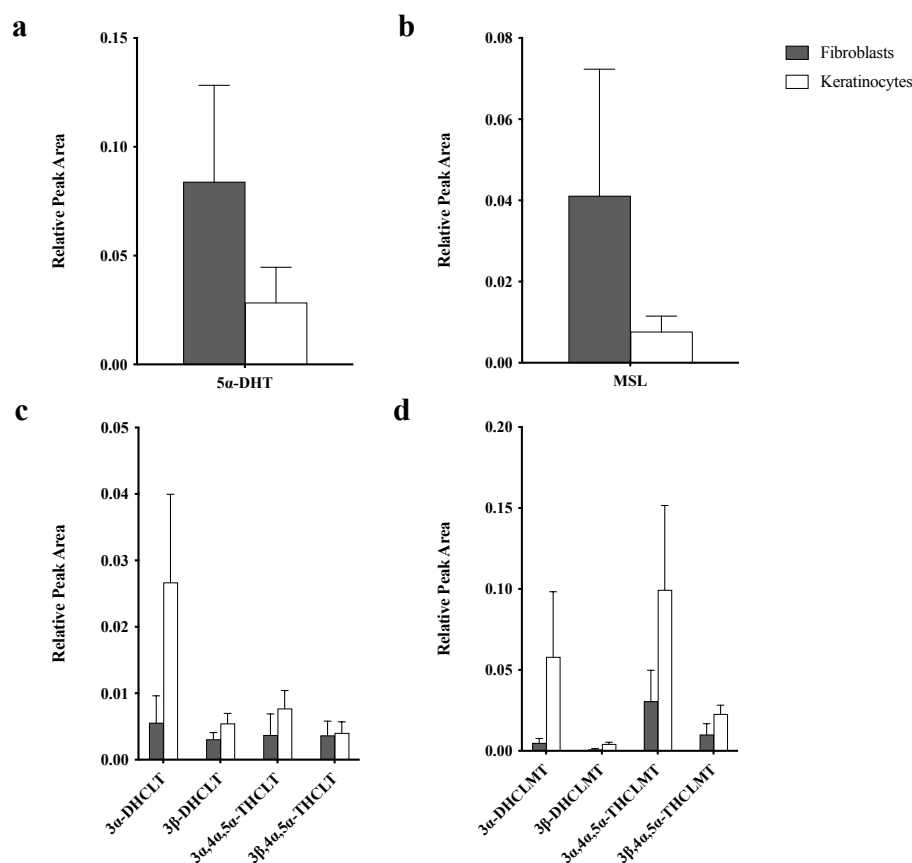


Figure 24: The peak area (relative to the internal standard ($T-d_3$)) of metabolites detected in fibroblasts and keratinocytes incubated with (a) T (EIC m/z 434), (b) MT (EIC m/z 143), (c) CLT (EIC m/z 433 and m/z 255), and (d) CLMT (EIC m/z 357 and m/z 143) (mean \pm SD; $n = 3$), in GC-EI-MS analysis. This figure is adapted from my published paper [140]

4.4 *In vivo* Biotransformation in Fish Embryo Model

To investigate whether medaka embryos might be an alternative, non-animal test model to study human-like metabolism, the anabolic steroid MD was used as a model substance. The results of MD metabolism and the discussion concerning the usability of the medaka embryo model as an adequate model are presented in the following chapter 4.4.1.

To further investigate the metabolic characteristics of anabolic steroids in the medaka embryo model, [$^{13}C_3$]-T and MT were used in the following study. The metabolic patterns of two compounds in medaka embryos are presented in chapter 4.4.2.

4.4.1 Evaluation of Medaka Embryo Model through Metabolite Analysis for MD

Sample extracts obtained from medaka embryo incubation with MD were diluted and analyzed by LC-ESI-MS/MS directly, or by GC-EI-QTOF-MS after derivatization. The results obtained show that the embryos produced four MD metabolites. Those were

postulated to be three mono-hydroxylation metabolites, including 6 β -hydroxy-metandienone (6 β OH-MD, **M1**), tentatively 18OH-MD (**M2**), tentatively 16OH-MD (**M3**), as well as one reduced metabolite, 5 β -DHMD (**M4**).

In the pilot experiment, a peak of metabolic capacity was shown after day 8 (8 dpf), which did not change until hatching. From 4 dpf, the reduced metabolite was detected, whereas the hydroxylated metabolites were observed from 8 dpf. During the 10 day-incubation period, no sex-dependent differences in metabolite pattern were observed. Developmental malformations were observed for the exposition to 50 μ M MD, while a significant elevation of the heart beat was also present in those embryos exposed to the lower dose (10 μ M) for 8 days. Therefore, an incubation from 6 to 8 days of development was established as standard protocol with strain d-rR.YHNI.

In LC-ESI-MS analysis, all four metabolites were detected after the incubation. **Figure 25** shows a typical chromatogram of the samples obtained after incubation of MD with the medaka embryos. The structure of **M1** was identified by comparison of the data obtained in extracted samples with authentic reference material. The retention time and product ion mass spectrum of **M1** matched with those from authentic material of 6 β OH-MD. The mass spectra of **M1** and its reference compound are available in **Figure 26** and **Figure 52** (Annex), respectively. The postulated fragments and their corresponding mass errors for **M1** are displayed in **Table 14**. **M4** can be tentatively identified as 5 α -DHMD or 5 β -DHMD by the comparison of the retention time with that of reference materials. However, due to the similarity of the product ion spectra among 5 α -DHMD, 5 β -DHMD, and **M4**, the stereochemistry at the C5 position of **M4** cannot be confirmed based on the LC-ESI-MS/MS analysis. **Figure 53** (Annex) displays the product ion spectrum of **M4**. Due to the lack of authentic materials, the structures of **M2** and **M3** can only be postulated based on the fragmentation analysis of their product ion spectra. The retention times of these four metabolites in LC-ESI-MS are given in **Table 38** (Annex).

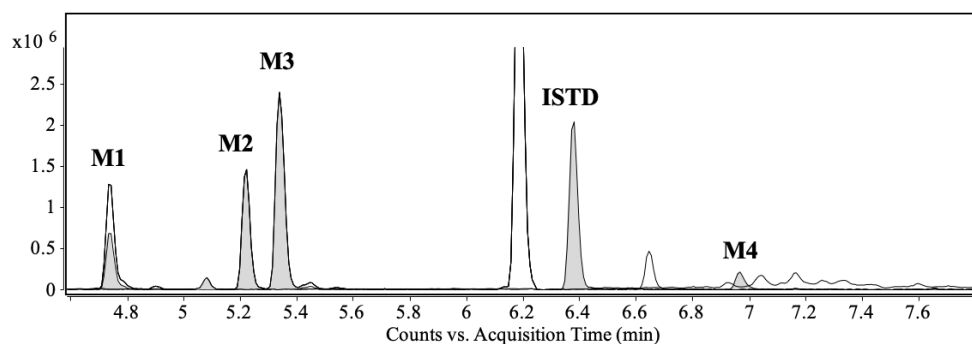


Figure 25: Overlay of EICs (LC-ESI-QTOF-MS) of a sample obtained after 2-day incubation of medaka embryos with 10 μ M MD. 6 β OH-MD (**M1**, RT 4.71 min; EIC m/z 317.2111 \pm 0.5000), mono-hydroxy MD (**M2**, RT 5.22 min; EIC m/z 317.2111 \pm 0.5000), mono-hydroxy MD (**M3**, RT 5.34 min; EIC m/z 317.2111 \pm 0.5000), T-d₃ (internal standard, **ISTD**, RT 6.38 min; EIC m/z 292.2350 \pm 0.5000), mono-reduced MD (**M4**, RT 6.97 min; EIC m/z 303.2319 \pm 0.5000). This figure and the following figures and tables in chapter 4.4.1 have been published, material from: Lingyu Liu, Medaka embryos as a model for metabolism of anabolic steroids, Archives of Toxicology, published [2022], [Springer] [168]

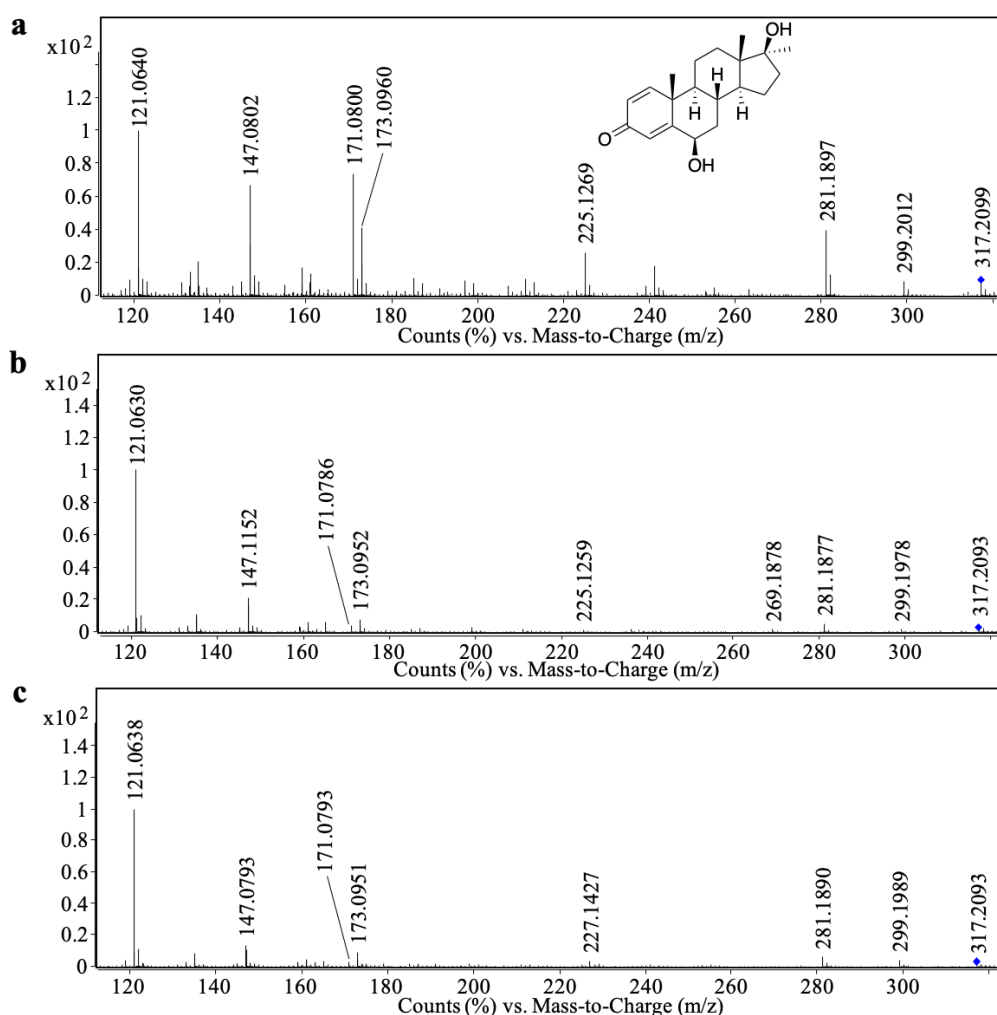


Figure 26: Product ion spectra (LC-ESI-QTOF-MS/MS) of (a) 6 β OH-MD (**M1**, $[M+H]^+$ =317.2112, mass error 0.32 ppm, RT 4.71 min), (b) mono-hydroxy MD (**M2**, $[M+H]^+$ =317.2100, mass error -3.47 ppm, RT 5.22 min), and (c) mono-hydroxy MD (**M3**, $[M+H]^+$ =317.2105, mass error -1.89 ppm, RT 5.34 min) formed by medaka embryos incubated with 10 μ M MD, collision energy 23.1 eV. This figure is adapted from my published paper [168]

Metabolites **M1**, **M2**, and **M3** have the same molecular ion m/z 317, suggesting a hydroxylation with respect to MD. **Figure 26** shows the product ion spectra of **M1**, **M2**, and **M3** obtained by LC-ESI-MS/MS. **Table 14**, **Table 15**, and **Table 16** show all fragments and their corresponding mass errors for **M1**, **M2**, and **M3**, respectively, which are discussed in this section. The fragment ions at m/z 299 and 281 were found in all the product ion spectra of these three metabolites, representing water losses from the molecular ion with m/z 317. The ions at m/z 121, 147, 171, and 173 were commonly observed and discussed for hydroxylated MD metabolites in literature [169-171], which were also detected in the product ion spectra of **M1**, **M2**, and **M3**. The 1,4-dien-3-one structure was identified by the product ions m/z 121 and m/z 147 [172, 173]. According to Schänzer *et al.*, the fragment at m/z 121 is proposed to result from fissions of C-C bonds between C6-C7 and C9-C10 [173]. However, two different product ions at nominal mass m/z 147 were observed in **M2** and **M3**. As proposed by Thevis *et al.* and Pozo *et al.*, m/z 147.0793 obtained from **M3** is suggested to result from the A-, B-, and C-rings of 1,4-dien-3-one steroids by fissions of the linkages between C-6 and C-7, C-8 and C-9, and C-11 and C-12, while the fragment at m/z 147.1152 from **M2** is generated from C- and D-ring [172, 174]. This indicates that the intact 1,4-dien-3-one structure has been substantiated in the structure of metabolites **M3**.

Table 14: Postulated fragments, exact masses, accurate masses, mass errors ($\Delta m/z$) for **M1**, LC-ESI-MS/MS. This table is adapted from my published paper [168]

Postulated fragment	Exact mass [m/z]	Accurate mass [m/z]	Mass error [ppm]	Rings involved
[M+H] ⁺	317.2111	317.2112	0.32	A-B-C-D
[M+H-H ₂ O] ⁺	299.2006	299.2012	2.01	A-B-C-D
[M+H-2H ₂ O] ⁺	281.1900	281.1897	-1.07	A-B-C-D
[M+H-3H ₂ O] ⁺	263.1794	263.1793	-0.38	A-B-C-D
[M+H-H ₂ O-74 Da] ⁺	225.1274	225.1269	-2.22	A-B-C
[C ₁₂ H ₁₃ O] ⁺	173.0961	173.0960	-0.58	A-B
[C ₁₂ H ₁₁ O] ⁺	171.0804	171.0800	-2.34	A-B
[C ₁₀ H ₁₁ O] ⁺	147.0804	147.0802	-1.36	A-B
[C ₈ H ₉ O] ⁺	121.0648	121.0640	-6.61	A

Table 15: Postulated fragments, exact masses, accurate masses, mass errors ($\Delta m/z$) for **M2**, LC-ESI-MS/MS. This table is adapted from my published paper [168]

Postulated fragment	Exact mass [m/z]	Accurate mass [m/z]	Mass error [ppm]	Rings involved
[M+H] ⁺	317.2111	317.2100	-3.47	A-B-C-D
[M+H-H ₂ O] ⁺	299.2006	299.1978	-9.36	A-B-C-D
[M+H-2H ₂ O] ⁺	281.1900	281.1877	-8.18	A-B-C-D
[M+H-H ₂ O-CH ₂ O] ⁺	269.1900	269.1878	-8.17	A-B-C-D
[C ₁₂ H ₁₃ O] ⁺	173.0961	173.0952	-5.20	A-B
[C ₁₂ H ₁₁ O] ⁺	171.0804	171.0786	-10.52	A-B
[C ₁₁ H ₁₅] ⁺	147.1168	147.1152	-10.88	C-D
[C ₈ H ₉ O] ⁺	121.0648	121.0630	-14.87	A

Table 16: Postulated fragments, exact masses, accurate masses, mass errors ($\Delta m/z$) for **M3**, LC-ESI-MS/MS. This table is adapted from my published paper [168]

Postulated fragment	Exact mass [m/z]	Accurate mass [m/z]	Mass error [ppm]	Rings involved
[M+H] ⁺	317.2111	317.2105	-1.89	A-B-C-D
[M+H-H ₂ O] ⁺	299.2006	299.1989	-5.68	A-B-C-D
[M+H-2H ₂ O] ⁺	281.1900	281.1890	-3.56	A-B-C-D
[C ₁₆ H ₁₉ O] ⁺	227.1430	227.1427	-1.32	A-B-C
[C ₁₂ H ₁₃ O] ⁺	173.0961	173.0951	-5.78	A-B
[C ₁₂ H ₁₁ O] ⁺	171.0804	171.0793	-6.43	A-B
[C ₁₀ H ₁₁ O] ⁺	147.0804	147.0793	-7.48	A-B
[C ₈ H ₉ O] ⁺	121.0648	121.0638	-8.26	A

As proposed by Musharraf *et al.*, the product ion at m/z 225 of **M1** was generated owing to the loss of 56 Da from the D-ring and two water losses from the quasi molecular ion [M+H]⁺, containing A-, B-, and C-ring. The hydroxy group at position 6 was eliminated in this process [170]. The similar fragment was observed in the product ion spectrum of **M3**, which is shifted towards m/z 227 (+2 Da). This is also in consistent with the postulation that **M3** remains the intact 1,4-dien-3-one structure as MD. Therefore, it is assumed that the additional hydroxy group of **M3** is located in the D-ring.

In the product ion spectrum of **M2** the fragment ion m/z 269 is proposed to be generated due to the neutral loss of formaldehyde (30 Da) from the molecular ion with an additional loss of water, indicating the presence of a hydroxylated methyl residue in the structure of **M2** [173]. Given that **M2** keeps the conserved structure of the D-ring with respect to MD, the position of the hydroxylated methyl residue can be assumed at C18 or C19. However, a comparison of spectra and retention time with authentic reference

material is necessary for the ultimate confirmation in the future (level 1 confidence according to [175]).

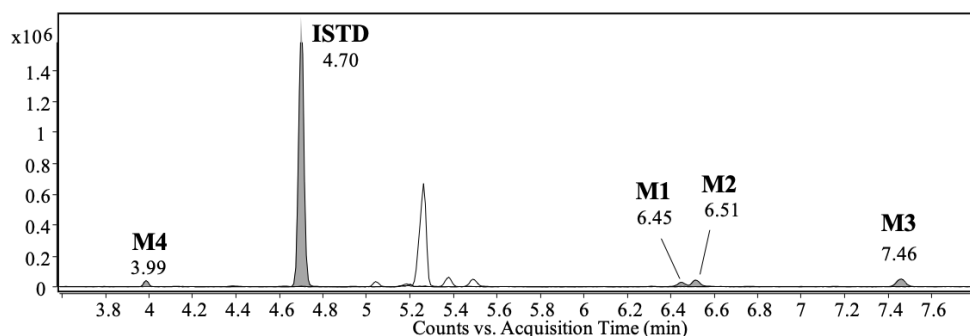


Figure 27: Overlay of EICs in GC-EI-QTOF-MS after TMIS derivatization showing five main products after 2-day incubation of medaka embryos with 10 μ M MD. 5 β -DHMD (**M4**, RT 3.99 min; EIC m/z 446.3031 \pm 0.5000), ISTD (*T-d₃*, RT 4.70 min; EIC m/z 435.3063 \pm 0.5000), 6 β OH-MD (**M1**, RT 6.45 min; EIC m/z 532.3219 \pm 0.5000), mono-hydroxy MD (**M2**, RT 6.51 min; EIC m/z 532.3219 \pm 0.5000), mono-hydroxy MD (**M3**, RT 7.46 min; EIC m/z 532.3219 \pm 0.5000). This figure is adapted from my published paper [168]

Table 17: Per-TMS derivatives of metabolites detected in samples obtained after 2-day incubation of medaka embryos with 10 μ M MD by GC-EI-QTOF-MS. This table is adapted from my published paper [168]

Analyte	Elemental Composition	[M] ⁺⁺ (calc)	[M] ⁺⁺ (exp)	Mass error [ppm]	Retention Time (min)	Assignment
1	[C ₂₆ H ₄₆ O ₂ Si ₂] ⁺⁺	446.3031	446.3038	1.57	3.99	5 β -DHMD (M4)
2	[C ₂₉ H ₅₂ O ₃ Si ₃] ⁺⁺	532.3219	532.3237	3.38	6.45	6 β OH-MD (M1)
3	[C ₂₉ H ₅₂ O ₃ Si ₃] ⁺⁺	532.3219	532.3228	1.69	6.51	18OH-MD* (M2)
4	[C ₂₉ H ₅₂ O ₃ Si ₃] ⁺⁺	532.3219	532.3231	2.25	7.46	16OH-MD* (M3)

* Tentative assignment.

To have more fragmentation information on the mono-hydroxylated metabolites, and to further confirm the stereochemistry of the C5 in **M4**, additional GC-EI-QTOF-MS analysis was performed. **Figure 27** shows the GC-EI-QTOF-MS chromatogram (EICs) after TMIS derivatization of the products. The retention times of metabolites detected in GC-EI-QTOF-MS are displayed in **Table 17**. The molecular ion of metabolite at 3.99 min is m/z 446, which was identified as 5 β -DHMD (i.e., **M4**) after the comparison of the retention time and mass spectra with those of reference material (**Figure 34** and **Figure 54** in Annex). **Table 39** (Annex) displays the postulated fragments and their corresponding mass errors. This is also in accordance with the results published before [38, 93], which report that almost all of the reduced metabolites produced from MD show a 5 β -stereochemistry structure.

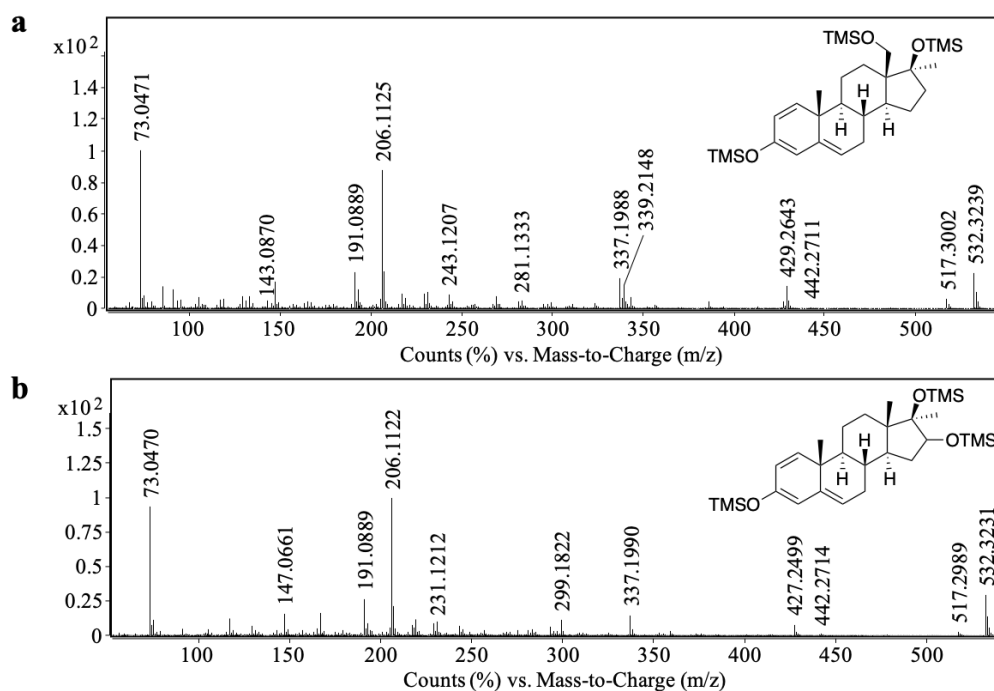


Figure 28: Normalized EI mass spectra (GC-QTOF-MS) of TMS derivatives of (a) mono-hydroxy MD (**M2**, $[M]^{+}=532.3239$, mass error 3.76 ppm, RT 6.51 min) and (b) mono-hydroxy MD (**M3**, $[M]^{+}=532.3231$, mass error 2.25 ppm, RT 7.46 min), formed by medaka embryos incubated with 10 μM MD. This figure is adapted from my published paper [168]

Table 18: Postulated fragments, exact masses, accurate masses, mass errors ($\Delta m/z$) for TMS-derivative of mono-hydroxy MD (**M2**), GC-EI-QTOF-MS. This table is adapted from my published paper [168]

Postulated fragment	Exact mass [m/z]	Accurate mass [m/z]	Mass error [ppm]
$[M]^{+}$	532.3219	532.3239	3.76
$[M-\text{CH}_3]^{+}$	517.2984	517.3002	3.48
$[M-\text{TMSOH}]^{+}$	442.2718	442.2711	-1.58
$[M-\text{CH}_2-\text{TMSO}]^{+}$	429.2645	429.2643	-0.47
$[M-\text{CH}_3-2x\text{TMSOH}]^{+}$	337.1982	337.1988	1.78
$[M-\text{CH}_2-\text{TMSO}-\text{TMSOH}]^{+}$	339.2139	339.2148	2.65
$[\text{TMS}]^{+}$	73.0468	73.0471	4.11

GC-EI-QTOF-MS analysis also showed three mono-hydroxylated metabolites formed by medaka embryos. The molecular ions (m/z 532) of tris-TMS-OH-MD derivatives were identified. The metabolite at 6.45 min was assigned to **M1** by comparison with authentic reference material (mass spectra in **Figure 55** in Annex). **Table 40** (Annex) shows all postulated fragments and their corresponding mass errors for **M1**. The mass spectrum of the metabolite at 6.51 min is displayed in **Figure 28**. **Table 18** shows all fragments and their corresponding mass errors for this metabolite (RT 6.51 min), which are discussed in this section. The fragment ions at m/z 517 ($[M-\text{CH}_3]^{+}$), and m/z 337

([M-CH₃-2xTMSOH]⁺) are generated by the losses of •CH₃ and/or TMSOH from the molecule. Notably, an exclusive fragment *m/z* 429 was observed in the mass spectrum of this metabolite (RT 6.51 min), which is correlated to the characteristic loss of TMS-O-CH₂• (103 Da) from the molecular ion (*m/z* 532) discussed for steroids bearing a hydroxymethyl group [176]. This is followed by a loss of TMSOH (90 Da) yielding *m/z* 339 [177]. The fragment *m/z* 206 is suggested to arise from the cleavage of the C9-C10 and C7-C8 bonds, comprising the A-ring and the C6 and C7 carbons [178], which indicates the unaltered 1,4-dien-3-one structure after enolization by means of trimethylsilylation [111]. This fragment was found for both metabolites at 6.51 min and 7.46 min. This substantiates an intact structure of A- and B-ring derived from MD in both analytes. Moreover, the mass spectrum of the metabolite at 6.51 min is in line with that of 18OH-MD previously reported by Parr, *et al.* [177], providing level 2 confidence in identification. Hence, this metabolite (RT 6.51 min) was postulated to be 18OH-MD (**M2**). However, the confirmation of its structure still needs further comparison with reference material in the future.

Table 19: Postulated fragments, exact masses, accurate masses, mass errors ($\Delta m/z$) for TMS-derivative of mono-hydroxy MD (**M3**), GC-ESI-QTOF-MS. This table is adapted from my published paper [168]

Postulated fragment	Exact mass [m/z]	Accurate mass [m/z]	Mass error [ppm]
[M] ⁺	532.3219	532.3231	2.25
[M-CH ₃] ⁺	517.2984	517.2989	0.97
[M-TMSOH] ⁺	442.2718	442.2714	-0.90
[M-CH ₃ -TMSOH] ⁺	427.2483	427.2499	3.74
[M-CH ₃ -2xTMSOH] ⁺	337.1982	337.1990	2.37
[TMS] ⁺	73.0468	73.0470	2.74

The mass spectrum of the metabolite at 7.46 min (**Figure 28**) shows ions at *m/z* 427 ([M-CH₃-TMSOH]⁺) and *m/z* 337 ([M-CH₃-2xTMSOH]⁺), indicating the losses of two TMSOH and •CH₃ from the molecular ion. **Table 19** shows all fragments and their corresponding mass errors for this metabolite (RT 7.46 min), which are discussed in this section. The ion at *m/z* 299 is proposed to result from the loss of D-ring [179]. Therefore, the combination of fragment ions *m/z* 206 and *m/z* 299 represents a conserved structure of A-, B-, and C-ring derived from MD. The fragment ion *m/z* 231 is proposed to originate from the cleavage of the D-ring, which is incremented by 88 Da from the typical fragment of 17-methyl steroids at *m/z* 143 due to the additional hydroxy group in the D-ring [177].

This supports the assumption that the hydroxy group in this metabolite (RT 7.46 min) is located at the D-ring. Accordingly, its mass spectrum is consistent with that of 16OH-MD reported in the literature [177].

In combination with the data from LC-ESI-MS/MS, the metabolite at 6.51 min was allocated to **M2**, tentatively assigned as 18OH-MD, while the metabolite at 7.46 min was proposed to correspond to **M3**, which was postulated to be 16OH-MD. However, for ultimate confirmation of the structures, but also stereochemical assignment of 16-hydroxylation, comparison with authentic reference materials is necessary in further investigations.

Since the first detection of MD in human urine samples in 1980, 6 β OH-MD has been one of the MD target metabolites investigated in routine doping analysis [180]. The other three metabolites generated by the medaka embryos are also known to be excreted in humans. 5 β -DHMD was first found after MD administration in human urine in 1991 [136]. While 16OH-MD was first detected as a phase I metabolite in horse urine in 1992, administration studies identified 16OH-MD and 18OH-MD as human urinary MD metabolites later [177, 181]. Although full confirmation of the two mono-hydroxylated metabolites **M2** and **M3** was not possible due to the lack of reference materials, the comparison of the data obtained with previous results allows for the shown postulation [177]. Thus, level 2 confidence in identification is achieved.

In the past few years, a couple of studies investigated the zebrafish (*Danio rerio*) as a species to model human metabolism of different doping-related compound classes (e.g., anabolic steroids, stimulants, cannabimimetics, secretagogues) [127, 128, 182]. The so-called zebrafish water tank model seems to be a promising model for metabolism studies. As this model uses adult zebrafish, every compound treatment represents an animal experiment and therefore needs approval by responsible governing animal welfare authorities. In contrast, the medaka embryo model investigated in the present study is a non-animal *in vivo* test system for which no approval is required. Furthermore, in comparison to *in vitro* metabolic models, the medaka embryo model allows for simultaneous analysis of biotransformation and potential toxicity. Based on the similar outcomes with human administration studies, medaka embryos may serve as an alternative model to identify potential metabolites for human biotransformation of doping-relevant compounds.

Further studies are necessary to substantiate the usability of the medaka embryo as a model for human biotransformation. Still, strong expertise and facilities are a prerequisite

to address this topic but if proven, this model may contribute to reducing and replacing animal experiments as defined by the 3R principle of animal welfare. Besides this, in contrast to the zebrafish, medaka offers another interesting feature that genotypic sex can be easily identified, which might be of interest for future studies. This part of the study includes material previously published. As one of the authors, I have the right to reuse the article in whole or in part in this thesis (Lingyu Liu, Medaka embryos as a model for metabolism of anabolic steroids, Archives of Toxicology, published [2022], [Springer]) [168].

4.4.2 Biotransformation of [$^{13}\text{C}_3$]-Testosterone and Methyltestosterone in Medaka Embryo Model

As described earlier, T and MT possess very similar structures with the additional 17 α -methyl group in MT. Thus, the metabolic patterns of these two compounds in medaka embryos are compared and discussed.

There are no significant sex-specific or substrate concentration differences in metabolite production. In all cases, the same metabolites were produced, albeit with slight differences in amounts.

The sample extracts were analyzed by GC-EI-MS. **Figure 29** shows the chromatogram of the sample obtained after medaka embryo incubation with [$^{13}\text{C}_3$]-T in GC-MS analysis. The metabolism of [$^{13}\text{C}_3$]-T in the medaka embryo model mainly involved hydrogenation of the 4,5-double bond, reduction at position 3, and oxidation of the 17-hydroxy group. The biotransformation of [$^{13}\text{C}_3$]-T mainly resulted in the formation of six metabolites, including four mono-reduced metabolites, i.e., [$^{13}\text{C}_3$]-5 β -DHT (mass spectrum in **Figure 56** in Annex), [$^{13}\text{C}_3$]-Etio (mass spectrum in **Figure 57** in Annex), and [$^{13}\text{C}_3$]-EA (mass spectrum in **Figure 58** in Annex), [$^{13}\text{C}_3$]-5 α -DHT (mass spectrum in **Figure 59** in Annex), one dehydrogenated metabolite [$^{13}\text{C}_3$]-AED (mass spectrum in **Figure 60** in Annex), as well as one unidentified hydroxylated metabolite (mass spectrum in **Figure 61** in Annex). The identification of metabolites was achieved by the comparison of retention times and mass spectra obtained from sample extracts with non-labeled authentic reference materials. The retention times of the per-TMS derivatives of the metabolites are given in **Table 41** (Annex). The proposed metabolic pathway is shown in **Figure 30**. It has been recognized that T and AED are interconvertible *in vivo* [42]. This may explain the high amount of AED detected after incubation. As described by Schänzer *et al.*, Etio

and EA are the main excreted metabolites detected in routine urine samples for drug testing [38].

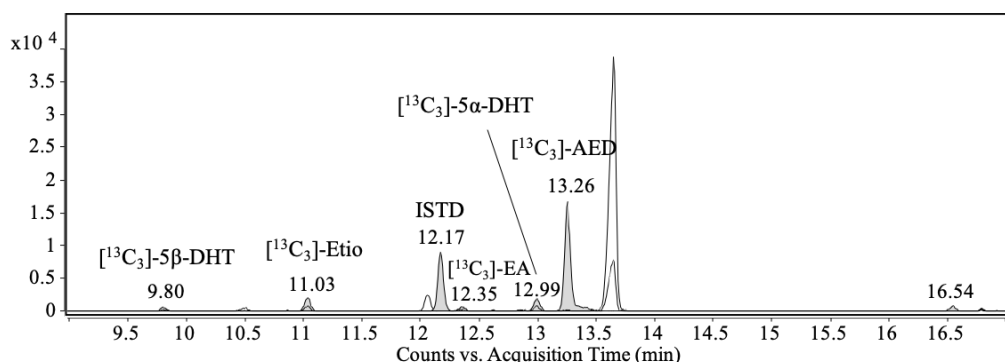


Figure 29: Overlay of EICs in GC-EI-MS after TMIS derivatization showing seven main products after 2-day incubation of medaka embryos with $[^{13}\text{C}_3]$ -T: $[^{13}\text{C}_3]$ -5 β -DHT (RT 9.80 min; EIC m/z 437), DHEA- d_6 (ISTD, RT 12.17 min; EIC m/z 438), $[^{13}\text{C}_3]$ -Etio (RT 11.03 min; EIC m/z 437), $[^{13}\text{C}_3]$ -EA (RT 12.35 min; EIC m/z 437), $[^{13}\text{C}_3]$ -5 α -DHT (RT 12.99 min; EIC m/z 437), $[^{13}\text{C}_3]$ -AED (13.26 min; EIC m/z 433), and $[^{13}\text{C}_3]$ -hydroxylated product (unidentified, RT 16.54 min; EIC m/z 521)

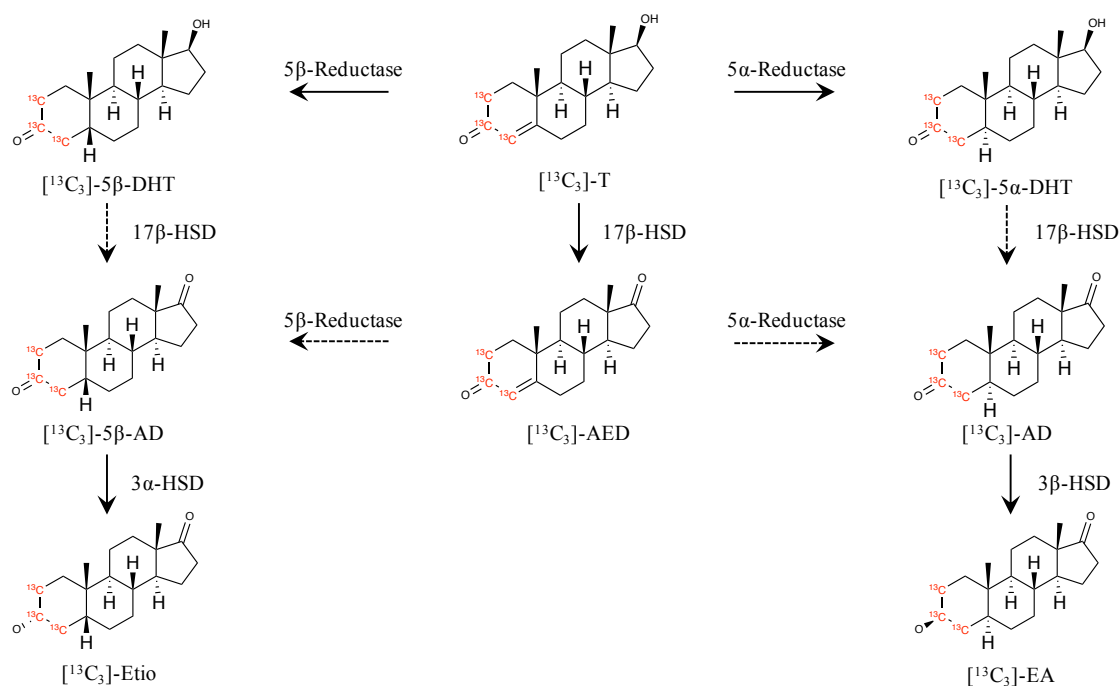


Figure 30: Proposed pathway of $[^{13}\text{C}_3]$ -T metabolism in medaka embryos; the dotted arrows indicate that the compounds were not detected in the incubation of medaka embryos with $[^{13}\text{C}_3]$ -T; AD, androstanedione (5 α -androstane-3,17-dione); 5 β -AD, 5 β -androstanedione (5 β -androstane-3,17-dione)

Figure 31 displays the chromatogram of the sample obtained after medaka embryo incubation with MT in GC-EI-MS analysis. Similar to $[^{13}\text{C}_3]$ -T, A-ring reductions were also observed in MT incubation. However, no oxidation reaction occurred at position 17 due to the presence of 17 α -methyl. The biotransformation of MT in medaka embryos resulted in the formation of five metabolites, including two mono-reduced metabolites,

17 β -hydroxy-17 α -methyl-5 β -androstane-3-one (5 β -mestanolone, 5 β -MSL) (mass spectrum in **Figure 62** in Annex) and MSL (mass spectrum in **Figure 66** in Annex), as well as three di-reduced metabolites, 3 β ,5 α -THMT (mass spectrum in **Figure 65** in Annex), 3 α ,5 β -THMT (mass spectrum in **Figure 64** in Annex), and 3 ξ ,5 ξ -THMT (mass spectrum in **Figure 63** in Annex). Due to the low-level abundance and the close retention time of 3 α ,5 α -THMT and 3 β ,5 β -THMT, the confirmation of the stereochemistry of 3 ξ ,5 ξ -THMT is not possible. Other compounds were identified by the comparison of retention time and mass spectra obtained from sample extracts with reference materials. No hydroxylated metabolites were observed in MT incubation. The metabolites were identified by comparison with authentic reference materials. 3 α ,5 β -THMT is one of the main metabolites of MT monitored by doping control laboratories and has a long detection window [93, 183]. The retention times of the per-TMS derivatives of the metabolites are given in **Table 42** (Annex). The main proposed metabolic pathway is shown in **Figure 32**.

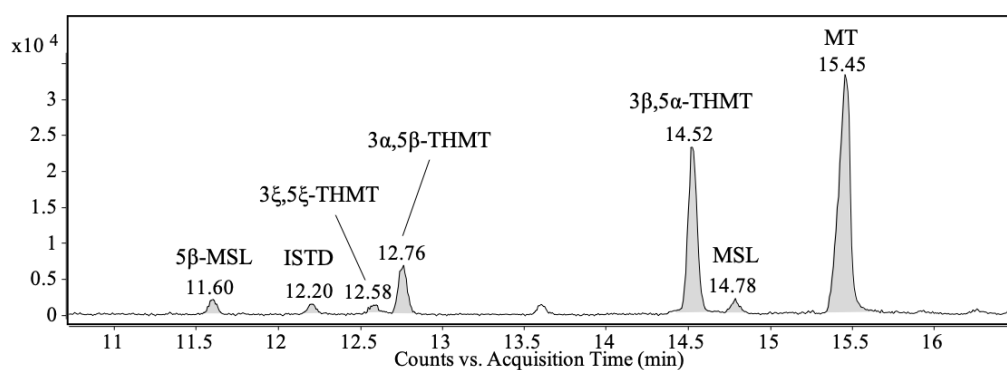


Figure 31: GC-EI-MS chromatogram (EIC m/z 143) after TMIS derivatization showing seven main products after 2-day incubation of medaka embryos with MT. 5 β -MSL (RT 11.60 min), DHEA- d_6 (ISTD, RT 12.20 min), 3 ξ ,5 ξ -THMT (RT 12.58 min), 3 α ,5 β -THMT (RT 12.76 min), 3 β ,5 α -THMT (RT 14.52 min), MSL (14.78 min), and MT (RT 15.45 min)

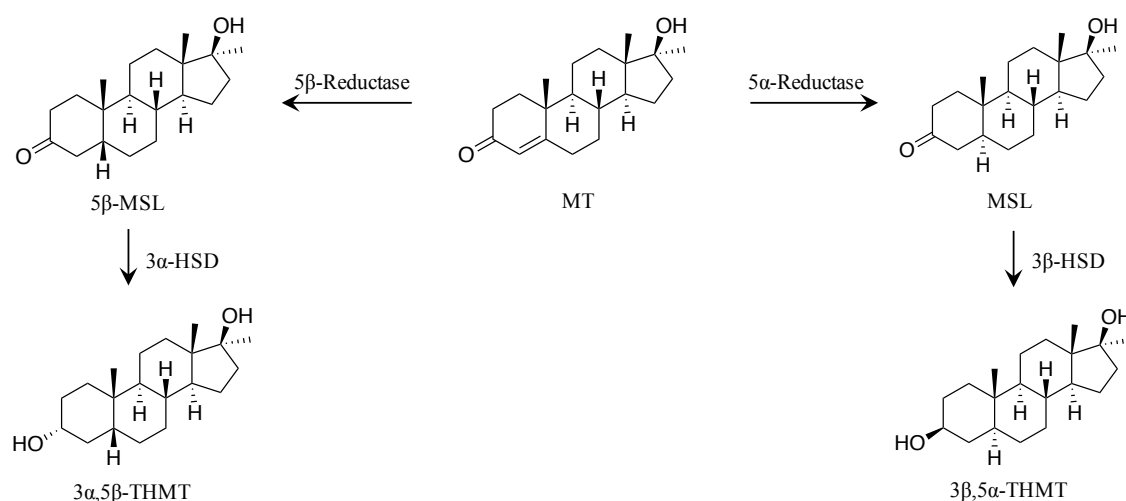


Figure 32: Main proposed pathway of MT metabolism in medaka embryos

In contrast to the medaka embryo incubations with MD, there are very few hydroxylation reactions occurring with [$^{13}\text{C}_3$]-T and MT. This may be attributed to the formation of tissues and organs at different development stages of medaka embryos. The liver as the main metabolizing organ is formed between day 2 and 4 of embryonic development [184], but it is not known when the full metabolic capacity is established. As stressed in chapter 4.4.1, the hydroxylated metabolites of MD first appeared during the incubation from 6 to 8 dpf, however, the exposure of [$^{13}\text{C}_3$]-T and MT was performed from 5 to 7 dpf. Based on the metabolites detected after the incubations, the dominant enzymes involved in the metabolic reactions include steroid 5 α /5 β -reductases, 3 α /3 β -HSDs as well as 17 β -HSD. As discussed in chapter 4.2 and chapter 4.3.2, steroids with a 4-ene-3-one structure have been considered to undergo a sequential reduction catalyzed by steroid 5 α - or 5 β - reductases to produce 5 α - or 5 β -dihydrosteroids, followed by the 3-oxo reduction to produce a series of isomeric tetrahydrosteroids [28]. The absence of metabolites with 4-ene-3 α / β -hydroxy structure substantiates the consistency of the reduction sequence observed in this study with the previous research findings. Among the four isomeric tetrahydro-metabolites, 3 β ,5 α - and 3 α ,5 β -isomers are the main metabolites detected in both [$^{13}\text{C}_3$]-T and MT incubations **Figure 33**. However, the fully reduced metabolites of MT mostly detected in humans are 3 α 5 α -THMT and 3 α 5 β -THMT [118]. According to Steckelbroeck *et al.*, AKR1C subfamily members display different preferences for the stereoselectivity of 3-oxo group reduction [34], which has also been supported by the enzyme incubation studies in chapter 4.2 to some extent. Therefore, the differences in THMT diastereoisomers observed in medaka embryo incubations and human urinary samples may be due to the varying levels of AKR1Cs enzyme expression.

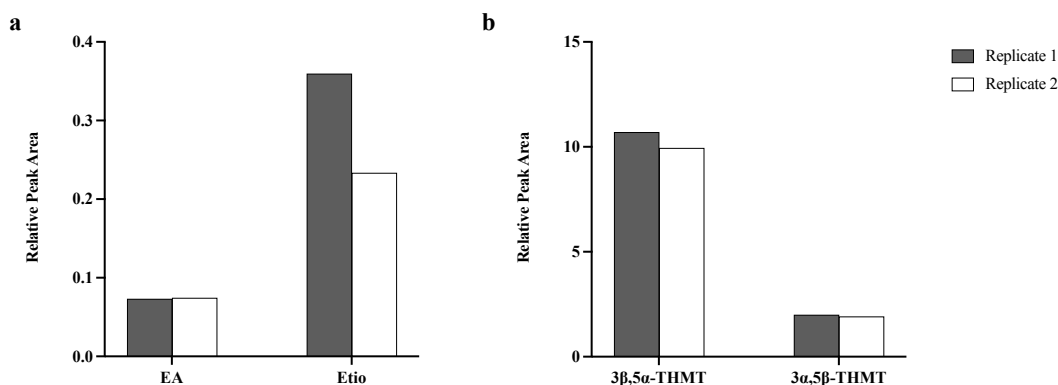


Figure 33: The peak area (relative to the internal standard (DHEA- d_6 ; EIC m/z 438)) (GC-EI-MS) of (a) EA (EIC m/z 437) and Etio (EIC m/z 437) detected in sample extracts obtained after 2-day incubation of medaka embryos (strain *d-rR.YHNI*) with 20 μM [$^{13}\text{C}_3$]-T, (b) 3 β ,5 α -THMT (EIC m/z 143) and 3 α ,5 β -THMT (EIC m/z 143) detected in sample extracts obtained after 2-day incubation of medaka embryos (strain *d-rR.YHNI*) with 20 μM MT, two technical replicates under fully sterile conditions

Moreover, it is worthy to note that compounds with a 1,2-double bond were detected in both incubations, which is not common in the metabolism of T and MT. There is no known enzyme in humans that catalyzes this dehydrogenation reaction, while many bacteria species possess enzyme systems responsible for catalyzing this reaction, such as the strain *Rhodococcus eryth.* [185, 186]. It is unclear whether this reaction was catalyzed by the embryos or contaminating bacteria. Therefore, medaka embryos were then exposed under sterile conditions to MT through autoclavation of the embryo-rearing medium and/or sterilization of the chorion. In the sample extracts obtained from the incubation after both medium and embryo sterilization, MD was not detectable in most of the samples, with the exception of one sample. However, the repetition of the experiments showed consistent results, in which MD was absent in all samples. In contrast, MD was detected to varying degrees in samples obtained from the incubation after the sterilization of either the embryos or the rearing medium. This may be attributed to the uncertainties of the amounts and activity of the bacteria among different incubations. The results indicate that the dehydrogenation of the 1,2-double bond was most likely catalyzed by contaminating bacteria from either the embryos or the rearing medium.

Although the presence of bacteria in the incubation system may result in the formation of C1,2-dehydrogenated products, the main metabolites detected after the incubation under varying degrees of sterility are identical, with only slight differences in abundance. However, to obtain consistent results in further studies, it is necessary to conduct experiments under sterile conditions.

5 Summary and Outlook

The knowledge of drug metabolism is fundamental for scientific fields where a comprehensive understanding of steroid metabolism is of high relevance, including but not only limited to anti-doping studies, endocrinology, forensic toxicology, and safety assessment in drug development. This work concentrates on the metabolism of anabolic androgenic steroids (AAS) in both *in vivo* and *in vitro* models, with a specific focus on the AAS compounds testosterone (T), metandienone (MD), methyltestosterone (MT), clostebol (CLT), dehydrochloromethyltestosterone (DHCMT), and methylclostebol (CLMT) due to their structural similarities. It introduces new alternative models for studying AAS metabolism and provides valuable knowledge on metabolic properties based on chemical structural characteristics, offering the possibility for the enhancement of AAS detection.

Firstly, in order to have a deep understanding of the A-ring reduction in MD, isolated enzyme assays (AKR1C2, AKR1C3, AKR1C4, and AKR1D1) were performed. The results obtained substantiate the sequence of A-ring reduction in MD, as previously suggested in the literature [93, 136, 137], i.e., the 4,5-double bond is reduced first, then the 3-oxo group, and finally the 1,2-double bond. Moreover, it appears that AKR1C2, AKR1C3, and AKR1C4 exhibited varying stereoselectivity in catalyzing the 3-oxo reduction in 5 α - or 5 β -DHMD. AKR1C2 and AKR1C4 showed both 3 α - and 3 β -HSD activities, whereas AKR1C3 functioned as 3 α -HSD only. The sequence of A-ring reduction provided valuable insights for the metabolic pathway analysis for subsequent *in vitro* studies in human skin cells.

The metabolism of T, MT, CLT, and CLMT by keratinocytes and fibroblasts derived from human foreskins produced metabolites with partially or fully reduced A-ring. However, no metabolites of MD or DHCMT could be detected. The metabolite profiles suggest that 3 α -HSD, 3 β -HSD, and 5 α -reductase activities play important roles in steroid metabolism by human keratinocytes and fibroblasts, whereas 17 β -HSD activity is weak. The stereochemistry of fully reduced metabolites (i.e., 3 α ,4 α ,5 α -THCLT, 3 β ,4 α ,5 α -THCLT, 3 α ,4 α ,5 α -THCLMT, and 3 β ,4 α ,5 α -THCLMT) of CLT and CLMT was newly identified and confirmed in this study. Differences in the chemical structures of compounds appear to affect A-ring reduction order and cellular metabolic capacities, especially the chlorine group at position 4. Keratinocytes appear to have a higher

metabolic capability for compounds containing a chlorine substituent in position 4, whereas the opposite is true in fibroblasts.

The medaka embryo model was used for the first time as an alternative model for *in vivo* studies of AAS. There were four metabolites detected after incubation of medaka embryos with MD, including 6 β OH-MD and 5 β -DHMD as well as tentatively assigned 18OH-MD and 16OH-MD. These metabolites have also been reported in previous human administration studies [136, 177, 180]. In comparison to the *in vitro* models, the medaka embryo model allows for simultaneous analysis of biotransformation and potential toxicity. Given the similar outcomes with human administration studies, medaka embryos may serve as an alternative model to identify potential metabolites for human biotransformation of doping-relevant compounds.

Investigations on the metabolism of [$^{13}\text{C}_3$]-T and MT in the medaka embryo model show that the main metabolic reactions for both two substrates include hydrogenation of the 4,5-double bond and reduction of the 3-oxo function. Additionally, the oxidation of 17 β -hydroxy group in [$^{13}\text{C}_3$]-T was also observed. The metabolites observed indicate the activities of steroid 5 α -reductases, steroid 5 β -reductases, 3 α -HSD, 3 β -HSD, and 17 β -HSD in medaka embryos. 3 β ,5 α - and 3 α ,5 β -isomers were detected as the main fully reduced A-ring metabolites in both incubations. However, this study only showed preliminary results, further studies are necessary.

In conclusion, appropriate *in vivo* and *in vitro* models were evaluated and used for metabolic studies of AAS. The findings presented in this thesis hold significant implications not only for doping control analysis, but also for other scientific areas where a comprehensive understanding of steroid metabolism is highly relevant, such as endocrinology, forensic toxicology, and safety assessment in drug development.

Further studies may focus on the refinement of the metabolic models. As the skin cells were isolated from the human foreskin (from the medically indicated circumcision of boys younger than 10 years), biases of the results due to sex, age, and race (Caucasians) might be present. Therefore, it would be valuable to study the metabolism in other sources of human skin cells, which may provide a more comprehensive elucidation of AAS metabolism in the skin. Moreover, the incorporation of a larger number of donors or the utilization of a pooled cell model derived from different donors may also be taken into consideration to minimize the individual variations of metabolism.

In addition, similar to the human skin cell model, it is worthy to further investigate the metabolism of AAS in the medaka embryo model using additional structurally related

compounds. Moreover, as only non-conjugated compounds were studied in this work, the analysis of intact phase II metabolites generated by medaka embryos can also be considered for further investigation. This may contribute to a more comprehensive understanding of the metabolic pathways of AAS in humans.

6 Zusammenfassung und Ausblick

Die Kenntnis des Wirkstoffmetabolismus ist von grundlegender Bedeutung für wissenschaftliche Bereiche, in denen ein umfassendes Verständnis des Steroidstoffwechsels von großer Relevanz ist, z. B. für Anti-Doping-Studien, die Endokrinologie, die forensische Toxikologie und die Sicherheitsbewertung bei der Arzneimittelentwicklung. Diese Arbeit konzentriert sich auf die Untersuchung des Metabolismus von anabolen androgenen Steroiden (AAS) sowohl in *in vivo*- als auch in *in vitro*-Modellen, wobei der Schwerpunkt auf den Verbindungen Testosteron (T), Metandienon (MD), Methyltestosteron (MT), Clostebol (CLT), Dehydrochlormethyltestosteron (DHCMT) und Methylclostebol (CLMT) liegt. Es werden neue alternative Modelle für die Untersuchung des AAS-Stoffwechsels vorgestellt und wertvolle Erkenntnisse über die metabolischen Eigenschaften auf der Grundlage der chemischen Strukturmerkmale gewonnen, die eine Verbesserung des AAS-Nachweises ermöglichen.

Um ein tieferes Verständnis der A-Ring-Reduktion in MD zu erhalten, wurden zunächst Tests mit isolierten Enzymen (AKR1C2, AK1C3, ALR1C4 und AKR1D1) durchgeführt. Die erzielten Ergebnisse bestätigen die Reihenfolge der A-Ring-Reduktion in MD, wie sie zuvor in der Literatur vorgeschlagen wurde [93, 136, 137], d.h. zuerst wird die 4,5-Doppelbindung reduziert, dann die 3-Oxo-Gruppe und schließlich die 1,2-Doppelbindung. Außerdem scheinen AKR1C2, AKR1C3 und AKR1C4 eine unterschiedliche Stereoselektivität bei der Katalyse der 3-Oxo-Reduktion in 5 α - oder 5 β -DHMD aufzuweisen. AKR1C2 und AKR1C4 zeigten sowohl 3 α - als auch 3 β -HSD-Aktivitäten, während AKR1C3 nur als 3 α -HSD fungierte. Die Sequenz der A-Ring-Reduktion lieferte wertvolle Erkenntnisse für die Analyse der Stoffwechselwege für nachfolgende *in vitro*-Studien in menschlichen Hautzellen.

Der Metabolismus von T, MT, CLT und CLMT durch Keratinozyten und Fibroblasten aus menschlicher Vorhaut produzierte Produkte mit teilweise oder vollständig reduziertem A-Ring. Es konnten jedoch keine Metabolite von MD oder DHCMT nachgewiesen werden. Die Metabolitenprofile deuten darauf hin, dass 3 α -HSD-, 3 β -HSD- und 5 α -Reduktase-Aktivitäten eine wichtige Rolle beim Steroidmetabolismus durch menschliche Keratinozyten und Fibroblasten spielen, während die 17 β -HSD-Aktivität gering war. Die Stereochemie der vollständig reduzierten Produkten (d. h.

3 α ,4 α ,5 α -THCLT, 3 β ,4 α ,5 α -THCLT, 3 α ,4 α ,5 α -THCLMT und 3 β ,4 α ,5 α -THCLMT) von CLT und CLMT wurde in dieser Studie neu identifiziert und bestätigt. Unterschiede in den chemischen Strukturen der Verbindungen scheinen die Reihenfolge der A-Ring-Reduktion und die zellulären Stoffwechsellkapazitäten zu beeinflussen, insbesondere die Gegenwart eines Chlorsubstituenten an Position 4. Keratinozyten scheinen eine höhere Stoffwechselfähigkeit für Verbindungen mit derartigen Chlorsubstituenten zu haben, während bei Fibroblasten das Gegenteil der Fall ist.

In dieser Arbeit wurde das Medaka-Embryo-Modell zum ersten Mal als alternatives Modell für *in vivo*-Studien von AAS verwendet. Nach der Inkubation von Medaka-Embryonen mit MD wurden vier Metaboliten nachgewiesen, darunter 6 β OH-MD und 5 β -DHMD, zusätzlich wurden 18OH-MD und 16OH-MD anhand ihrer Fragmentierung identifiziert und postuliert. Diese Metaboliten wurden auch in früheren Studien zur Verabreichung an den Menschen festgestellt [136, 177, 180]. Im Vergleich zu den *in vitro*-Modellen ermöglicht das Medaka-Embryo-Modell eine gleichzeitige Untersuchung der Biotransformation und der potenziellen Toxizität. Angesichts der vergleichbaren Ergebnisse mit Studien zur Verabreichung beim Menschen könnten Medaka-Embryonen als alternatives Modell zur Identifizierung potenzieller Metaboliten für die Biotransformation von dopingrelevanten Verbindungen beim Menschen dienen.

Weitere Untersuchungen zum Stoffwechsel von [¹³C₃]-T und MT im Medaka-Embryo-Modell zeigen, dass die wichtigsten Stoffwechselreaktionen für beide Substrate die Hydrierung der 4,5-Doppelbindung und die Reduktion der 3-Oxo-Funktion umfassen. Darüber hinaus wurde auch die Oxidation der 17 β -Hydroxygruppe bei [¹³C₃]-T beobachtet. Die beobachteten Metabolite weisen auf die Aktivitäten von Steroid-5 α -Reduktasen, Steroid-5 β -Reduktasen, 3 α -HSD, 3 β -HSD und 17 β -HSD in Medaka-Embryonen hin. 3 β ,5 α - und 3 α ,5 β -Isomere wurden als die wichtigsten vollständig reduzierten A-Ring-Metaboliten in beiden Inkubationen nachgewiesen. Diese Studie zeigte jedoch nur vorläufige Ergebnisse, weitere Studien sind notwendig.

Zusammenfassend kann festgestellt werden, daß geeignete *in vivo*- und *in vitro*-Modelle evaluiert und für Stoffwechselstudien von AAS verwendet wurden. Die in dieser Arbeit vorgestellten Ergebnisse sind nicht nur für die Dopingkontrollanalyse von Bedeutung, sondern auch für andere wissenschaftliche Bereiche, in denen ein umfassendes Verständnis des Steroidstoffwechsels von großer Bedeutung ist, z. B. für die Endokrinologie, die forensische Toxikologie und die Sicherheitsbewertung bei der Arzneimittelentwicklung.

Anschließende Studien könnten sich auf die Verfeinerung der Stoffwechselmodelle konzentrieren. Da die Hautzellen aus der menschlichen Vorhaut isoliert wurden (aus der medizinisch indizierten Beschneidung von Jungen, die jünger als 10 Jahre sind), gibt es mögliche Verzerrungen der Ergebnisse hinsichtlich Geschlecht, Alter und Rasse (Kaukasier). Daher wäre es wertvoll, den Stoffwechsel in verschiedenen verfügbaren Quellen menschlicher Hautzellen zu untersuchen, was eine umfassendere Aufklärung des AAS-Stoffwechsels in der Haut ermöglichen würde. Darüber hinaus könnte auch die Einbeziehung einer größeren Anzahl von Spendern oder die Verwendung eines gepoolten Zellmodells, das von verschiedenen Spendern stammt, in Betracht gezogen werden, um die individuellen Schwankungen des Stoffwechsels zu minimieren.

Ähnlich wie beim menschlichen Hautzellmodell ist es außerdem lohnenswert, den Metabolismus von AAS im Medaka-Embryo-Modell unter Verwendung zusätzlicher strukturell verwandter Verbindungen weiter zu untersuchen. Da in dieser Arbeit nur nicht konjugierte Verbindungen untersucht wurden, kann die Analyse von intakten Phase-II-Metaboliten, die von Medaka-Embryonen erzeugt werden, für weitere Untersuchungen in Betracht gezogen werden. Dies könnte zu einem umfassenderen Verständnis der Stoffwechselwege von AAS beim Menschen beitragen.

7 References

- [1] Fraser AD. Doping control from a global and national perspective. *Ther Drug Monit* 26 (2004) 171-174
- [2] Botre F. New and old challenges of sports drug testing. *J Mass Spectrom* 43 (2008) 903-907
- [3] Bowers LD. Anti-dope testing in sport: the history and the science. *Faseb J* 26 (2012) 3933-3936
- [4] World Anti-Doping Code. World Anti-Doping Agency. 2021. <https://www.wada-ama.org/en/resources/world-anti-doping-program/world-anti-doping-code>
- [5] Parr MK, Schänzer W. Detection of the misuse of steroids in doping control. *J Steroid Biochem Mol Biol* 121 (2010) 528-537
- [6] WADA Prohibited List. World Anti-Doping Agency. 2023. (accessed on 2023.08.22). <https://www.wada-ama.org/en/prohibited-list>
- [7] International Standard for Results Management (ISRM) 2023. World Anti-Doping Agency. 2023. (accessed on 2023.09.13). https://www.wada-ama.org/sites/default/files/2023-01/international_standard_isrm_-_abp_update_2023_final_0.pdf
- [8] Schiffer L, Barnard L, Baranowski ES, Gilligan LC, Taylor AE, Arlt W, Shackleton CHL, Storbeck KH. Human steroid biosynthesis, metabolism and excretion are differentially reflected by serum and urine steroid metabolomes: A comprehensive review. *J Steroid Biochem Mol Biol* 194 (2019) 105439
- [9] Joseph JF, Parr MK. Synthetic androgens as designer supplements. *Curr Neuropharmacol* 13 (2015) 89-100
- [10] Mosa A, Neunzig J, Gerber A, Zapp J, Hannemann F, Pilak P, Bernhardt R. 2beta- and 16beta-hydroxylase activity of CYP11A1 and direct stimulatory effect of estrogens on pregnenolone formation. *J Steroid Biochem Mol Biol* 150 (2015) 1-10
- [11] Rasheed A, Qasim M. A review of natural steroids and their applications. *International Journal of Pharmaceutical Sciences and Research* 4 (2013) 520
- [12] Sanderson JT. The steroid hormone biosynthesis pathway as a target for endocrine-disrupting chemicals. *Toxicol Sci* 94 (2006) 3-21

-
- [13] Bernhardt R. Cytochromes P450 as versatile biocatalysts. *J Biotechnol* 124 (2006) 128-145
- [14] Zollner A, Buchheit D, Meyer MR, Maurer HH, Peters FT, Bureik M. Production of human phase 1 and 2 metabolites by whole-cell biotransformation with recombinant microbes. *Bioanalysis* 2 (2010) 1277-1290
- [15] Schumacher SD, Jose J. Expression of active human P450 3A4 on the cell surface of *Escherichia coli* by Autodisplay. *J Biotechnol* 161 (2012) 113-120
- [16] Pikuleva IA, Waterman MR. Cytochromes p450: roles in diseases. *J Biol Chem* 288 (2013) 17091-17098
- [17] Achour B, Barber J, Rostami-Hodjegan A. Expression of hepatic drug-metabolizing cytochrome p450 enzymes and their intercorrelations: a meta-analysis. *Drug Metab Dispos* 42 (2014) 1349-1356
- [18] Durairaj P, Fan L, Du W, Ahmad S, Mebrahtu D, Sharma S, Ashraf RA, Liu J, Liu Q, Bureik M. Functional expression and activity screening of all human cytochrome P450 enzymes in fission yeast. *FEBS Lett* 593 (2019) 1372-1380
- [19] Joseph JF. Metabolism of androstane derivatives with focus on hydroxylation reactions. Freie Universitaet Berlin (Germany) (2016)
- [20] Penning TM. Human hydroxysteroid dehydrogenases and pre-receptor regulation: insights into inhibitor design and evaluation. *J Steroid Biochem Mol Biol* 125 (2011) 46-56
- [21] Savill R, Baues H, Voigt E, Zierau O, Thieme D, Keiler AM. Cell culture as a toolbox to generate phase I metabolites for antidoping screening. *Drug Test Anal* 13 (2021) 1169-1177
- [22] Penning TM, Wangtrakuldee P, Auchus RJ. Structural and Functional Biology of Aldo-Keto Reductase Steroid-Transforming Enzymes. *Endocr Rev* 40 (2019) 447-475
- [23] Simard J, Ricketts ML, Gingras S, Soucy P, Feltus FA, Melner MH. Molecular biology of the 3beta-hydroxysteroid dehydrogenase/delta5-delta4 isomerase gene family. *Endocr Rev* 26 (2005) 525-582
- [24] Lorence MC, Murry BA, Trant JM, Mason JI. Human 3 beta-hydroxysteroid dehydrogenase/delta 5→4 isomerase from placenta: expression in nonsteroidogenic cells of a protein that catalyzes the dehydrogenation/isomerization of C21 and C19 steroids. *Endocrinology* 126 (1990) 2493-2498

- [25] Luu-The V, Zhang Y, Poirier D, Labrie F. Characteristics of human types 1, 2 and 3 17 beta-hydroxysteroid dehydrogenase activities: oxidation/reduction and inhibition. *J Steroid Biochem Mol Biol* 55 (1995) 581-587
- [26] Penning TM, Jin Y, Heredia VV, Lewis M. Structure-function relationships in 3alpha-hydroxysteroid dehydrogenases: a comparison of the rat and human isoforms. *J Steroid Biochem Mol Biol* 85 (2003) 247-255
- [27] Penning TM, Burczynski ME, Jez JM, Hung CF, Lin HK, Ma H, Moore M, Palackal N, Ratnam K. Human 3alpha-hydroxysteroid dehydrogenase isoforms (AKR1C1-AKR1C4) of the aldo-keto reductase superfamily: functional plasticity and tissue distribution reveals roles in the inactivation and formation of male and female sex hormones. *Biochem J* 351 (2000) 67-77
- [28] Penning TM, Chen M, Jin Y. Promiscuity and diversity in 3-ketosteroid reductases. *J Steroid Biochem Mol Biol* 151 (2015) 93-101
- [29] Seo KS, Naidansuren P, Kim SH, Yun SJ, Park JJ, Sim BW, Park CW, Nanjidsuren T, Kang MH, Seo H, Ka H, Kim NH, Hwang SY, Yoon JT, Yamanouchi K, Min KS. Expression of aldo-keto reductase family 1 member C1 (AKR1C1) gene in porcine ovary and uterine endometrium during the estrous cycle and pregnancy. *Reprod Biol Endocrinol* 9 (2011) 139
- [30] Dufort I, Labrie F, Luu-The V. Human types 1 and 3 3 alpha-hydroxysteroid dehydrogenases: differential lability and tissue distribution. *J Clin Endocrinol Metab* 86 (2001) 841-846
- [31] Khanna M, Qin KN, Wang RW, Cheng KC. Substrate specificity, gene structure, and tissue-specific distribution of multiple human 3 alpha-hydroxysteroid dehydrogenases. *J Biol Chem* 270 (1995) 20162-20168
- [32] Fung KM, Samara EN, Wong C, Metwalli A, Krlin R, Bane B, Liu CZ, Yang JT, Pitha JV, Culkin DJ, Kropp BP, Penning TM, Lin HK. Increased expression of type 2 3alpha-hydroxysteroid dehydrogenase/type 5 17beta-hydroxysteroid dehydrogenase (AKR1C3) and its relationship with androgen receptor in prostate carcinoma. *Endocr Relat Cancer* 13 (2006) 169-180
- [33] Yepuru M, Wu Z, Kulkarni A, Yin F, Barrett CM, Kim J, Steiner MS, Miller DD, Dalton JT, Narayanan R. Steroidogenic enzyme AKR1C3 is a novel androgen receptor-selective coactivator that promotes prostate cancer growth. *Clin Cancer Res* 19 (2013) 5613-5625

- [34] Steckelbroeck S, Jin Y, Gopishetty S, Oyesanmi B, Penning TM. Human cytosolic 3 α -hydroxysteroid dehydrogenases of the aldo-keto reductase superfamily display significant 3 β -hydroxysteroid dehydrogenase activity: implications for steroid hormone metabolism and action. *J Biol Chem* 279 (2004) 10784-10795
- [35] Weldon SM, Brown NF. Inhibitors of Aldosterone Synthase. *Vitam Horm* 109 (2019) 211-239
- [36] Stoll A. Investigations on Phase I Metabolism of Anabolic Androgenic Steroids and Its Influenceability as Tool to Refine Steroid Detection and Evaluation. Freie Universitaet Berlin (Germany) (2021)
- [37] Loke S. Optimizing the Process of Introducing New Metabolites of Anabolic-Androgenic Steroids–Method Evaluation, Synthesis, Verification. Freie Universitaet Berlin (Germany) (2021)
- [38] Schänzer W. Metabolism of anabolic androgenic steroids. *Clin Chem* 42 (1996) 1001-1020
- [39] Mazzeo F. Anabolic steroid use in sports and in physical activity: overview and analysis. *Sport Mont* 16 (2018) 113-118
- [40] Slaunwhite Jr WR, Sandberg AA. Metabolism of 4-C¹⁴-testosterone in human subjects III. Fate of androsterone and etiocholanolone. *The Journal of Clinical Endocrinology & Metabolism* 18 (1958) 1056-1066
- [41] Baulieu E-E, Mauvais-Jarvis P. Studies on testosterone metabolism. I. Conversion of testosterone-17- α -3h to 5- α - and 5- β -androstane-3- α , 17- β -deol-17- α -3h: a new “17- β -hydroxyl pathway”. *J Biol Chem* 239 (1964) 1569-1577
- [42] Baulieu EE, Mauvais-Jarvis P. Studies on testosterone metabolism: II. Metabolism of Testosterone-4-¹⁴C and androst-4-ene-3, 17-dione-1, 2-³H. *J Biol Chem* 239 (1964) 1578-1584
- [43] Gomez EC, Hsia SL. In vitro metabolism of testosterone-4-¹⁴C and delta-4-androstene-3,17-dione-4-¹⁴C in human skin. *Biochemistry* 7 (1968) 24-32
- [44] Mauvais-Jarvis P, Floch HH, Bercovici JP. Studies on testosterone metabolism in human subjects with normal and pathological sexual differentiation. *J Clin Endocrinol Metab* 28 (1968) 460-471
- [45] Deslypere JP, Wiers PW, Sayed A, Vermeulen A. Urinary excretion of androgen metabolites, comparison with excretion of radioactive metabolites after injection

- of [4-14C]testosterone. Influence of age. *Acta Endocrinol (Copenh)* 96 (1981) 265-272
- [46] Penning TM. New frontiers in androgen biosynthesis and metabolism. *Curr Opin Endocrinol Diabetes Obes* 17 (2010) 233-239
- [47] Escobar-Wilches DC, Ventura-Bahena A, De Lourdes Lopez-Gonzalez M, Torres-Sanchez L, Figueroa M, Sierra-Santoyo A. Analysis of testosterone-hydroxylated metabolites in human urine by ultra high performance liquid chromatography-Mass Spectrometry. *Anal Biochem* 597 (2020) 113670
- [48] Drury JE, Mindnich R, Penning TM. Characterization of disease-related 5beta-reductase (AKR1D1) mutations reveals their potential to cause bile acid deficiency. *J Biol Chem* 285 (2010) 24529-24537
- [49] Jin Y, Chen M, Penning TM. Rate of steroid double-bond reduction catalysed by the human steroid 5beta-reductase (AKR1D1) is sensitive to steroid structure: implications for steroid metabolism and bile acid synthesis. *Biochem J* 462 (2014) 163-171
- [50] Rizner TL, Penning TM. Role of aldo-keto reductase family 1 (AKR1) enzymes in human steroid metabolism. *Steroids* 79 (2014) 49-63
- [51] Jin Y, Penning TM. Steroid 5alpha-reductases and 3alpha-hydroxysteroid dehydrogenases: key enzymes in androgen metabolism. *Best Pract Res Clin Endocrinol Metab* 15 (2001) 79-94
- [52] Kumar T, Chaiyasut C, Rungsevijitprapa W, Suttajit M. Screening of steroid 5alpha-reductase inhibitory activity and total phenolic content of Thai plants. *J Med Plant Res* 5 (2011) 1265-1271
- [53] Brown TR. Androgen metabolism and action. *Male reproductive function* (1999) 65-84
- [54] Hutchison JB, Steimer T. Androgen metabolism in the brain: behavioural correlates. *Prog Brain Res* 61 (1984) 23-51
- [55] Fabregat A, Marcos J, Ventura R, Casals G, Jimenez W, Reichenbach V, Segura J, Pozo OJ. Formation of Delta(1) and Delta(6) testosterone metabolites by human hepatocytes. *Steroids* 95 (2015) 66-72
- [56] Monostory K, Dvorak Z. Steroid regulation of drug-metabolizing cytochromes P450. *Curr Drug Metab* 12 (2011) 154-172

-
- [57] Bredendiek F. Orthogonal Analytical Approaches for the Investigation of Specific Metabolic Pathways of 17 α -Methyltestosterone with the Focus on Hydroxylation Reactions. (2021)
- [58] Mazzarino M, Khevenhuller-Metsch FL, Fiacco I, Parr MK, De La Torre X, Botre F. Drug-drug interaction and doping: Effect of non-prohibited drugs on the urinary excretion profile of methandienone. *Drug Test Anal* 10 (2018) 1554-1565
- [59] Pozo OJ, Marcos J, Ventura R, Fabregat A, Segura J. Testosterone metabolism revisited: discovery of new metabolites. *Anal Bioanal Chem* 398 (2010) 1759-1770
- [60] 2021 Anti-Doping Testing Figures. World Anti-Doping Agency. 2021. (accessed on 2023.08.29). https://www.wada-ama.org/sites/default/files/2023-01/2021_anti-doping_testing_figures_en.pdf
- [61] 2020 Anti-Doping Testing Figures. World Anti-Doping Agency. 2020. (accessed on 2023.08.29). https://www.wada-ama.org/sites/default/files/2022-01/2020_anti-doping_testing_figures_en.pdf
- [62] 2019 Anti-Doping Testing Figures. World Anti-Doping Agency. 2019. (accessed on 2023.08.29). https://www.wada-ama.org/sites/default/files/resources/files/2019_anti-doping_testing_figures_en.pdf
- [63] 2018 Anti-Doping Testing Figures. World Anti-Doping Agency. 2018. (accessed on 2023.08.29). https://www.wada-ama.org/sites/default/files/resources/files/2018_testing_figures_report.pdf
- [64] 2017 Anti-Doping Testing Figures. World Anti-Doping Agency. 2017. (accessed on 2023.08.29). https://www.wada-ama.org/sites/default/files/resources/files/2017_anti-doping_testing_figures_en_0.pdf
- [65] 2016 Anti-Doping Testing Figures. World Anti-Doping Agency. 2016. (accessed on 2023.08.29). https://www.wada-ama.org/sites/default/files/resources/files/2016_anti-doping_testing_figures.pdf
- [66] 2015 Anti-Doping Testing Figures. World Anti-Doping Agency. 2015. (accessed on 2023.08.29). https://www.wada-ama.org/sites/default/files/resources/files/2015_wada_anti-doping_testing_figures_report_0.pdf

-
- [67] 2014 Anti-Doping Testing Figures. World Anti-Doping Agency. 2014. (accessed on 2023.08.29). https://www.wada-ama.org/sites/default/files/wada_2014_anti-doping-testing-figures_full-report_en.pdf
- [68] 2013 Anti-Doping Testing Figures. World Anti-Doping Agency. 2013. (accessed on 2023.08.29). https://www.wada-ama.org/sites/default/files/wada_2013_anti-doping_testing_figures_report_en.pdf
- [69] 2012 Anti-Doping Testing Figures. World Anti-Doping Agency. 2012. (accessed on 2023.08.29). <https://www.wada-ama.org/sites/default/files/resources/files/WADA-2012-Anti-Doping-Testing-Figures-Report-EN.pdf>
- [70] 2011 Laboratory Testing Figures. World Anti-Doping Agency. 2011. (accessed on 2023.08.29). <https://www.wada-ama.org/sites/default/files/resources/files/WADA-2011-Laboratory-Testing-Figures.pdf>
- [71] 2010 Adverse Analytical Findings and Atypical Findings World Anti-Doping Agency. 2010. (accessed on 2023.08.29). https://www.wada-ama.org/sites/default/files/resources/files/WADA_2010_Laboratory_Statistics_Report.pdf
- [72] 2009 Adverse Analytical Findings and Atypical Findings World Anti-Doping Agency. 2009. (accessed on 2023.08.29). https://www.wada-ama.org/sites/default/files/resources/files/WADA_2009_LaboratoryStatisticsReport_Final.pdf
- [73] 2008 Adverse Analytical Findings and Atypical Findings World Anti-Doping Agency. 2008. (accessed on 2023.08.29). https://www.wada-ama.org/sites/default/files/resources/files/WADA_LaboStatistics_2008.pdf
- [74] 2007 Adverse Analytical Findings Reported by Accredited Laboratories. World Anti-Doping Agency. 2007. (accessed on 2023.08.29). https://www.wada-ama.org/sites/default/files/resources/files/WADA_LaboStatistics_2007.pdf
- [75] 2006 Adverse Analytical Findings Reported by Accredited Laboratories. World Anti-Doping Agency. 2006. (accessed on 2023.08.29). https://www.wada-ama.org/sites/default/files/resources/files/WADA_LaboStatistics_2006.pdf

- [76] 2005 Adverse Analytical Findings Reported by Accredited Laboratories. World Anti-Doping Agency. 2005. (accessed on 2023.08.29). https://www.wada-ama.org/sites/default/files/resources/files/WADA_LaboStatistics_2005.pdf
- [77] 2004 Adverse Analytical Findings Reported by Accredited Laboratories. World Anti-Doping Agency. 2004. (accessed on 2023.08.29). https://www.wada-ama.org/sites/default/files/resources/files/WADA_LaboStatistics_2004.pdf
- [78] WADA Statistics 2003. World Anti-Doping Agency. 2003. (accessed on 2023.08.29). <https://www.nada.at/files/doc/Statistiken/WADA-Statistik-2003.pdf>
- [79] Hoffmann U. Anabolic steroids—a problem in popular sports. *Toxichem Krimtech* 69 (2002) 136-142
- [80] Skoupa K, Stastny K, Sladek Z. Anabolic Steroids in Fattening Food-Producing Animals-A Review. *Animals (Basel)* 12 (2022)
- [81] Parr MK, Flenker U, Schanzer W. Sports-related issues and biochemistry of natural and synthetic anabolic substances. *Endocrinol Metab Clin North Am* 39 (2010) 45-57, viii
- [82] Kicman AT, Houghton E, Gower DB. Anabolic steroids: Metabolism, doping and detection in human and equestrian sports. *Steroid Analysis* (2010) 743-836
- [83] Parr MK, Müller-Schöll A. Pharmacology of doping agents—mechanisms promoting muscle hypertrophy. *AIMS Molecular Science* 5 (2018) 131-159
- [84] Bird SR, Goebel C, Burke LM, Greaves RF. Doping in sport and exercise: anabolic, ergogenic, health and clinical issues. *Ann Clin Biochem* 53 (2016) 196-221
- [85] Fabregat A, Pozo OJ, Van Renterghem P, Van Eenoo P, Marcos J, Segura J, Ventura R. Detection of dihydrotestosterone gel, oral dehydroepiandrosterone, and testosterone gel misuse through the quantification of testosterone metabolites released after alkaline treatment. *Drug Test Anal* 3 (2011) 828-835
- [86] Kicman AT, Gower DB. Anabolic steroids in sport: biochemical, clinical and analytical perspectives. *Ann Clin Biochem* 40 (2003) 321-356
- [87] Graham MR, Davies B, Grace FM, Baker JS. Exercise, science and designer doping: Traditional and emerging trends. *J Sports Med Doping Stud* 2 (2012) 2161-0673.100011
- [88] Stojanovic BJ, Goschl L, Forsdahl G, Gunter G. Metabolism of steroids and sport drug testing. *Bioanalysis* 12 (2020) 561-563

- [89] George AJ. The actions and side effects of anabolic steroids in sport and social abuse. *Andrologie* 13 (2003) 354-366
- [90] Schänzer W, Geyer H, Fuschöller G, Halatcheva N, Kohler M, Parr MK, Guddat S, Thomas A, Thevis M. Mass spectrometric identification and characterization of a new long-term metabolite of metandienone in human urine. *Rapid Commun Mass Spectrom* 20 (2006) 2252-2258
- [91] Cole BC. *The East German sports system: Image and reality*, Texas Tech University, (2000)
- [92] Balcells G, Gomez C, Garrosta L, Pozo OJ, Ventura R. Sulfate metabolites as alternative markers for the detection of 4-chlorometandienone misuse in doping control. *Drug Test Anal* 9 (2017) 983-993
- [93] Loke S, Liu L, Wenzel M, Scheffler H, Iannone M, De La Torre X, Schlörer N, Botre F, Keiler AM, Bureik M, Parr MK. New Insights into the Metabolism of Methyltestosterone and Metandienone: Detection of Novel A-Ring Reduced Metabolites. *Molecules* 26 (2021)
- [94] Schänzer W, Opfermann G, Donike M. 17-Epimerization of 17 alpha-methyl anabolic steroids in humans: metabolism and synthesis of 17 alpha-hydroxy-17 beta-methyl steroids. *Steroids* 57 (1992) 537-550
- [95] Esquivel López A. Control of anabolic steroids misuse in sport: potential of direct detection of phase II metabolites. Universitat Pompeu Fabra (2018)
- [96] Stoll A, Loke S, Joseph JF, Machalz D, De La Torre X, Botre F, Wolber G, Bureik M, Parr MK. Fine-mapping of the substrate specificity of human steroid 21-hydroxylase (CYP21A2). *J Steroid Biochem Mol Biol* 194 (2019) 105446
- [97] Basaria S, Wahlstrom JT, Dobs AS. Clinical review 138: Anabolic-androgenic steroid therapy in the treatment of chronic diseases. *J Clin Endocrinol Metab* 86 (2001) 5108-5117
- [98] Albano GD, Amico F, Cocimano G, Liberto A, Maglietta F, Esposito M, Rosi GL, Di Nunno N, Salerno M, Montana A. Adverse Effects of Anabolic-Androgenic Steroids: A Literature Review. *Healthcare (Basel)* 9 (2021)
- [99] Patane FG, Liberto A, Maria Maglitta AN, Malandrino P, Esposito M, Amico F, Cocimano G, Rosi GL, Condorelli D, Nunno ND, Montana A. Nandrolone Decanoate: Use, Abuse and Side Effects. *Medicina (Kaunas)* 56 (2020)

- [100] Falqueto H, Dos Santos MR, Manfredi LH. Anabolic-Androgenic Steroids and Exercise Training: Breaking the Myths and Dealing With Better Outcome in Sarcopenia. *Front Physiol* 13 (2022) 838526
- [101] Arver S, Dobs AS, Meikle AW, Caramelli KE, Rajaram L, Sanders SW, Mazer NA. Long-term efficacy and safety of a permeation-enhanced testosterone transdermal system in hypogonadal men. *Clin Endocrinol (Oxf)* 47 (1997) 727-737
- [102] Donovitz GS. A Personal Prospective on Testosterone Therapy in Women-What We Know in 2022. *J Pers Med* 12 (2022)
- [103] De La Torre X, Colamonici C, Iannone M, Jardines D, Molaioni F, Botre F. Detection of clostebol in sports: Accidental doping? *Drug Test Anal* 12 (2020) 1561-1569
- [104] International Standard for Laboratories (ISL). World Anti-Doping Agency. 2021. <https://www.wada-ama.org/en/resources/world-anti-doping-program/international-standard-laboratories-isl>
- [105] WADA Technical Document – TD2023INDEX. World Anti-Doping Agency. 2023. https://www.wada-ama.org/sites/default/files/2023-02/td2023_index_v2.0_wada_technical_document_index_february_2023.pdf
- [106] Marcos J, Pascual JA, De La Torre X, Segura J. Fast screening of anabolic steroids and other banned doping substances in human urine by gas chromatography/tandem mass spectrometry. *J Mass Spectrom* 37 (2002) 1059-1073
- [107] Parr MK, Schanzer W. Detection of the misuse of steroids in doping control. *J Steroid Biochem Mol Biol* 121 (2010) 528-537
- [108] Pozo OJ, De Brabanter N, Fabregat A, Segura J, Ventura R, Van Eenoo P, Deventer K. Current status and bioanalytical challenges in the detection of unknown anabolic androgenic steroids in doping control analysis. *Bioanalysis* 5 (2013) 2661-2677
- [109] Donike M. N-methyl-N-trimethylsilyl-trifluoroacetamide a new silylating agent from series of silylated amides. *Journal of Chromatography* 42 (1969) 103
- [110] Piper T, Geyer H, Haenelt N, Huelsemann F, Schaenzer W, Thevis M. Current insights into the steroidal module of the athlete biological passport. *International Journal of Sports Medicine* 42 (2021) 863-878

- [111] Thevis M, Schanzer W. Mass spectrometry in sports drug testing: Structure characterization and analytical assays. *Mass Spectrom Rev* 26 (2007) 79-107
- [112] Fragkaki AG, Angelis YS, Tsantili-Kakoulidou A, Koupparis M, Georgakopoulos C. Statistical analysis of fragmentation patterns of electron ionization mass spectra of enolized-trimethylsilylated anabolic androgenic steroids. *Int J Mass Spectrom* 285 (2009) 58-69
- [113] Kollmeier AS, Parr MK. Mass spectral fragmentation analyses of isotopically labelled hydroxy steroids using gas chromatography/electron ionization low - resolution mass spectrometry: A practical approach. *Rapid Commun Mass Sp* 34 (2020) 0951-4198
- [114] Marcos J, Pozo OJ. Derivatization of steroids in biological samples for GC-MS and LC-MS analyses. *Bioanalysis* 7 (2015) 2515-2536
- [115] Balcells G, Gómez C, Garrosta L, Pozo ÓJ, Ventura R. Sulfate metabolites as alternative markers for the detection of 4 - chlorometandienone misuse in doping control. *Drug Test Anal* 9 (2017) 983-993
- [116] Esquivel A, Pozo OJ, Garrosta L, Balcells G, Gomez C, Kotronoulas A, Joglar J, Ventura R. LC-MS/MS detection of unaltered glucuronoconjugated metabolites of metandienone. *Drug Test Anal* 9 (2017) 534-544
- [117] Pozo OJ, Van Eenoo P, Van Thuyne W, Deventer K, Delbeke FT. Direct quantification of steroid glucuronides in human urine by liquid chromatography-electrospray tandem mass spectrometry. *J Chromatogr A* 1183 (2008) 108-118
- [118] Schänzer W, Donike M. Metabolism of anabolic steroids in man: synthesis and use of reference substances for identification of anabolic steroid metabolites. *Anal Chim Acta* 275 (1993) 23-48
- [119] Research Ethics Policy. World Anti-Doping Agency. 2014. <https://www.wada-ama.org/en/resources/research-ethics-policy>
- [120] Sanchini V, Devriendt T, Borry P. Anti-doping research and the Helsinki Declaration: (mis)match? *Account Res* 27 (2020) 179-194
- [121] Devriendt T, Sanchini V, Borry P. Ethics Review in Anti-Doping Research: Experiences of Stakeholders. *AJOB Empir Bioeth* 11 (2020) 125-133
- [122] Tannenbaum J, Bennett BT. Russell and Burch's 3Rs then and now: the need for clarity in definition and purpose. *Journal of the American association for laboratory animal science* 54 (2015) 120-132

- [123] Klipper WA. Biotransformation Capacity of Reconstructed Human Skin versus Human Skin ex vivo—analysing Prednicarbate and Testosterone as Example. *Freie Universität Berlin, Berlin* (2013)
- [124] Svensson CK. Biotransformation of drugs in human skin. *Drug Metab Dispos* 37 (2009) 247-253
- [125] Münster U, Hammer S, Blume-Peytavi U, Schäfer-Korting M. Testosterone metabolism in human skin cells in vitro and its interaction with estradiol and dutasteride. *Skin Pharmacol Appl Skin Physiol* 16 (2003) 356-366
- [126] Lleras-Forero L, Winkler C, Schulte-Merker S. Zebrafish and medaka as models for biomedical research of bone diseases. *Developmental biology* 457 (2020) 191-205
- [127] Sardela VF, Anselmo CS, Nunes I, Carneiro GRA, Dos Santos GRC, De Carvalho AR, Labanca BJ, Silva Oliveira D, Ribeiro WD, De Araujo ALD, Padilha MC, De Lima CKF, De Sousa VP, De Aquino Neto FR, Gualberto Pereira HM. Zebrafish (*Danio rerio*) water tank model for the investigation of drug metabolism: Progress, outlook, and challenges. *Drug Test Anal* 10 (2018) 1657-1669
- [128] De Souza Anselmo C, Sardela VF, Matias BF, De Carvalho AR, De Sousa VP, Pereira HMG, De Aquino Neto FR. Is zebrafish (*Danio rerio*) a tool for human-like metabolism study? *Drug Test Anal* 9 (2017) 1685-1694
- [129] Strähle U, Scholz S, Geisler R, Greiner P, Hollert H, Rastegar S, Schumacher A, Selderslaghs I, Weiss C, Witters H. Zebrafish embryos as an alternative to animal experiments—a commentary on the definition of the onset of protected life stages in animal welfare regulations. *Reproductive Toxicology* 33 (2012) 128-132
- [130] Van Wijk RC, Hu W, Dijkema SM, Van Den Berg DJ, Liu J, Bahi R, Verbeek FJ, Simonsson USH, Spaink HP, Van Der Graaf PH, Krekels EHJ. Anti-tuberculosis effect of isoniazid scales accurately from zebrafish to humans. *Br J Pharmacol* 177 (2020) 5518-5533
- [131] Union E. Directive 2010/63/EU on the protection of animals used for scientific purposes. *Official Journal of the European Union* L276(33) (2010)
- [132] Naruse K, Tanaka M, Mita K, Shima A, Postlethwait J, Mitani H. A medaka gene map: the trace of ancestral vertebrate proto-chromosomes revealed by comparative gene mapping. *Genome Res* 14 (2004) 820-828

- [133] Scholz S, Rosler S, Schaffer M, Hornung U, Scharl M, Gutzeit HO. Hormonal induction and stability of monosex populations in the medaka (*Oryzias latipes*): expression of sex-specific marker genes. *Biol Reprod* 69 (2003) 673-678
- [134] Tong SK, Hsu HJ, Chung BC. Zebrafish monosex population reveals female dominance in sex determination and earliest events of gonad differentiation. *Dev Biol* 344 (2010) 849-856
- [135] Orrego R, Guchardi J, Beyger L, Barra R, Hewitt LM, Holdway D. Sex-Related Embryotoxicity of Pulp Mill Effluent Extracts in Medaka (*Oryzias latipes*) Female Leucophore-free FLFII Strain. *Environ Toxicol Chem* 40 (2021) 2297-2305
- [136] Schänzer W, Geyer H, Donike M. Metabolism of metandienone in man: identification and synthesis of conjugated excreted urinary metabolites, determination of excretion rates and gas chromatographic-mass spectrometric identification of bis-hydroxylated metabolites. *J Steroid Biochem Mol Biol* 38 (1991) 441-464
- [137] Massé R, Bi HG, Ayotte C, Du P, Gélinas H, Dugal R. Studies on anabolic steroids. V. Sequential reduction of methandienone and structurally related steroid A-ring substituents in humans: gas chromatographic-mass spectrometric study of the corresponding urinary metabolites. *J Chromatogr* 562 (1991) 323-340
- [138] Da Silva EJT, Roleira FMF, E Melo MLS, Neves ASC, Paixão JA, De Almeida MJ, Silva MR, Andrade LCR. X-ray and deuterium labeling studies on the abnormal ring cleavages of a 5 β -epoxide precursor of formestane. *Steroids* 67 (2002) 311-319
- [139] Kratena N, Pilz SM, Weil M, Gmeiner G, Enev VS, Gärtner P. Synthesis and structural elucidation of a dehydrochloromethyltestosterone metabolite. *Org Biomol Chem* 16 (2018) 2508-2521
- [140] Liu L, Karim Z, Schlörer N, De La Torre X, Botrè F, Zoschke C, Parr MK. Human skin cells as an in vitro model for metabolism of anabolic steroids. *J Steroid Biochem Mol Biol*, In Press (Available online 12 December 2023. <https://doi.org/10.1016/j.jsbmb.2023.106444>)
- [141] Wakamatsu Y. Establishment of new medaka (*Oryzias latipes*) stocks carrying genotypic sex markers. *Environ Sci* 10 (2003) 291

- [142] Parr MK, Zapp J, Becker M, Opfermann G, Bartz U, Schänzer W. Steroidal isomers with uniform mass spectra of their per-TMS derivatives: synthesis of 17-hydroxyandrost-3-ones, androst-1-, and -4-ene-3,17-diols. *Steroids* 72 (2007) 545-551
- [143] Geyer H, Parr MK, Koehler K, Mareck U, Schänzer W, Thevis M. Nutritional supplements cross-contaminated and faked with doping substances. *J Mass Spectrom* 43 (2008) 892-902
- [144] Fragkaki AG, Angelis YS, Tsantili-Kakoulidou A, Koupparis M, Georgakopoulos C. Statistical analysis of fragmentation patterns of electron ionization mass spectra of enolized-trimethylsilylated anabolic androgenic steroids. *Int J Mass Spectrom* 285 (2009) 58-69
- [145] Smyrniotopoulos V, Rae M, Soldatou S, Ding Y, Wolff CW, McCormack G, Coleman CM, Ferreira D, Tasdemir D. Sulfated steroid-amino acid conjugates from the Irish marine sponge *Polymastia boletiformis*. *Mar Drugs* 13 (2015) 1632-1646
- [146] Wu D, Carillo KJ, Shie JJ, Yu SS, Tzou DM. Resolving Entangled J(H-H)-Coupling Patterns for Steroidal Structure Determinations by NMR Spectroscopy. *Molecules* 26 (2021)
- [147] Lootens L, Van Eenoo P, Pozo Mendoza OJ, Meulemans P, Leroux-Roels G, Delbeke F. Application of in vivo urinary steroid detection in uPA+/+-SCID chimeric mice. in, Sportverlag Strauss, (2010) 52-61
- [148] Parr MK, Zapp J, Becker M, Opfermann G, Bartz U, Schanzer W. Steroidal isomers with uniform mass spectra of their per-TMS derivatives: synthesis of 17-hydroxyandrost-3-ones, androst-1-, and -4-ene-3,17-diols. *Steroids* 72 (2007) 545-551
- [149] Verheyden K, Le Bizec B, Courtheyn D, Mortier V, Vandewiele M, Gillis W, Vanthemsche P, De Brabander HF, Noppe H. Mass spectrometric detection of and similarities between 1-androgens. *Anal Chim Acta* 586 (2007) 57-72
- [150] Schänzer W, Donike M. Metabolism of boldenone in man: gas chromatographic/mass spectrometric identification of urinary excreted metabolites and determination of excretion rates. *Biol Mass Spectrom* 21 (1992) 3-16

- [151] Milewich L, Kaimal V, Shaw CB, Sontheimer. Epidermal keratinocytes: a source of 5 alpha-dihydrotestosterone production in human skin. *J Clin Endocrinol Metab* 62 (1986) 739-746
- [152] Maudelonde T, Rosenfield RL, Shuler CF, Schwartz SA. Studies of androgen metabolism and action in cultured hair and skin cells. *J Steroid Biochem* 24 (1986) 1053-1060
- [153] Morimoto I, Nagataki S, Ishimaru T. [Dihydrotestosterone formation (5 alpha-reductase activity) in cultured human skin fibroblasts]. *Nihon Naibunpi Gakkai Zasshi* 60 (1984) 1281-1291
- [154] Gómez C, Pozo OJ, Marcos J, Segura J, Ventura R. Alternative long-term markers for the detection of methyltestosterone misuse. *Steroids* 78 (2013) 44-52
- [155] Parr MK, Fußhöller G, Gütschow M, Hess C, Schänzer W. GC-MS (/MS) investigations on long-term metabolites of 17-methyl steroids. *Recent advances in doping analysis* 18 (2010) 64-73
- [156] Martinez-Brito D, Iannone M, Tatangelo MA, Molaioni F, De La Torre X, Botre F. A further insight into methyltestosterone metabolism: New evidences from in vitro and in vivo experiments. *Rapid Commun Mass Spectrom* 34 (2020) e8870
- [157] Pozo OJ, Van Eenoo P, Deventer K, Lootens L, Van Thuyne W, Parr MK, Schänzer W, Sancho JV, Hernández F, Meuleman P. Detection and characterization of a new metabolite of 17 α -methyltestosterone. *Drug Metab Dispos* 37 (2009) 2153-2162
- [158] Yamada M, Aramaki S, Okayasu T, Hosoe T, Kurosawa M, Kijima-Suda I, Saito K, Nakazawa H. Identification and quantification of metabolites common to 17alpha-methyltestosterone and mestanolone in horse urine. *J Pharm Biomed Anal* 45 (2007) 125-133
- [159] Leyssens L, Royackers E, Gielen B, Missotten M, Schoofs J, Czech J, Noben JP, Hendriks L, Raus J. Metabolites of 4-chlorotestosterone acetate in cattle urine as diagnostic markers for its illegal use. *J Chromatogr B Biomed Appl* 654 (1994) 43-54
- [160] André F, Le Bizec B, Montrade M-P, Maume D, Monteau F, Marchand P. Developments in residue assay and metabolism study of growth-promoters by mass spectrometric analysis. *Analyst* 119 (1994) 2529-2535

- [161] Lu J, Fernandez-Alvarez M, Yang S, He G, Xu Y, Aguilera R. New clostebol metabolites in human urine by liquid chromatography time-of-flight tandem mass spectrometry and their application for doping control. *J Mass Spectrom* 50 (2015) 191-197
- [162] Kaufmann G, Schumann G, Horhold C. Influence of 1-double bond and 11 beta-hydroxy group on stereospecific microbial reductions of 4-en-3-oxo-steroids. *J Steroid Biochem* 25 (1986) 561-566
- [163] Swizdor A, Kolek T. Transformations of 4- and 17alpha-substituted testosterone analogues by *Fusarium culmorum*. *Steroids* 70 (2005) 817-824
- [164] Lootens L, Meuleman P, Leroux-Roels G, Van Eenoo P. Metabolic studies with promagnon, methylclostebol and methasterone in the uPA^{+/+}-SCID chimeric mice. *J Steroid Biochem Mol Biol* 127 (2011) 374-381
- [165] Franke WW, Berendonk B. Hormonal doping and androgenization of athletes: a secret program of the German Democratic Republic government. *Clin Chem* 43 (1997) 1262-1279
- [166] Bull HG, Garcia-Calvo M, Andersson S, Baginsky WF, Chan HK, Ellsworth DE, Miller RR, Stearns RA, Bakshi RK, Rasmusson GH, Tolman RL, Myers RW, Kozarich JW, Harris GS. Mechanism-based inhibition of human steroid 5 alpha-reductase by finasteride: Enzyme-catalyzed formation of NADP-dihydrofinasteride, a potent bisubstrate analog inhibitor. *J Am Chem Soc* 118 (1996) 2359-2365
- [167] Loke S, De La Torre X, Iannone M, La Piana G, Schlörer N, Botre F, Bureik M, Parr MK. Controlled administration of dehydrochloromethyltestosterone in humans: Urinary excretion and long-term detection of metabolites for anti-doping purpose. *J Steroid Biochem Mol Biol* 214 (2021) 105978
- [168] Liu LY, Hobohm L, Bredendiek F, Froschauer A, Zierau O, Parr MK, Keiler AM. Medaka embryos as a model for metabolism of anabolic steroids. *Arch Toxicol* 96 (2022) 1963-1974
- [169] Kwok WH, Leung GN, Wan TS, Curl P, Schiff PJ. Metabolic study of androsta-1,4,6-triene-3,17-dione in horses using liquid chromatography/high resolution mass spectrometry. *J Steroid Biochem Mol Biol* 152 (2015) 142-154
- [170] Musharraf SG, Ali A, Khan NT, Yousuf M, Choudhary MI, Atta Ur R. Tandem mass spectrometry approach for the investigation of the steroidal metabolism:

- structure-fragmentation relationship (SFR) in anabolic steroids and their metabolites by ESI-MS/MS analysis. *Steroids* 78 (2013) 171-181
- [171] Pozo OJ, Lootens L, Van Eenoo P, Deventer K, Meuleman P, Leroux-Roels G, Parr MK, Schanzer W, Delbeke FT. Combination of liquid-chromatography tandem mass spectrometry in different scan modes with human and chimeric mouse urine for the study of steroid metabolism. *Drug Test Anal* 1 (2009) 554-567
- [172] Thevis M, Schänzer W. Mass spectrometric analysis of androstan-17 β -ol-3-one and androstadiene-17 β -ol-3-one isomers. *J Am Soc Mass Spectr* 16 (2005) 1660-1669
- [173] Schanzer W, Geyer H, Fusholler G, Halatcheva N, Kohler M, Parr MK, Guddat S, Thomas A, Thevis M. Mass spectrometric identification and characterization of a new long-term metabolite of metandienone in human urine. *Rapid Commun Mass Spectrom* 20 (2006) 2252-2258
- [174] Pozo OJ, Van Eenoo P, Deventer K, Grimalt S, Sancho JV, Hernandez F, Delbeke FT. Collision-induced dissociation of 3-keto anabolic steroids and related compounds after electrospray ionization. Considerations for structural elucidation. *Rapid Commun Mass Sp* 22 (2008) 4009-4024
- [175] Schymanski EL, Jeon J, Gulde R, Fenner K, Ruff M, Singer HP, Hollender J. Identifying small molecules via high resolution mass spectrometry: communicating confidence. *Environ Sci Technol* 48 (2014) 2097-2098
- [176] Geldof L, Lootens L, Polet M, Eichner D, Campbell T, Nair V, Botre F, Meuleman P, Leroux-Roels G, Deventer K, Eenoo PV. Metabolism of methylstenbolone studied with human liver microsomes and the uPA(+)/(+)-SCID chimeric mouse model. *Biomed Chromatogr* 28 (2014) 974-985
- [177] Parr MK, Zollner A, Fusholler G, Opfermann G, Schlorer N, Zorio M, Bureik M, Schanzer W. Unexpected contribution of cytochrome P450 enzymes CYP11B2 and CYP21, as well as CYP3A4 in xenobiotic androgen elimination - insights from metandienone metabolism. *Toxicol Lett* 213 (2012) 381-391
- [178] Bi H, Masse R. Studies on anabolic steroids--12. Epimerization and degradation of anabolic 17 beta-sulfate-17 alpha-methyl steroids in human: qualitative and quantitative GC/MS analysis. *J Steroid Biochem Mol Biol* 42 (1992) 533-546
- [179] Pozo OJ, Van Eenoo P, Deventer K, Lootens L, Van Thuyne W, Parr MK, Schanzer W, Sancho JV, Hernandez F, Meuleman P, Leroux-Roels G, Delbeke

- FT. Detection and characterization of a new metabolite of 17alpha-methyltestosterone. *Drug Metab Dispos* 37 (2009) 2153-2162
- [180] Durbeck HW, Buker I. Studies on anabolic steroids. The mass spectra of 17 alpha-methyl-17 beta-hydroxy-1,4-androstadien-3-one (Dianabol) and its metabolites. *Biomed Mass Spectrom* 7 (1980) 437-445
- [181] Hagedorn HW, Schulz R, Friedrich A. Detection of methandienone (methandrostenolone) and metabolites in horse urine by gas chromatography-mass spectrometry. *J Chromatogr* 577 (1992) 195-203
- [182] Matos RR, Anselmo CS, Sardela VF, Pereira HMG. Phase II stanozolol metabolism study using the zebrafish water tank (ZWT) model. *J Pharm Biomed Anal* 195 (2021) 113886
- [183] Parr MK, Fussholler G, Schlorer N, Opfermann G, Geyer H, Rodchenkov G, Schanzer W. Detection of Delta6-methyltestosterone in a "dietary supplement" and GC-MS/MS investigations on its urinary metabolism. *Toxicol Lett* 201 (2011) 101-104
- [184] Iwamatsu T. Stages of normal development in the medaka *Oryzias latipes*. *Mech Dev* 121 (2004) 605-618
- [185] Kaufmann G, Thole H, Kraft R, Atrat P. Steroid-1-dehydrogenase of *Rhodococcus erythropolis*: purification and N-terminal amino acid sequence. *J Steroid Biochem Mol Biol* 43 (1992) 297-301
- [186] Rautenberg C, Grosse J, Thieme D, Wassill L, Ganghofner D, Mueller R. Testosterone degradation induced by *Rh. erythropolis*. *Recent Advances in Doping Analysis (14), Köln* (2006) 379-382

8 List of Figures

- Figure 1:** Backbones of (a): pregnane with exemplary numbering of carbon atoms (C1-C19) and rings (A-D), (b): estrane, (c): androstane..... 3
- Figure 2:** The simplified biosynthetic pathway of endogenous steroids starting from cholesterol. Progestogens: PREG, P4, 17 α -OHPREG, and 17 α -OHP; androgens: DHEA, AED, Δ^5 -diol and T; estrogen: E1 and E2; partially adapted from [8, 12, 35-37] 5
- Figure 3:** Possible positions of metabolism reactions for T in humans; blue: hydrogenation catalyzed by steroid 5 α - or 5 β -reductases; red: oxidations or reductions catalyzed by AKR1Cs; green: hydroxylation catalyzed by CYPs; orange: dehydrogenation 7
- Figure 4:** AAFs of AAS in relation to the total amount of AAFs of all groups between 2003 and 2021 by WADA accredited laboratories [60-78] 7
- Figure 5:** Main chemical modifications of AAS derived from T. Red arrow: the first type enables depot activity; blue arrows: the second type confers oral activity; green arrows: the third type hinders the aromatization and reduces 5 α -reduction..... 9
- Figure 6:** Chemical structures of T, MT, MD, CLT, CLMT, and DHCMT 10
- Figure 7:** AAFs of MT, MD, CLT, CLMT, and DHCMT between 2003 and 2021[60-78] 10
- Figure 8:** Reaction scheme for 4 α -chloro-5 α -androstane-3 ξ ,17 β -diol (**13a**, **13b**) and 4 α -chloro-17 α -methyl-5 α -androstane-3 ξ ,17 β -diol (**14a**, **14b**) steroids: (a) Zn, AcOH, reflux; (b) H₂O₂, HCO₂H, CH₂Cl₂, rt, 6 h; (c) conc. HCl, CHCl₃, rt, 30 min; (d) DMP, CH₂Cl₂, rt, 1 h; (e) KOH, MeOH, rt; (f) NaBH₄, rt, 1 h. This figure is adapted from my published paper [140] 22
- Figure 9:** Reaction scheme for 4-chloroandrost-4-ene-3 ξ ,17 β -diol (**17a**, **17b**) and 4-chloro-17 α -methylandrost-4-ene-3 ξ ,17 β -diol (**18a**, **18b**) steroids: (a) NaBH₄, rt, 1 h. This figure is adapted from my published paper [140]..... 26
- Figure 10:** Normalized EI mass spectra (GC-QTOF-MS) of TMS derivatives of (a) 3 α ,4 α ,5 α -THCLT (**13a**, [M]⁺=470.2777, mass error -4.47 ppm, RT 5.03 min), (b) 3 β ,4 α ,5 α -THCLT (**13b**, [M]⁺=470.2799, mass error 0.21 ppm, RT 5.67 min) at 70 eV. This figure is adapted from my published paper [140]..... 34

- Figure 11:** Normalized EI mass spectra (GC-QTOF-MS) of TMS derivatives of (a) 3 α ,4 α ,5 α -THCLMT (**14a**, [M]⁺=484.2941, mass error -2.68 ppm, RT 5.60 min), (b) 3 β ,4 α ,5 α -THCLMT (**14b**, [M]⁺=484.2947, mass error -1.45 ppm, RT 6.47 min) at 70 eV. This figure is adapted from my published paper [140]..... 36
- Figure 12:** Normalized EI mass spectra (GC-QTOF-MS) of TMS derivatives of (a) 3 α -DHCLT (**17a**, [M]⁺=468.2636, mass error -1.07 ppm, RT 4.62 min), (b) 3 β -DHCLT (**17b**, [M]⁺=468.2612, mass error -6.19 ppm, RT 5.20 min) at 70 eV. This figure is adapted from my published paper [140] 38
- Figure 13:** Normalized EI mass spectra (GC-QTOF-MS) of TMS derivatives of (a) 3 α -DHCLMT (**18a**, [M]⁺=482.2769, mass error -6.01 ppm, RT 5.16 min), and (b) 3 β -DHCLMT (**18b**, [M]⁺=482.2761, mass error -7.67 ppm, RT 5.88 min) at 70 eV. This figure is adapted from my published paper [140]..... 39
- Figure 14:** Extracted ion chromatogram (EIC) in GC-EI-MS (m/z 143) of a sample obtained after enzyme incubation of AKR1D1 with MD, showing 5 β -DHMD (RT 11.81 min) as per-TMS derivative..... 41
- Figure 15:** EICs in GC-EI-MS (m/z 143) of samples obtained after enzyme incubations of AKR14 with (a) 5 α -DHMD, showing tentatively assigned 3 α , 5 α -THMD (RT 13.53 min), 5 α -DHMD (RT 14.74 min), tentatively assigned 3 β , 5 α -THMD (RT 14.83 min), and MT (ISTD, RT 15.91 min) as per-TMS derivatives; (b) 5 β -DHMD, showing 5 β -DHMD, (RT 11.80 min), 3 α , 5 β -THMD (RT 13.03 min), tentatively assigned 3 β , 5 β -THMD (RT 13.48 min), and MT (ISTD, RT 15.90 min) as per-TMS derivatives 42
- Figure 16:** Normalized EI mass spectra (GC-QTOF-MS) of TMS derivatives of (a) tentatively assigned 3 α ,5 α -THMD ([M]⁺=448.3201, mass error 3.12 ppm, RT 4.49 min) detected in the incubation of AKR1C4 with 5 α -DHMD, (b) 3 α ,5 β -THMD ([M]⁺=448.3201, mass error 3.12 ppm, RT 4.32 min), formed by the incubation of AKR1C4 with 5 β -DHMD, at 70 eV 43
- Figure 17:** The peak area (relative to the internal standard (MT; EIC m/z 143)) of metabolites detected in the incubation of AKR1C2-AKR1C4 enzymes with (a) 5 α -DHMD (EIC m/z 143), (b) 5 β -DHMD (EIC m/z 143); the relative peak area is the peak area of the substances in correlation to the complete peak area of all detected substances (substrate and metabolites for each incubation), in GC-EI-MS analysis..... 45
- Figure 18:** Proposed sequence of A-ring reduction 46

- Figure 19:** Overlay of EICs of samples obtained after incubation of human keratinocytes with T, showing metabolites 5 α Adiol (RT 3.94 min; EIC m/z 241.1951 \pm 0.5000) and 5 α -DHT (RT 4.50 min; EIC m/z 434.3031 \pm 0.5000) as per-TMS derivatives. This figure is adapted from my published paper [140] 47
- Figure 20:** EIC of metabolites detected after incubation of human keratinocytes with MT (EIC m/z 448.3187 \pm 0.5000), showing metabolite MSL (RT 5.12 min) as per-TMS derivative. This figure is adapted from my published paper [140]..... 48
- Figure 21:** Overlay of EICs of metabolites detected after incubation of human keratinocytes with CLT, showing metabolites 4-chloro-3 α -hydroxy-androst-4-ene-17-one (RT 4.48 min; EIC m/z 466.2485 \pm 0.5000), 3 α -DHCLT (RT 4.63 min; EIC m/z 433.2953 \pm 0.5000), 3 α ,4 α ,5 α -THCLT (RT 5.02 min; EIC m/z 455.2563 \pm 0.5000), 3 β -DHCLT (RT 5.20 min; EIC m/z 433.2953 \pm 0.5000), and 3 β ,4 α ,5 α -THCLT (RT 5.64 min; EIC m/z 455.2563 \pm 0.5000) as per-TMS derivatives. This figure is adapted from my published paper [140]..... 49
- Figure 22:** Overlay of EICs of metabolites detected after incubation of human keratinocytes with CLMT, showing metabolites 3 α -DHCLMT (RT 5.16 min; EIC m/z 357.2608 \pm 0.5000), 3 α ,4 α ,5 α -THCLMT (RT 5.59 min; EIC m/z 469.2719 \pm 0.5000), 3 β -DHCLMT (RT 5.89 min; EIC m/z 357.2608 \pm 0.5000), and 3 β ,4 α ,5 α -THCLMT (RT 6.46 min; EIC m/z 469.2719 \pm 0.5000) as per-TMS derivatives. This figure is adapted from my published paper [140] 50
- Figure 23:** Proposed A-ring reduction sequence of (a) T and (b) CLT..... 52
- Figure 24:** The peak area (relative to the internal standard (T-d₃)) of metabolites detected in fibroblasts and keratinocytes incubated with (a) T (EIC m/z 434), (b) MT (EIC m/z 143), (c) CLT (EIC m/z 433 and m/z 255), and (d) CLMT (EIC m/z 357 and m/z 143) (mean \pm SD; n = 3), in GC-EI-MS analysis. This figure is adapted from my published paper [140] 53
- Figure 25:** Overlay of EICs (LC-ESI-QTOF-MS) of a sample obtained after 2-day incubation of medaka embryos with 10 μ M MD. 6 β OH-MD (**M1**, RT 4.71 min; EIC m/z 317.2111 \pm 0.5000), mono-hydroxy MD (**M2**, RT 5.22 min; EIC m/z 317.2111 \pm 0.5000), mono-hydroxy MD (**M3**, RT 5.34 min; EIC m/z 317.2111 \pm 0.5000), T-d₃ (internal standard, **ISTD**, RT 6.38 min; EIC m/z 292.2350 \pm 0.5000), mono-reduced MD (**M4**, RT 6.97 min; EIC m/z 303.2319 \pm 0.5000). This figure and the following figures and tables

in chapter 4.4.1 have been published, material from: Lingyu Liu, Medaka embryos as a model for metabolism of anabolic steroids, Archives of Toxicology, published [2022], [Springer] [168] 55

Figure 26: Product ion spectra (LC-ESI-QTOF-MS/MS) of (a) 6 β OH-MD (**M1**, [M+H]⁺=317.2112, mass error 0.32 ppm, RT 4.71 min), (b) mono-hydroxy MD (**M2**, [M+H]⁺=317.2100, mass error -3.47 ppm, RT 5.22 min), and (c) mono-hydroxy MD (**M3**, [M+H]⁺=317.2105, mass error -1.89 ppm, RT 5.34 min) formed by medaka embryos incubated with 10 μ M MD, collision energy 23.1 eV. This figure is adapted from my published paper [168]..... 55

Figure 27: Overlay of EICs in GC-EI-QTOF-MS after TMIS derivatization showing five main products after 2-day incubation of medaka embryos with 10 μ M MD. 5 β -DHMD (**M4**, RT 3.99 min; EIC m/z 446.3031 \pm 0.5000), ISTD (T-d₃, RT 4.70 min; EIC m/z 435.3063 \pm 0.5000), 6 β OH-MD (**M1**, RT 6.45 min; EIC m/z 532.3219 \pm 0.5000), mono-hydroxy MD (**M2**, RT 6.51 min; EIC m/z 532.3219 \pm 0.5000), mono-hydroxy MD (**M3**, RT 7.46 min; EIC m/z 532.3219 \pm 0.5000). This figure is adapted from my published paper [168]..... 58

Figure 28: Normalized EI mass spectra (GC-QTOF-MS) of TMS derivatives of (a) mono-hydroxy MD (**M2**, [M]⁺=532.3239, mass error 3.76 ppm, RT 6.51 min) and (b) mono-hydroxy MD (**M3**, [M]⁺=532.3231, mass error 2.25 ppm, RT 7.46 min), formed by medaka embryos incubated with 10 μ M MD. This figure is adapted from my published paper [168]..... 59

Figure 29: Overlay of EICs in GC-EI-MS after TMIS derivatization showing seven main products after 2-day incubation of medaka embryos with [¹³C₃]-T: [¹³C₃]-5 β -DHT (RT 9.80 min; EIC m/z 437), DHEA-d₆ (ISTD, RT 12.17 min; EIC m/z 438), [¹³C₃]-Etio (RT 11.03 min; EIC m/z 437), [¹³C₃]-EA (RT 12.35 min; EIC m/z 437), [¹³C₃]-5 α -DHT (RT 12.99 min; EIC m/z 437), [¹³C₃]-AED (13.26 min; EIC m/z 433), and [¹³C₃]-hydroxylated product (unidentified, RT 16.54 min; EIC m/z 521) 63

Figure 30: Proposed pathway of [¹³C₃]-T metabolism in medaka embryos; the dotted arrows indicate that the compounds were not detected in the incubation of medaka embryos with [¹³C₃]-T; AD, androstenedione (5 α -androstane-3,17-dione); 5 β -AD, 5 β -androstenedione (5 β -androstane-3,17-dione)..... 63

- Figure 31:** GC-EI-MS chromatogram (EIC m/z 143) after TMS derivatization showing seven main products after 2-day incubation of medaka embryos with MT. 5 β -MSL (RT 11.60 min), DHEA-d₆ (ISTD, RT 12.20 min), 3 ξ ,5 ξ -THMT (RT 12.58 min), 3 α ,5 β -THMT (RT 12.76 min), 3 β ,5 α -THMT (RT 14.52 min), MSL (14.78 min), and MT (RT 15.45 min) 64
- Figure 32:** Main proposed pathway of MT metabolism in medaka embryos 65
- Figure 33:** The peak area (relative to the internal standard (DHEA-d₆; EIC m/z 438)) (GC-EI-MS) of (a) EA (EIC m/z 437) and Etio (EIC m/z 437) detected in sample extracts obtained after 2-day incubation of medaka embryos (strain d-rR.YHNI) with 20 μ M [¹³C₃]-T, (b) 3 β ,5 α -THMT (EIC m/z 143) and 3 α ,5 β -THMT (EIC m/z 143) detected in sample extracts obtained after 2-day incubation of medaka embryos (strain d-rR.YHNI) with 20 μ M MT, two technical replicates under fully sterile conditions 66
- Figure 34:** Normalized EI mass spectra (GC-QTOF-MS) of TMS derivatives of (a) the metabolite 5 β -DHMD formed by the incubation of AKR1D1 with MD ([M]⁺=446.3057, mass error 5.83 ppm, RT 3.98 min), and (b) reference compound 5 β -DHMD ([M]⁺=446.3045, mass error 3.14 ppm, RT 3.98 min), at 70 eV 106
- Figure 35:** EICs in GC-EI-MS (m/z 143) of samples obtained after enzyme incubations of AKR1C2 with (a) 5 α -DHMD, showing tentatively assigned 3 α , 5 α -THMD (RT 13.66 min), 5 α -DHMD (RT 14.88 min), tentatively assigned 3 β , 5 α -THMD (RT 14.99 min), and MT (ISTD, RT 16.10 min) as per-TMS derivatives; (b) 5 β -DHMD, showing 5 β -DHMD, (RT 11.96 min), 3 α , 5 β -THMD (RT 13.19 min), tentatively assigned 3 β , 5 β -THMD (RT 13.61 min), and MT (ISTD, RT 16.08 min) as per-TMS derivatives 107
- Figure 36:** EICs in GC-EI-MS (m/z 143) of samples obtained after enzyme incubations of AKR1C3 with (a) 5 α -DHMD, showing tentatively assigned 3 α , 5 α -THMD (RT 13.65 min), 5 α -DHMD (RT 14.88 min), and MT (ISTD, RT 16.09 min) as per-TMS derivatives; (b) 5 β -DHMD, showing 5 β -DHMD, (RT 11.97 min), 3 α ,5 β -THMD (RT 13.18 min), and MT (ISTD, RT 16.11 min) as per-TMS derivatives 107
- Figure 37:** Normalized EI mass spectrum (GC-QTOF-MS) of TMS derivative of the reference compound 3 α ,5 β -THMD ([M]⁺=448.3205, mass error 4.02 ppm, RT 4.32 min) at 70 eV 108

- Figure 38:** Normalized EI mass spectrum (GC-QTOF-MS) of TMS derivative of the metabolite tentatively assigned as 3 β ,5 α -THMD, formed by the incubation of AKR1C4 with 5 α -DHMD ($[M]^{+}=448.3149$, mass error -8.48 ppm, RT 4.97 min) at 70 eV 108
- Figure 39:** Normalized EI mass spectrum (GC-QTOF-MS) of TMS derivative of the metabolite tentatively assigned as 3 β ,5 β -THMD, formed by the incubation of AKR1C4 with 5 β -DHMD ($[M]^{+}=448.3208$, mass error 4.68 ppm, RT 4.49 min) at 70 eV 108
- Figure 40:** Normalized mass spectra (GC-QTOF-MS) of TMS derivatives of (a) 5 α -DHT ($[M]^{+}=434.3059$, mass error 6.45 ppm, RT 4.49 min), formed by human keratinocytes incubated with T, and (b) reference compound 5 α -DHT ($[M]^{+}=434.3045$, mass error 3.22 ppm, RT 4.50 min), at 70 eV 110
- Figure 41:** Normalized mass spectra (GC-QTOF-MS) of TMS derivatives of (a) 5 α Adiol ($[M]^{+}=436.3150$, mass error -8.48 ppm, RT 3.94 min), formed by human keratinocytes incubated with T, and (b) reference compound 5 α Adiol ($[M]^{+}=436.3194$, mass error 1.60 ppm, RT 3.94 min), at 70 eV 111
- Figure 42:** Normalized mass spectra (GC-QTOF-MS) of TMS derivatives of (a) MSL ($[M]^{+}=448.3197$, mass error 2.23 ppm, RT 5.12 min), formed by human keratinocytes incubated with MT, and (b) reference compound MSL ($[M]^{+}=448.3190$, mass error 0.67 ppm, RT 5.13 min), at 70 eV 112
- Figure 43:** Normalized mass spectra (GC-QTOF-MS) of TMS derivative of 3 α -DHCLT ($[M]^{+}=468.2634$, mass error -1.49 ppm, RT 4.63 min), formed by human keratinocytes incubated with CLT, at 70 eV 113
- Figure 44:** Normalized mass spectra (GC-QTOF-MS) of TMS derivative of 3 α ,4 α ,5 α -THCLT ($[M]^{+}=470.2820$, mass error 4.68 ppm, RT 5.02 min), formed by human keratinocytes incubated with CLT, at 70 eV 113
- Figure 45:** Normalized mass spectra (GC-QTOF-MS) of TMS derivative of 3 β -DHCLT ($[M-CH_3]^{+}=453.2461$, mass error 12.13 ppm, RT 5.20 min), formed by human keratinocytes incubated with CLT, at 70 eV 114
- Figure 46:** Normalized mass spectra (GC-QTOF-MS) of TMS derivative of 3 β ,4 α ,5 α -THCLT ($[M-CH_3]^{+}=455.2603$, mass error 8.79 ppm, RT 5.64 min), formed by human keratinocytes incubated with CLT, at 70 eV 115

- Figure 47:** Normalized mass spectra (GC-QTOF-MS) of TMS derivatives of (a) 4-chloro-3 α -hydroxy-androst-4-ene-17-one ($[M]^{*+}=466.2508$, mass error 4.93 ppm, RT 4.48 min), formed by human keratinocytes incubated with CLT, and (b) reference compound 4-chloro-3 α -hydroxy-androst-4-ene-17-one ($[M]^{*+}=466.2480$, mass error -1.07 ppm, RT 4.49 min), at 70 eV 116
- Figure 48:** Normalized mass spectra (GC-QTOF-MS) of TMS derivative of 3 α -DHCLMT ($[M-CH_3]^{*+}=467.2609$, mass error 9.84 ppm, RT 5.16 min), formed by human keratinocytes incubated with CLMT, at 70 eV 116
- Figure 49:** Normalized mass spectra (GC-QTOF-MS) of TMS derivative of 3 $\alpha,4\alpha,5\alpha$ -THCLMT ($[M]^{*+}=484.2929$, mass error -5.16 ppm, RT 5.59 min), formed by human keratinocytes incubated with CLMT, at 70 eV 117
- Figure 50:** Normalized mass spectra (GC-QTOF-MS) of TMS derivative of 3 β -DHCLMT ($[M-CH_3]^{*+}=467.2570$, mass error 1.50 ppm, RT 5.89 min), formed by human keratinocytes incubated with CLMT, at 70 eV 118
- Figure 51:** Normalized mass spectra (GC-QTOF-MS) of TMS derivative of 3 $\beta,4\alpha,5\alpha$ -THCLMT ($[M]^{*+}=484.2962$, mass error 1.65 ppm, RT 6.46 min), formed by human keratinocytes incubated with CLMT, at 70 eV 118
- Figure 52:** Product ion spectra (LC-ESI-MS/MS) of reference compound 6 β OH-MD, $[M+H]^{*+}=317.2077$, mass error -10.72 ppm, RT 4.78 min, collision energy 23.1 eV .. 119
- Figure 53:** Product ion spectra (LC-ESI-MS/MS) of (a) 5 β -DHMD (**M4**) formed by medaka embryos incubated with 10 μ M MD, $[M+H]^{*+}=303.2318$, mass error 0.33 ppm, RT 6.97 min, collision energy 22.3 eV, and (b) reference compound 5 β -DHMD, $[M+H]^{*+}=303.2303$, mass error -5.28 ppm, RT 6.96 min, collision energy 22.3 eV 120
- Figure 54:** Normalized EI mass spectrum (GC-QTOF-MS) of TMS derivative of 5 β -DHMD (**M4**) formed by medaka embryos incubated with 10 μ M MD, $[M]^{*+}=446.3038$, mass error 1.57 ppm, RT 3.99 min, at 70 eV. This figure is adapted from my published paper [168] 120
- Figure 55:** Normalized EI mass spectra (GC-QTOF-MS) of TMS derivatives of (a) 6 β OH-MD (**M1**) formed by medaka embryos incubated with 10 μ M MD, $[M]^{*+}=532.3237$, mass error 3.38 ppm, RT 6.45 min, and (b) reference compound 6 β OH-

- MD, $[M]^{+}=532.3238$, mass error 3.57 ppm, RT 6.45 min, at 70 eV. This figure is adapted from my published paper [168]..... 121
- Figure 56:** Normalized mass spectra (GC-EI-MS) of TMS derivatives of (a) $[^{13}\text{C}_3]$ -5 β -DHT ($[M]^{+}=437$, RT 9.80 min), formed by medaka embryos incubated with $[^{13}\text{C}_3]$ -T, and (b) reference compound 5 β -DHT ($[M]^{+}=434$, RT 9.87 min), at 70 eV 122
- Figure 57:** Normalized mass spectra (GC-EI-MS) of TMS derivatives of (a) $[^{13}\text{C}_3]$ -Etio ($[M]^{+}=437$, RT 11.03 min), formed by medaka embryos incubated with $[^{13}\text{C}_3]$ -T, and (b) reference compound Etio ($[M]^{+}=434$, RT 11.08 min), at 70 eV..... 122
- Figure 58:** Normalized mass spectra (GC-EI-MS) of TMS derivatives of (a) $[^{13}\text{C}_3]$ -EA ($[M]^{+}=437$, RT 12.35 min), formed by medaka embryos incubated with $[^{13}\text{C}_3]$ -T, and (b) reference compound EA ($[M]^{+}=434$, RT 12.36 min), at 70 eV 123
- Figure 59:** Normalized mass spectra (GC-EI-MS) of TMS derivatives of (a) $[^{13}\text{C}_3]$ -5 α -DHT ($[M]^{+}=437$, RT 12.99 min), formed by medaka embryos incubated with $[^{13}\text{C}_3]$ -T, and (b) reference compound 5 α -DHT ($[M]^{+}=434$, RT 13.03 min), at 70 eV 123
- Figure 60:** Normalized mass spectra (GC-EI-MS) of TMS derivatives of (a) $[^{13}\text{C}_3]$ -AED ($[M]^{+}=433$, RT 13.26 min), formed by medaka embryos incubated with $[^{13}\text{C}_3]$ -T, and (b) reference compound AED ($[M]^{+}=430$, RT 13.26 min), at 70 eV 124
- Figure 61:** Normalized mass spectra (GC-EI-MS) of TMS derivative of an unidentified hydroxylated metabolite of $[^{13}\text{C}_3]$ -T ($[M]^{+}=521$, RT 16.54 min), at 70 eV 124
- Figure 62:** Normalized mass spectra (GC-EI-MS) of TMS derivatives of (a) 5 β -MSL ($[M]^{+}=448$, RT 11.60 min), formed by medaka embryos incubated with MT, and (b) reference compound at 5 β -MSL ($[M]^{+}=448$, RT 11.58 min), 70 eV 125
- Figure 63:** Normalized mass spectra (GC-EI-MS) of TMS derivative of 3 ξ ,5 ξ -THMT ($[M-\text{CH}_3]^{+}=435$, RT 12.58 min), formed by medaka embryos incubated with MT, at 70 eV 125
- Figure 64:** Normalized mass spectra (GC-EI-MS) of TMS derivatives of (a) 3 α ,5 β -THMT ($[M]^{+}=450$, RT 12.76 min), formed by medaka embryos incubated with MT, and (b) reference compound 3 α ,5 β -THMT ($[M]^{+}=450$, RT 12.87 min), at 70 eV..... 126
- Figure 65:** Normalized mass spectra (GC-EI-MS) TMS derivatives of (a) 3 β ,5 α -THMT ($[M]^{+}=450$, RT 14.52 min), formed by medaka embryos incubated with MT, and (b) reference compound 3 β ,5 α -THMT ($[M]^{+}=450$, RT 14.57 min) at 70 eV..... 126

Figure 66: Normalized mass spectra (GC-EI-MS) of TMS derivatives of (a) MSL ($[M]^{*+}=448$, RT 14.78 min), formed by medaka embryos incubated with MT, and (b) reference compound MSL ($[M]^{*+}=448$, RT 14.88 min), at 70 eV	127
--	-----

9 List of Tables

Table 1: Groups of the Prohibited List 2023 of WADA	2
Table 2: Steroids and reference materials.....	19
Table 3: Solvents, reagents, and materials.....	20
Table 4: Retention times, molecular ions (M^+) at 70 eV, and mass difference to exact mass of synthesized reference compounds 13a , 13b , 14a , 14b , 17a , 17b , 18a , and 18b as per-TMS derivatives (GC-EI-QTOF-MS). This table is adapted from my published paper [140]	32
Table 5: 1H and ^{13}C NMR chemical shifts of $3\alpha,4\alpha,5\alpha$ -THCLT (13a), $3\beta,4\alpha,5\alpha$ -THCLT (13b), $3\alpha,4\alpha,5\alpha$ -THCLMT (14a), and $3\beta,4\alpha,5\alpha$ -THCLMT (14b) in $CDCl_3$, δ in ppm. This table is adapted from my published paper [140]	33
Table 6: Postulated fragments, exact masses, accurate masses, mass errors ($\Delta m/z$) for $3\alpha,4\alpha,5\alpha$ -THCLT (13a) (GC-EI-QTOF-MS). This table is adapted from my published paper [140].....	35
Table 7: Postulated fragments, exact masses, accurate masses, mass errors ($\Delta m/z$) for $3\beta,4\alpha,5\alpha$ -THCLT (13b) (GC-EI-QTOF-MS). This table is adapted from my published paper [140].....	35
Table 8: Postulated fragments, exact masses, accurate masses, mass errors ($\Delta m/z$) for $3\alpha,4\alpha,5\alpha$ -THCLMT (14a) (GC-EI-QTOF-MS). This table is adapted from my published paper [140].....	37
Table 9: Postulated fragments, exact masses, accurate masses, mass errors ($\Delta m/z$) for $3\beta,4\alpha,5\alpha$ -THCLMT (14b) (GC-EI-QTOF-MS). This table is adapted from my published paper [140].....	37
Table 10: Postulated fragments, exact masses, accurate masses, mass errors ($\Delta m/z$) for 3α -DHCLT (17a) (GC-EI-QTOF-MS). This table is adapted from my published paper [140]	39
Table 11: Postulated fragments, exact masses, accurate masses, mass errors ($\Delta m/z$) for 3α -DHCLMT (18a) (GC-EI-QTOF-MS). This table is adapted from my published paper [140]	40

Table 12: Postulated fragments, mass errors ($\Delta m/z$) for the metabolite tentatively assigned as $3\alpha,5\alpha$ -THMD, formed by the incubation of AKR1C4 with 5α -DHMD (GC-EI-QTOF-MS)	44
Table 13: Postulated fragments, exact masses, accurate masses, mass errors ($\Delta m/z$) for the metabolite $3\alpha,5\beta$ -THMD, formed by the incubation of AKR1C4 with 5β -DHMD (GC-EI-QTOF-MS)	44
Table 14: Postulated fragments, exact masses, accurate masses, mass errors ($\Delta m/z$) for M1 , LC-ESI-MS/MS. This table is adapted from my published paper [168].....	56
Table 15: Postulated fragments, exact masses, accurate masses, mass errors ($\Delta m/z$) for M2 , LC-ESI-MS/MS. This table is adapted from my published paper [168].....	57
Table 16: Postulated fragments, exact masses, accurate masses, mass errors ($\Delta m/z$) for M3 , LC-ESI-MS/MS. This table is adapted from my published paper [168].....	57
Table 17: Per-TMS derivatives of metabolites detected in samples obtained after 2-day incubation of medaka embryos with 10 μ M MD by GC-EI-QTOF-MS. This table is adapted from my published paper [168]	58
Table 18: Postulated fragments, exact masses, accurate masses, mass errors ($\Delta m/z$) for TMS-derivative of mono-hydroxy MD (M2), GC-EI-QTOF-MS. This table is adapted from my published paper [168]	59
Table 19: Postulated fragments, exact masses, accurate masses, mass errors ($\Delta m/z$) for TMS-derivative of mono-hydroxy MD (M3), GC-EI-QTOF-MS. This table is adapted from my published paper [168]	60
Table 20: Postulated fragments, exact masses, accurate masses, mass errors ($\Delta m/z$) for 3β -DHCLT (17b) (GC-EI-QTOF-MS). This table is adapted from my published paper [140].....	105
Table 21: Postulated fragments, exact masses, accurate masses, mass errors ($\Delta m/z$) for 3β -DHCLMT (18b) (GC-EI-QTOF-MS). This table is adapted from my published paper [140].....	105
Table 22: Postulated fragments, exact masses, accurate masses, mass errors ($\Delta m/z$) for the metabolite 5β -DHMD, formed by the incubation of AKR1D1 with MD (GC-EI-QTOF-MS)	106

Table 23: Per-TMS derivatives of metabolites detected in samples obtained after AKR1C4 incubation with 5 α -DHMD or 5 β -DHMD, respectively (GC-EI-MS).....	106
Table 24: Postulated fragments, exact masses, accurate masses, mass errors ($\Delta m/z$) for the metabolite tentatively assigned as 3 β ,5 α -THMD, formed by the incubation of AKR1C4 with 5 α -DHMD (GC-EI-QTOF-MS)	109
Table 25: Postulated fragments, exact masses, accurate masses, mass errors ($\Delta m/z$) for the metabolite tentatively assigned as 3 β ,5 β -THMD, formed by the incubation of AKR1C4 with 5 β -DHMD (GC-EI-QTOF-MS)	109
Table 26: Postulated fragments, exact masses, accurate masses, mass errors ($\Delta m/z$) for the metabolite 5 α -DHT formed by human keratinocytes incubated with T (GC-EI-QTOF-MS).....	110
Table 27: Postulated fragments, exact masses, accurate masses, mass errors ($\Delta m/z$) for the metabolite 5 α Adiol formed by human keratinocytes incubated with T (GC-EI-QTOF-MS).....	111
Table 28: Postulated fragments, exact masses, accurate masses, mass errors ($\Delta m/z$) for the metabolite MSL formed by human keratinocytes incubated with MT (GC-EI-QTOF-MS).....	112
Table 29: Postulated fragments, exact masses, accurate masses, mass errors ($\Delta m/z$) for the metabolite 3 α -DHCLT formed by human keratinocytes incubated with CLT (GC-EI-QTOF-MS)	113
Table 30: Postulated fragments, exact masses, accurate masses, mass errors ($\Delta m/z$) for the metabolite 3 α ,4 α ,5 α -THCLT formed by human keratinocytes incubated with CLT (GC-EI-QTOF-MS)	114
Table 31: Postulated fragments, exact masses, accurate masses, mass errors ($\Delta m/z$) for the metabolite 3 β -DHCLT formed by human keratinocytes incubated with CLT (GC-EI-QTOF-MS)	114
Table 32: Postulated fragments, exact masses, accurate masses, mass errors ($\Delta m/z$) for the metabolite 3 β ,4 α ,5 α -THCLT formed by human keratinocytes incubated with CLT (GC-EI-QTOF-MS)	115

Table 33: Postulated fragments, exact masses, accurate masses, mass errors ($\Delta m/z$) for the metabolite 4-chloro-3 α -hydroxy-androst-4-ene-17-one formed by human keratinocytes incubated with CLT (GC-EI-QTOF-MS).....	116
Table 34: Postulated fragments, exact masses, accurate masses, mass errors ($\Delta m/z$) for the metabolite 3 α -DHCLMT formed by human keratinocytes incubated with CLMT (GC-EI-QTOF-MS).....	117
Table 35: Postulated fragments, exact masses, accurate masses, mass errors ($\Delta m/z$) for the metabolite 3 α ,4 α ,5 α -THCLMT formed by human keratinocytes incubated with CLMT (GC-EI-QTOF-MS).....	117
Table 36: Postulated fragments, exact masses, accurate masses, mass errors ($\Delta m/z$) for the metabolite 3 β -DHCLMT formed by human keratinocytes incubated with CLMT (GC-EI-QTOF-MS).....	118
Table 37: Postulated fragments, exact masses, accurate masses, mass errors ($\Delta m/z$) for the metabolite 3 β ,4 α ,5 α -THCLMT formed by human keratinocytes incubated with CLMT (GC-EI-QTOF-MS).....	119
Table 38: Results of the metabolites detected in samples obtained after 2-day incubation of medaka embryos with 10 μ M MD by LC-ESI-MS. This table is adapted from my published paper [168]	119
Table 39: Postulated fragments, exact masses, accurate masses, mass errors ($\Delta m/z$) for TMS-derivative of M4 , GC-EI-QTOF-MS.....	121
Table 40: Postulated fragments, exact masses, accurate masses, mass errors ($\Delta m/z$) for TMS-derivative of M1 , GC-EI-QTOF-MS. This table is adapted from my published paper [168]	121
Table 41: Per-TMS derivatives of metabolites detected in samples obtained after incubation of medaka embryos with [$^{13}\text{C}_3$]-T by GC-EI-MS	124
Table 42: Per-TMS derivatives of metabolites detected in samples obtained after incubation of medaka embryos with MT by GC-EI-MS	127
Table 43: List of anabolic-androgenic steroids, metabolites, and derivatives involved the synthesis of reference materials in chapter 3.2.1	128

10 Annex

Table 20: Postulated fragments, exact masses, accurate masses, mass errors ($\Delta m/z$) for 3 β -DHCLT (17b) (GC-EI-QTOF-MS). This table is adapted from my published paper [140]

Postulated fragment	Exact mass [m/z]	Accurate mass [m/z]	$\Delta m/z$ [ppm]
[M] ⁺	468.2641	468.2612	-6.19
[M-CH ₃] ⁺	453.2406	453.2397	-1.99
[M-Cl] ⁺	433.2953	433.2957	0.92
[M-Cl-TMSOH] ⁺	343.2452	343.2447	-1.46
[M-Cl-2xTMSOH] ⁺	253.1951	253.1948	-1.18
[M-TMSOH] ⁺	378.2140	378.2147	1.85
[M-CH ₃ -TMSOH] ⁺	363.1905	363.1903	-0.55
[M-CH ₃ -2xTMSOH] ⁺	273.1405	273.1422	6.22
[C ₆ H ₁₃ OSi] ⁺	129.0730	129.0720	-7.75
[TMS] ⁺	73.0468	73.0471	4.11

Table 21: Postulated fragments, exact masses, accurate masses, mass errors ($\Delta m/z$) for 3 β -DHCLMT (18b) (GC-EI-QTOF-MS). This table is adapted from my published paper [140]

Postulated fragment	Exact mass [m/z]	Accurate mass [m/z]	$\Delta m/z$ [ppm]
[M] ⁺	482.2798	482.2761	-7.67
[M-CH ₃] ⁺	467.2563	467.2556	-1.50
[M-Cl] ⁺	447.3109	447.3113	0.89
[M-Cl-TMSOH] ⁺	357.2608	357.2616	2.24
[M-Cl-2xTMSOH] ⁺	267.2107	267.2105	-0.75
[M-TMSOH] ⁺	392.2297	392.2273	-6.12
[M-CH ₃ -TMSOH] ⁺	377.2062	377.2059	-0.80
[M-CH ₃ -2xTMSOH] ⁺	287.1561	287.1582	7.31
[C ₇ H ₁₅ OSi] ⁺	143.0887	143.0890	2.10
[TMS] ⁺	73.0468	73.0472	5.48

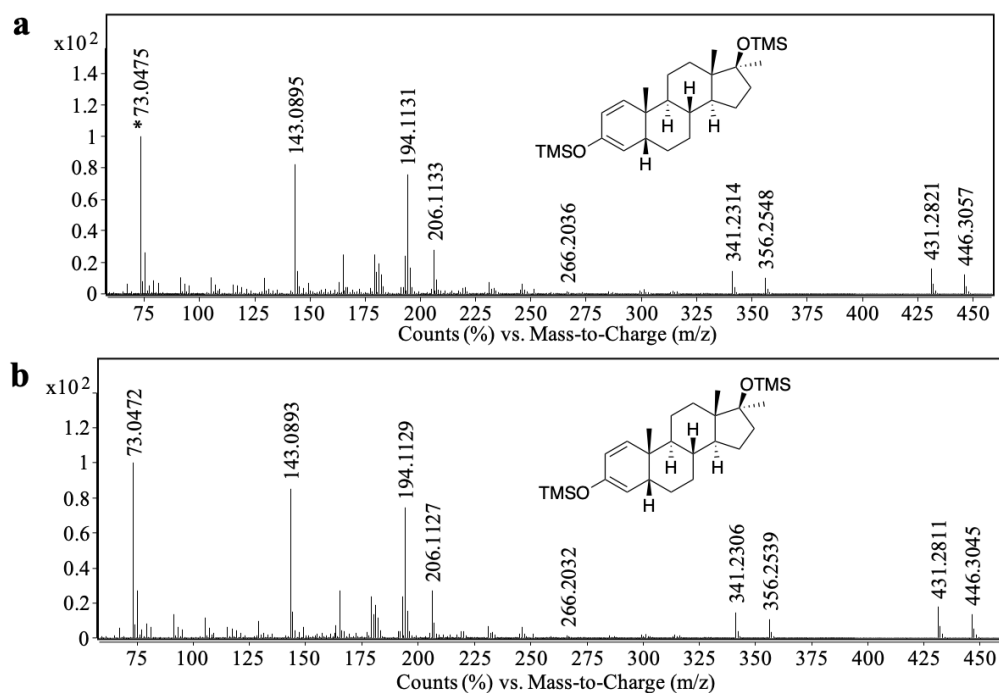


Figure 34: Normalized EI mass spectra (GC-QTOF-MS) of TMS derivatives of (a) the metabolite 5 β -DHMD formed by the incubation of AKR1D1 with MD ($[M]^{++}=446.3057$, mass error 5.83 ppm, RT 3.98 min), and (b) reference compound 5 β -DHMD ($[M]^{++}=446.3045$, mass error 3.14 ppm, RT 3.98 min), at 70 eV

Table 22: Postulated fragments, exact masses, accurate masses, mass errors ($\Delta m/z$) for the metabolite 5 β -DHMD, formed by the incubation of AKR1D1 with MD (GC-EI-QTOF-MS)

Postulated fragment	Exact mass [m/z]	Accurate mass [m/z]	$\Delta m/z$ [ppm]
$[M]^{++}$	446.3031	446.3057	5.83
$[M-CH_3]^+$	431.2796	431.2821	5.80
$[M-TMSOH]^{++}$	356.2530	356.2548	5.05
$[M-CH_3-TMSOH]^+$	341.2295	341.2314	5.57
$[M-2xTMSOH]^{++}$	266.2029	266.2036	2.63
$[C_7H_{15}OSi]^+$	143.0887	143.0895	5.59
$[TMS]^+$	73.0468	73.0475	9.58

Table 23: Per-TMS derivatives of metabolites detected in samples obtained after AKR1C4 incubation with 5 α -DHMD or 5 β -DHMD, respectively (GC-EI-MS)

Analyte	Elemental Composition	$[M]^{++}$	Retention Time (min)
3 α ,5 α -THMD*	$[C_{26}H_{48}O_2Si_2]^{++}$	448	13.53
3 β ,5 α -THMD*	$[C_{26}H_{48}O_2Si_2]^{++}$	448	14.83
3 α ,5 β -THMD	$[C_{26}H_{48}O_2Si_2]^{++}$	448	13.03
3 β ,5 β -THMD*	$[C_{26}H_{48}O_2Si_2]^{++}$	448	13.48

* Tentative assignment.

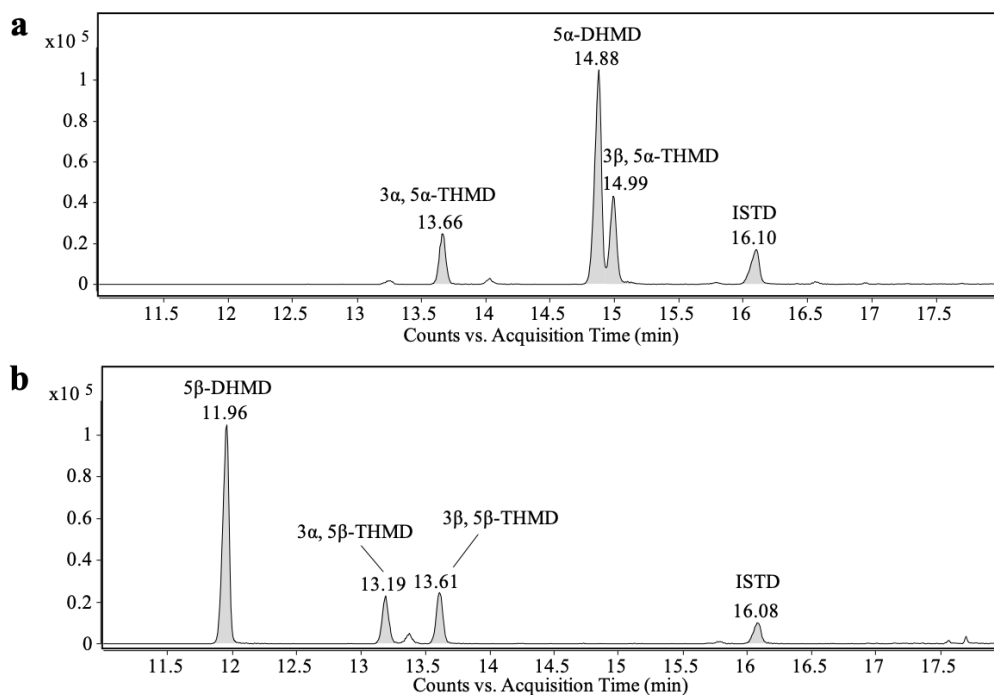


Figure 35: EICs in GC-EI-MS (m/z 143) of samples obtained after enzyme incubations of AKR1C2 with (a) 5 α -DHMD, showing tentatively assigned 3 α , 5 α -THMD (RT 13.66 min), 5 α -DHMD (RT 14.88 min), tentatively assigned 3 β , 5 α -THMD (RT 14.99 min), and MT (ISTD, RT 16.10 min) as per-TMS derivatives; (b) 5 β -DHMD, showing 5 β -DHMD, (RT 11.96 min), 3 α , 5 β -THMD (RT 13.19 min), tentatively assigned 3 β , 5 β -THMD (RT 13.61 min), and MT (ISTD, RT 16.08 min) as per-TMS derivatives

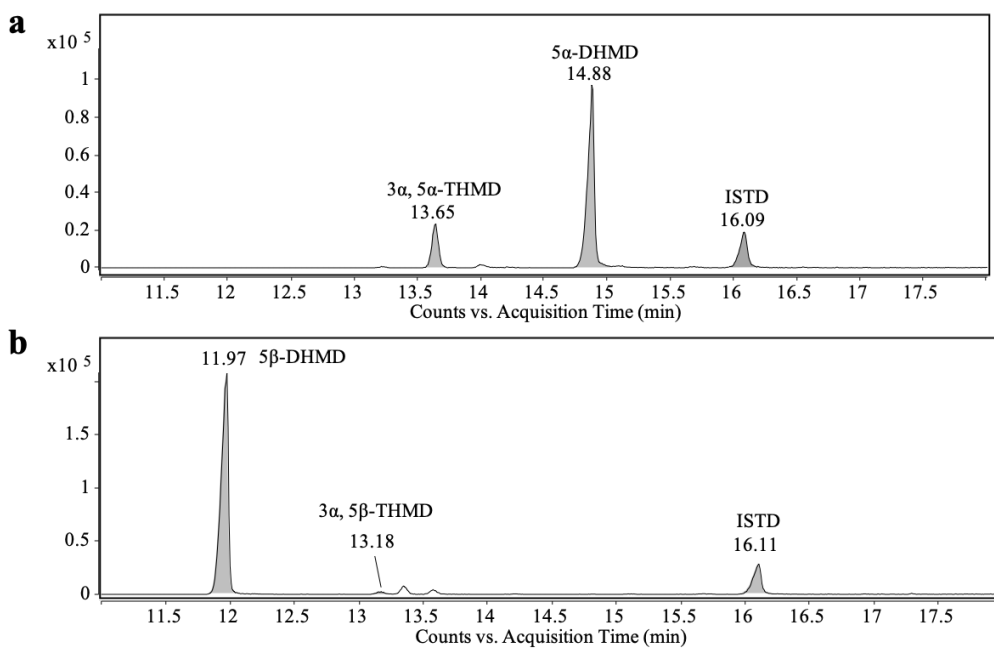


Figure 36: EICs in GC-EI-MS (m/z 143) of samples obtained after enzyme incubations of AKR1C3 with (a) 5 α -DHMD, showing tentatively assigned 3 α , 5 α -THMD (RT 13.65 min), 5 α -DHMD (RT 14.88 min), and MT (ISTD, RT 16.09 min) as per-TMS derivatives; (b) 5 β -DHMD, showing 5 β -DHMD, (RT 11.97 min), 3 α , 5 β -THMD (RT 13.18 min), and MT (ISTD, RT 16.11 min) as per-TMS derivatives

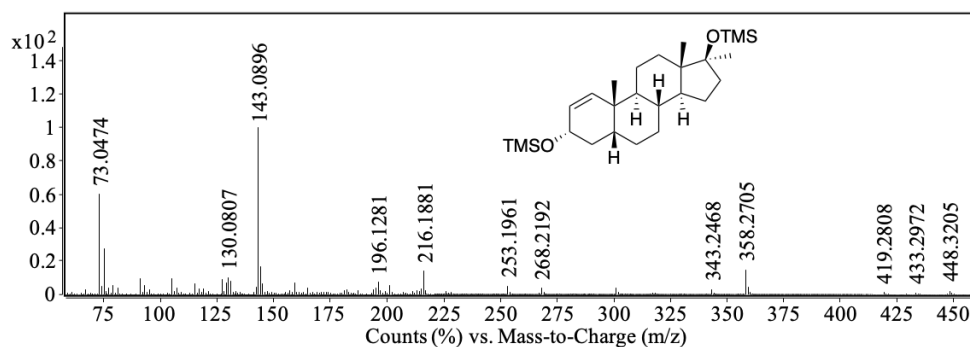


Figure 37: Normalized EI mass spectrum (GC-QTOF-MS) of TMS derivative of the reference compound 3 α ,5 β -THMD ($[M]^{++}=448.3205$, mass error 4.02 ppm, RT 4.32 min) at 70 eV

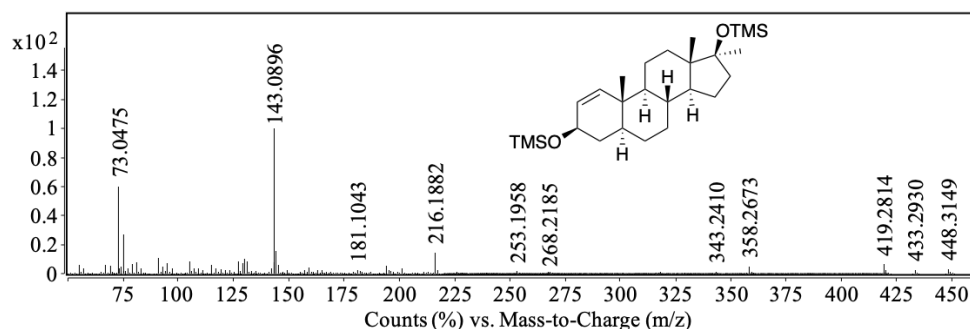


Figure 38: Normalized EI mass spectrum (GC-QTOF-MS) of TMS derivative of the metabolite tentatively assigned as 3 β ,5 α -THMD, formed by the incubation of AKR1C4 with 5 α -DHMD ($[M]^{++}=448.3149$, mass error -8.48 ppm, RT 4.97 min) at 70 eV

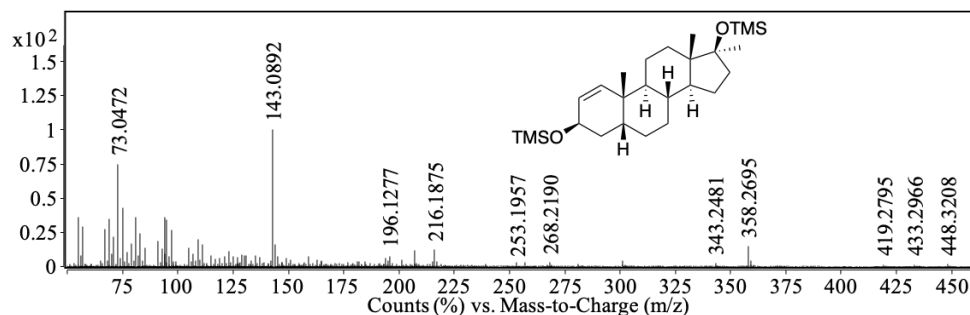


Figure 39: Normalized EI mass spectrum (GC-QTOF-MS) of TMS derivative of the metabolite tentatively assigned as 3 β ,5 β -THMD, formed by the incubation of AKR1C4 with 5 β -DHMD ($[M]^{++}=448.3208$, mass error 4.68 ppm, RT 4.49 min) at 70 eV

Table 24: Postulated fragments, exact masses, accurate masses, mass errors ($\Delta m/z$) for the metabolite tentatively assigned as 3 β ,5 α -THMD, formed by the incubation of AKR1C4 with 5 α -DHMD (GC-EI-QTOF-MS)

Postulated fragment	Exact mass [m/z]	Accurate mass [m/z]	$\Delta m/z$ [ppm]
[M] ⁺⁺	448.3187	448.3149	-8.48
[M-CH ₃] ⁺	433.2953	433.2930	-5.31
[M-TMSOH] ⁺⁺	358.2686	358.2673	-3.63
[M-CH ₃ -TMSOH] ⁺	343.2452	343.2410	-12.24
[M-2xTMSOH] ⁺⁺	268.2186	268.2185	-0.37
[M-CH ₃ -2xTMSOH] ⁺	253.1951	253.1958	2.76
[C ₁₀ H ₁₇ OSi] ⁺	181.1043	181.1043	0
[C ₇ H ₁₅ OSi] ⁺	143.0887	143.0896	6.29
[TMS] ⁺	73.0468	73.0475	9.58

Table 25: Postulated fragments, exact masses, accurate masses, mass errors ($\Delta m/z$) for the metabolite tentatively assigned as 3 β ,5 β -THMD, formed by the incubation of AKR1C4 with 5 β -DHMD (GC-EI-QTOF-MS)

Postulated fragment	Exact mass [m/z]	Accurate mass [m/z]	$\Delta m/z$ [ppm]
[M] ⁺⁺	448.3187	448.3208	4.68
[M-CH ₃] ⁺	433.2953	433.2966	3.00
[M-TMSOH] ⁺⁺	358.2686	358.2695	2.51
[M-CH ₃ -TMSOH] ⁺	343.2452	343.2481	8.45
[M-2xTMSOH] ⁺⁺	268.2186	268.2190	1.49
[M-CH ₃ -2xTMSOH] ⁺	253.1951	253.1957	2.37
[C ₁₁ H ₂₀ OSi] ⁺	196.1278	196.1277	-0.51
[C ₇ H ₁₅ OSi] ⁺	143.0887	143.0892	3.49
[TMS] ⁺	73.0468	73.0472	5.48

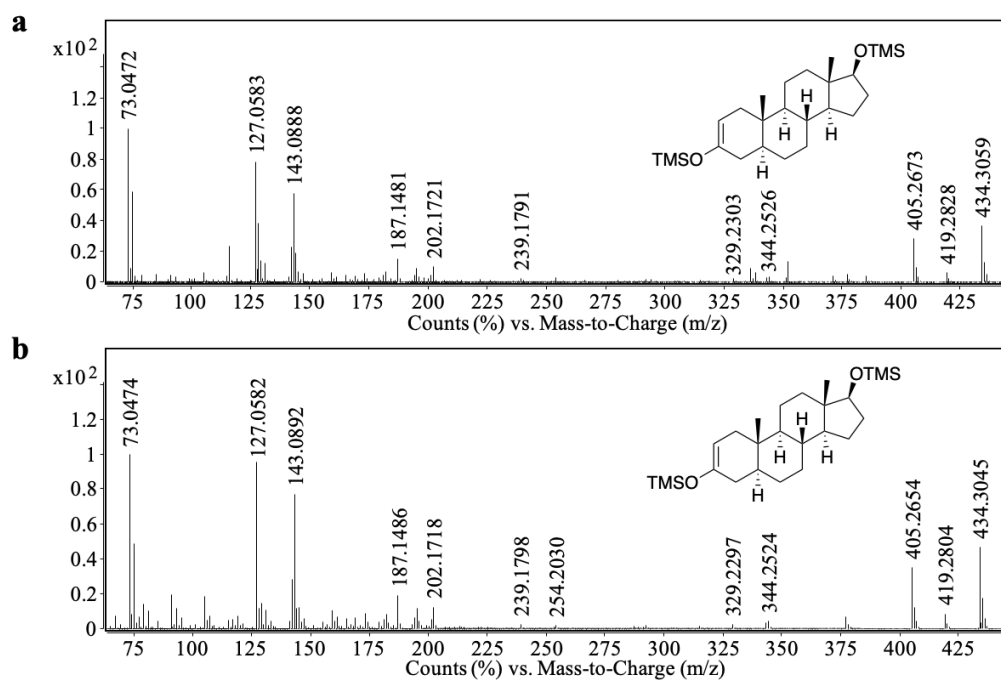


Figure 40: Normalized mass spectra (GC-QTOF-MS) of TMS derivatives of (a) 5 α -DHT ($[M]^{++}=434.3059$, mass error 6.45 ppm, RT 4.49 min), formed by human keratinocytes incubated with T, and (b) reference compound 5 α -DHT ($[M]^{++}=434.3045$, mass error 3.22 ppm, RT 4.50 min), at 70 eV

Table 26: Postulated fragments, exact masses, accurate masses, mass errors ($\Delta m/z$) for the metabolite 5 α -DHT formed by human keratinocytes incubated with T (GC-EI-QTOF-MS)

Postulated fragment	Exact mass [m/z]	Accurate mass [m/z]	$\Delta m/z$ [ppm]
$[M]^{++}$	434.3031	434.3059	6.45
$[M-CH_3]^+$	419.2796	419.2828	7.63
$[M-TMSOH]^{++}$	344.2530	344.2526	-1.16
$[M-CH_3-TMSOH]^+$	329.2295	329.2303	2.43
$[M-CH_3-2xTMSOH]^+$	239.1794	239.1791	-1.25
$[TMS]^+$	73.0468	73.0474	8.21

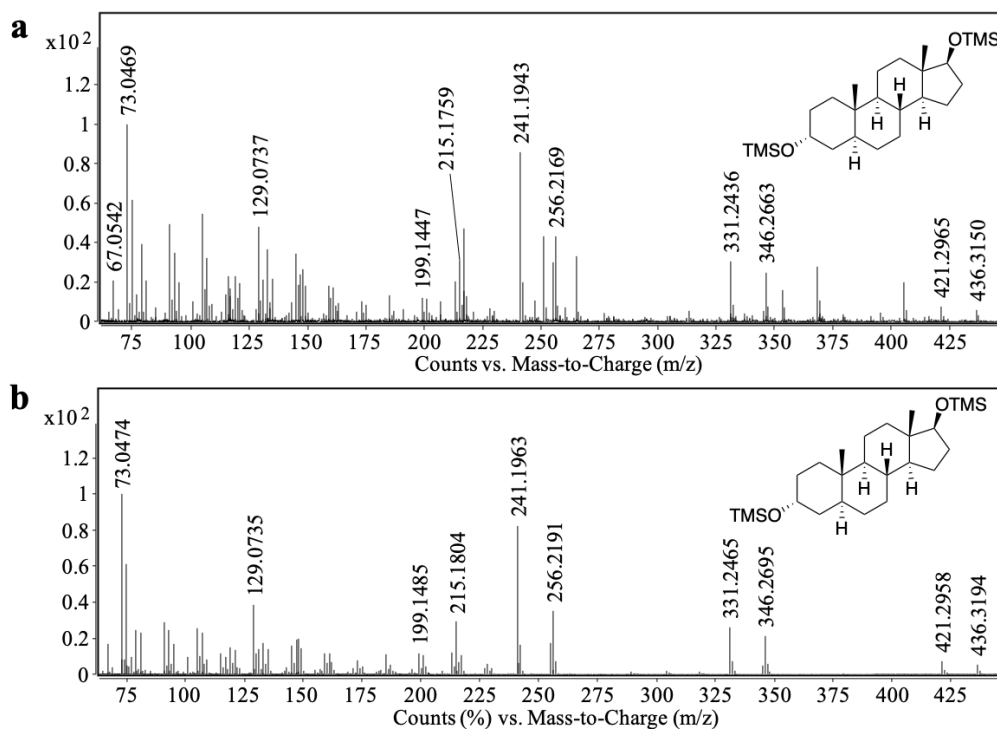


Figure 41: Normalized mass spectra (GC-QTOF-MS) of TMS derivatives of (a) 5 α -Adiol ($[M]^{++}=436.3150$, mass error -8.48 ppm, RT 3.94 min), formed by human keratinocytes incubated with T, and (b) reference compound 5 α -Adiol ($[M]^{++}=436.3194$, mass error 1.60 ppm, RT 3.94 min), at 70 eV

Table 27: Postulated fragments, exact masses, accurate masses, mass errors ($\Delta m/z$) for the metabolite 5 α -Adiol formed by human keratinocytes incubated with T (GC-EI-QTOF-MS)

Postulated fragment	Exact mass [m/z]	Accurate mass [m/z]	$\Delta m/z$ [ppm]
$[M]^{++}$	436.3187	436.3150	-8.48
$[M-CH_3]^+$	421.2953	421.2965	2.85
$[M-TMSOH]^+$	346.2686	346.2663	-6.64
$[M-CH_3-TMSOH]^+$	331.2452	331.2436	-4.83
$[M-2xTMSOH]^+$	256.2186	256.2169	-6.63
$[M-CH_3-2xTMSOH]^+$	241.1951	241.1943	-3.32
$[C_6H_{13}OSi]^+$	129.0730	129.0737	5.42
$[TMS]^+$	73.0468	73.0469	1.37

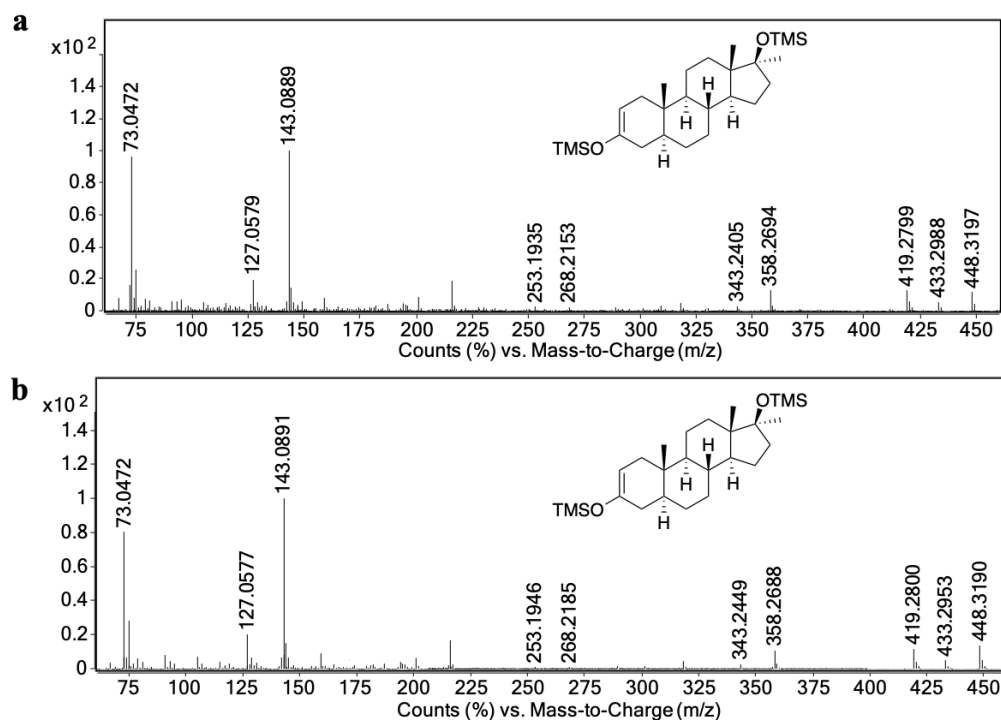


Figure 42: Normalized mass spectra (GC-QTOF-MS) of TMS derivatives of (a) MSL ($[M]^{++}=448.3197$, mass error 2.23 ppm, RT 5.12 min), formed by human keratinocytes incubated with MT, and (b) reference compound MSL ($[M]^{++}=448.3190$, mass error 0.67 ppm, RT 5.13 min), at 70 eV

Table 28: Postulated fragments, exact masses, accurate masses, mass errors ($\Delta m/z$) for the metabolite MSL formed by human keratinocytes incubated with MT (GC-EI-QTOF-MS)

Postulated fragment	Exact mass [m/z]	Accurate mass [m/z]	$\Delta m/z$ [ppm]
$[M]^{++}$	448.3187	448.3197	2.23
$[M-CH_3]^+$	433.2953	433.2988	8.08
$[M-TMSOH]^{++}$	358.2686	358.2694	2.23
$[M-CH_3-TMSOH]^+$	343.2452	343.2405	-13.69
$[M-2xTMSOH]^{++}$	268.2186	268.2153	-12.30
$[M-CH_3-2xTMSOH]^+$	253.1951	253.1935	-6.32
$[C_7H_{15}OSi]^+$	143.0887	143.0889	1.40
$[TMS]^+$	73.0468	73.0472	5.48

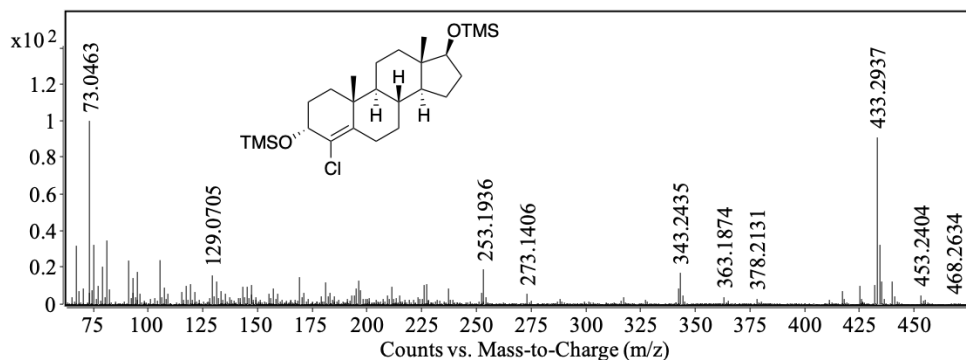


Figure 43: Normalized mass spectra (GC-QTOF-MS) of TMS derivative of 3 α -DHCLT ($[M]^{++}=468.2634$, mass error -1.49 ppm, RT 4.63 min), formed by human keratinocytes incubated with CLT, at 70 eV

Table 29: Postulated fragments, exact masses, accurate masses, mass errors ($\Delta m/z$) for the metabolite 3 α -DHCLT formed by human keratinocytes incubated with CLT (GC-EI-QTOF-MS)

Postulated fragment	Exact mass [m/z]	Accurate mass [m/z]	$\Delta m/z$ [ppm]
$[M]^{++}$	468.2641	468.2634	-1.49
$[M-CH_3]^+$	453.2406	453.2404	-0.44
$[M-Cl]^+$	433.2953	433.2937	-3.69
$[M-Cl-TMSOH]^+$	343.2452	343.2435	-4.95
$[M-Cl-2xTMSOH]^+$	253.1951	253.1936	-5.92
$[M-TMSOH]^+$	378.2140	378.2131	-2.38
$[M-CH_3-TMSOH]^+$	363.1905	363.1874	-8.54
$[M-CH_3-2xTMSOH]^+$	273.1405	273.1406	0.37
$[TMS]^+$	73.0468	73.0463	-6.84

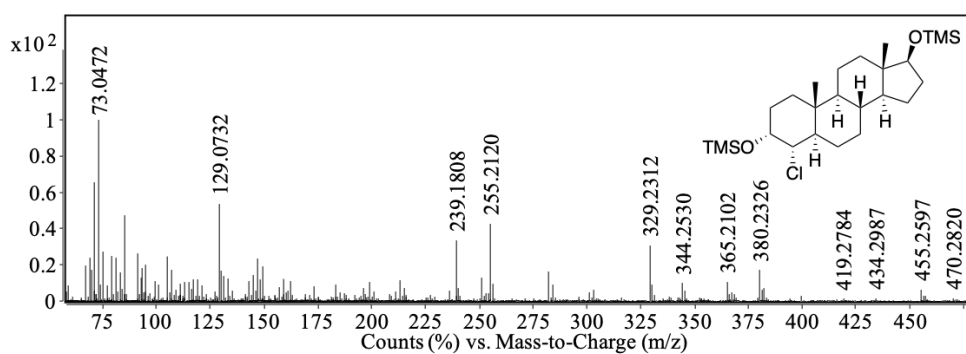


Figure 44: Normalized mass spectra (GC-QTOF-MS) of TMS derivative of 3 α ,4 α ,5 α -THCLT ($[M]^{++}=470.2820$, mass error 4.68 ppm, RT 5.02 min), formed by human keratinocytes incubated with CLT, at 70 eV

Table 30: Postulated fragments, exact masses, accurate masses, mass errors ($\Delta m/z$) for the metabolite 3 α ,4 α ,5 α -THCLT formed by human keratinocytes incubated with CLT (GC-EI-QTOF-MS)

Postulated fragment	Exact mass [m/z]	Accurate mass [m/z]	$\Delta m/z$ [ppm]
[M] ⁺	470.2798	470.2820	4.68
[M-CH ₃] ⁺	455.2563	455.2597	7.47
[M-HCl] ⁺	434.3031	434.2987	-10.13
[M-CH ₃ -HCl] ⁺	419.2796	419.2784	-2.86
[M-HCl-TMSOH] ⁺	344.2530	344.2530	0.00
[M-HCl-TMSOH-CH ₃] ⁺	329.2295	329.2312	5.16
[M-HCl-TMSOH-TMSO] ⁺	255.2107	255.2120	5.09
[M-TMSOH] ⁺	380.2297	380.2326	7.63
[M-CH ₃ -TMSOH] ⁺	365.2062	365.2102	10.95
[M-HCl-2xTMSOH-CH ₃] ⁺	239.1794	239.1808	5.85
[C ₆ H ₁₃ OSi] ⁺	129.0730	129.0732	1.55
[TMS] ⁺	73.0468	73.0472	5.48

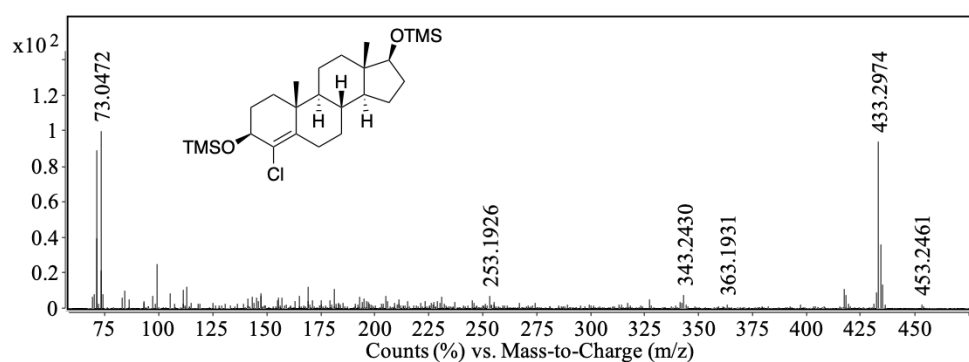


Figure 45: Normalized mass spectra (GC-QTOF-MS) of TMS derivative of 3 β -DHCLT ([M-CH₃]⁺=453.2461, mass error 12.13 ppm, RT 5.20 min), formed by human keratinocytes incubated with CLT, at 70 eV

Table 31: Postulated fragments, exact masses, accurate masses, mass errors ($\Delta m/z$) for the metabolite 3 β -DHCLT formed by human keratinocytes incubated with CLT (GC-EI-QTOF-MS)

Postulated fragment	Exact mass [m/z]	Accurate mass [m/z]	$\Delta m/z$ [ppm]
[M-CH ₃] ⁺	453.2406	453.2461	12.13
[M-Cl] ⁺	433.2953	433.2974	4.85
[M-Cl-TMSOH] ⁺	343.2452	343.2430	-6.41
[M-Cl-2xTMSOH] ⁺	253.1951	253.1926	-9.87
[M-CH ₃ -TMSOH] ⁺	363.1905	363.1931	7.16
[TMS] ⁺	73.0468	73.0472	5.48

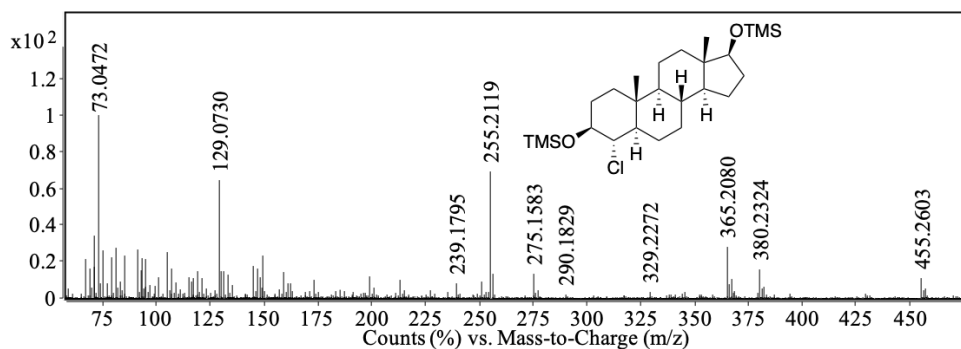


Figure 46: Normalized mass spectra (GC-QTOF-MS) of TMS derivative of 3β,4α,5α-THCLT ($[M-CH_3]^+$ =455.2603, mass error 8.79 ppm, RT 5.64 min), formed by human keratinocytes incubated with CLT, at 70 eV

Table 32: Postulated fragments, exact masses, accurate masses, mass errors ($\Delta m/z$) for the metabolite 3β,4α,5α-THCLT formed by human keratinocytes incubated with CLT (GC-EI-QTOF-MS)

Postulated fragment	Exact mass [m/z]	Accurate mass [m/z]	$\Delta m/z$ [ppm]
$[M-CH_3]^+$	455.2563	455.2603	8.79
$[M-HCl-TMSOH-CH_3]^+$	329.2295	329.2272	-6.99
$[M-HCl-TMSOH-TMSO]^+$	255.2107	255.2119	4.70
$[M-TMSOH]^+$	380.2297	380.2324	7.10
$[M-CH_3-TMSOH]^+$	365.2062	365.2080	4.93
$[M-2xTMSOH]^+$	290.1796	290.1829	11.37
$[M-CH_3-2xTMSOH]^+$	275.1561	275.1583	8.00
$[M-HCl-2xTMSOH-CH_3]^+$	239.1794	239.1795	0.42
$[C_6H_{13}OSi]^+$	129.0730	129.0730	0.00
$[TMS]^+$	73.0468	73.0472	5.48

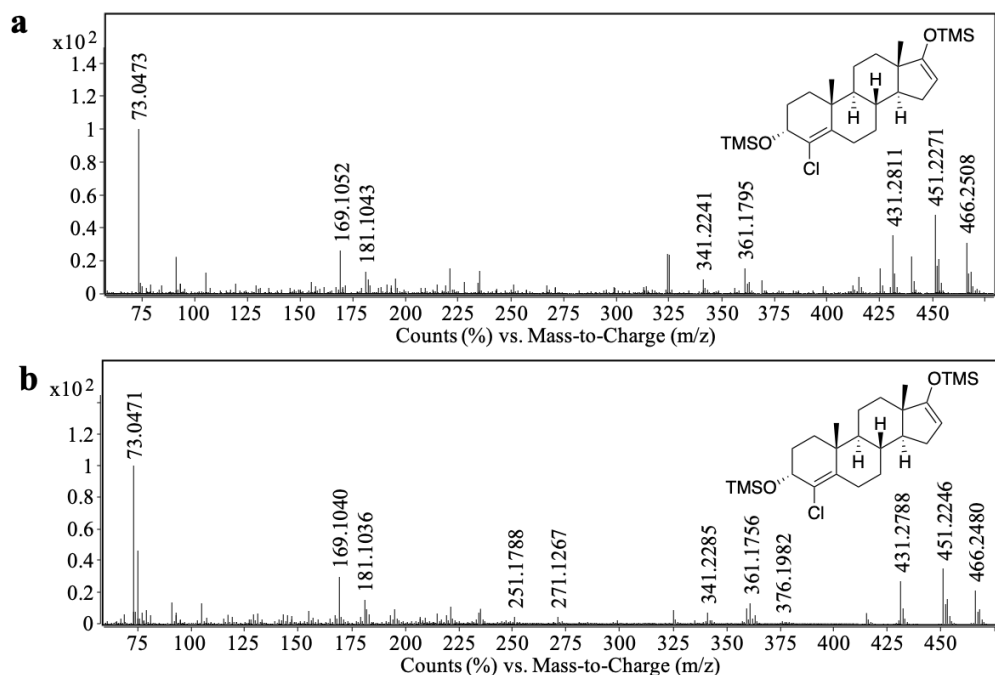


Figure 47: Normalized mass spectra (GC-QTOF-MS) of TMS derivatives of (a) 4-chloro-3 α -hydroxy-androst-4-ene-17-one ($[M]^{++}=466.2508$, mass error 4.93 ppm, RT 4.48 min), formed by human keratinocytes incubated with CLT, and (b) reference compound 4-chloro-3 α -hydroxy-androst-4-ene-17-one ($[M]^{++}=466.2480$, mass error -1.07 ppm, RT 4.49 min), at 70 eV

Table 33: Postulated fragments, exact masses, accurate masses, mass errors ($\Delta m/z$) for the metabolite 4-chloro-3 α -hydroxy-androst-4-ene-17-one formed by human keratinocytes incubated with CLT (GC-EI-QTOF-MS)

Postulated fragment	Exact mass [m/z]	Accurate mass [m/z]	$\Delta m/z$ [ppm]
$[M]^{++}$	466.2485	466.2508	4.93
$[M-CH_3]^+$	451.2250	451.2271	4.65
$[M-Cl]^+$	431.2796	431.2811	3.48
$[M-Cl-TMSOH]^+$	341.2295	341.2241	-15.83
$[M-CH_3-TMSOH]^+$	361.1749	361.1795	12.74
$[TMS]^+$	73.0468	73.0473	6.84

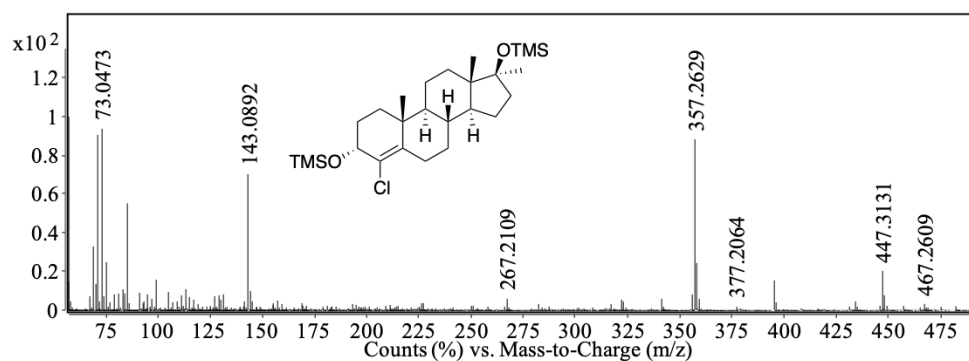


Figure 48: Normalized mass spectra (GC-QTOF-MS) of TMS derivative of 3 α -DHCLMT ($[M-CH_3]^+=467.2609$, mass error 9.84 ppm, RT 5.16 min), formed by human keratinocytes incubated with CLMT, at 70 eV

Table 34: Postulated fragments, exact masses, accurate masses, mass errors ($\Delta m/z$) for the metabolite 3 α -DHCLMT formed by human keratinocytes incubated with CLMT (GC-EI-QTOF-MS)

Postulated fragment	Exact mass [m/z]	Accurate mass [m/z]	$\Delta m/z$ [ppm]
[M-CH ₃] ⁺	467.2563	467.2609	9.84
[M-Cl] ⁺	447.3109	447.3131	4.92
[M-Cl-TMSOH] ⁺	357.2608	357.2629	5.88
[M-Cl-2xTMSOH] ⁺	267.2107	267.2109	0.75
[M-CH ₃ -TMSOH] ⁺	377.2062	377.2064	0.53
[C ₇ H ₁₅ OSi] ⁺	143.0887	143.0892	3.49
[TMS] ⁺	73.0468	73.0473	6.84

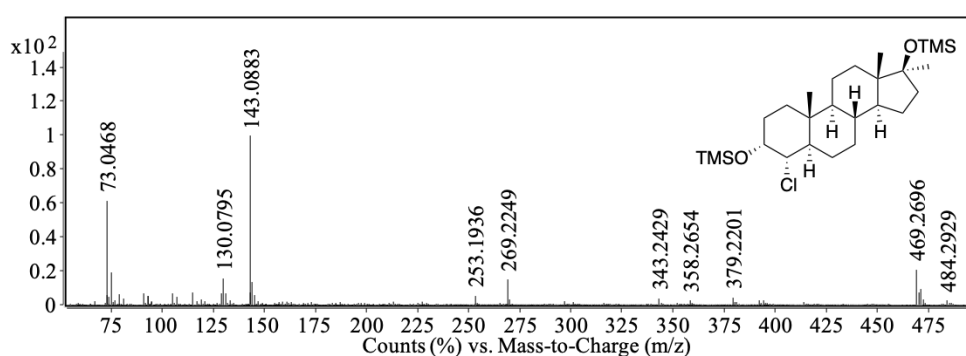


Figure 49: Normalized mass spectra (GC-QTOF-MS) of TMS derivative of 3 α ,4 α ,5 α -THCLMT ($[M]^{*+}=484.2929$, mass error -5.16 ppm, RT 5.59 min), formed by human keratinocytes incubated with CLMT, at 70 eV

Table 35: Postulated fragments, exact masses, accurate masses, mass errors ($\Delta m/z$) for the metabolite 3 α ,4 α ,5 α -THCLMT formed by human keratinocytes incubated with CLMT (GC-EI-QTOF-MS)

Postulated fragment	Exact mass [m/z]	Accurate mass [m/z]	$\Delta m/z$ [ppm]
[M] ⁺	484.2954	484.2929	-5.16
[M-CH ₃] ⁺	469.2719	469.2696	-4.90
[M-HCl-TMSOH] ⁺	358.2686	358.2654	-8.93
[M-HCl-TMSOH-CH ₃] ⁺	343.2452	343.2429	-6.70
[M-HCl-TMSOH-TMSO] ⁺	269.2264	269.2249	-5.57
[M-CH ₃ -TMSOH] ⁺	379.2218	379.2201	-4.48
[M-HCl-TMSOH-CH ₃] ⁺	253.1951	253.1936	-5.92
[C ₇ H ₁₅ OSi] ⁺	143.0887	143.0883	-2.80
[TMS] ⁺	73.0468	73.0468	0.00

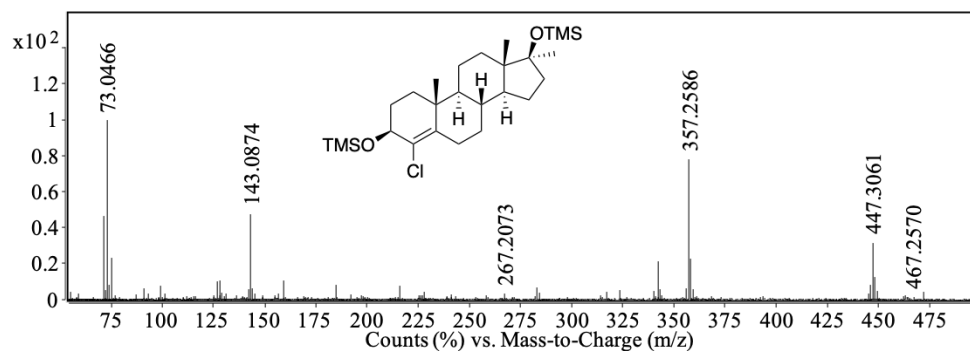


Figure 50: Normalized mass spectra (GC-QTOF-MS) of TMS derivative of 3 β -DHCLMT ($[M-CH_3]^+$ =467.2570, mass error 1.50 ppm, RT 5.89 min), formed by human keratinocytes incubated with CLMT, at 70 eV

Table 36: Postulated fragments, exact masses, accurate masses, mass errors ($\Delta m/z$) for the metabolite 3 β -DHCLMT formed by human keratinocytes incubated with CLMT (GC-EI-QTOF-MS)

Postulated fragment	Exact mass [m/z]	Accurate mass [m/z]	$\Delta m/z$ [ppm]
$[M-CH_3]^+$	467.2563	467.2570	1.50
$[M-Cl]^+$	447.3109	447.3061	-10.73
$[M-Cl-TMSOH]^+$	357.2608	357.2586	-6.16
$[M-Cl-2xTMSOH]^+$	267.2107	267.2073	-12.72
$[C_7H_{15}OSi]^+$	143.0887	143.0874	-9.09
$[TMS]^+$	73.0468	73.0466	-2.74

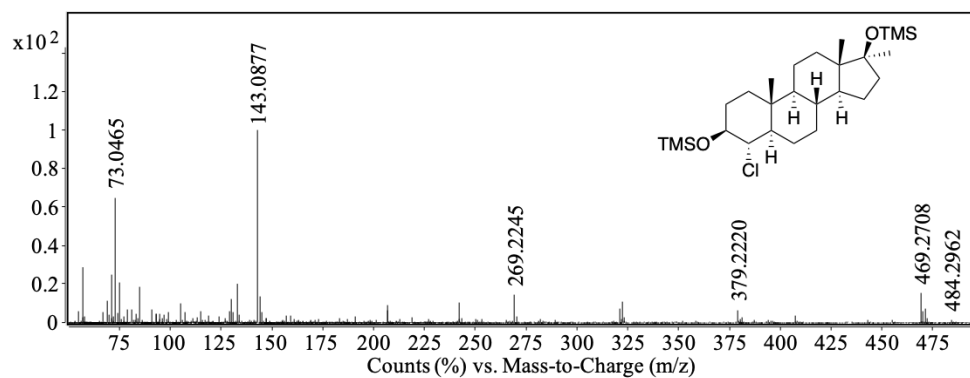


Figure 51: Normalized mass spectra (GC-QTOF-MS) of TMS derivative of 3 β ,4 α ,5 α -THCLMT ($[M]^+$ =484.2962, mass error 1.65 ppm, RT 6.46 min), formed by human keratinocytes incubated with CLMT, at 70 eV

Table 37: Postulated fragments, exact masses, accurate masses, mass errors ($\Delta m/z$) for the metabolite 3 β ,4 α ,5 α -THCLMT formed by human keratinocytes incubated with CLMT (GC-EI-QTOF-MS)

Postulated fragment	Exact mass [m/z]	Accurate mass [m/z]	$\Delta m/z$ [ppm]
[M] ⁺	484.2954	484.2962	1.65
[M-CH ₃] ⁺	469.2719	469.2708	-2.34
[M-HCl-TMSOH-TMSO] ⁺	269.2264	269.2245	-7.06
[M-CH ₃ -TMSOH] ⁺	379.2218	379.2220	0.53
[C ₇ H ₁₅ OSi] ⁺	143.0887	143.0877	-6.99
[TMS] ⁺	73.0468	73.0465	-4.11

Table 38: Results of the metabolites detected in samples obtained after 2-day incubation of medaka embryos with 10 μ M MD by LC-ESI-MS. This table is adapted from my published paper [168]

ID	Elemental Composition	[M+H] ⁺ (calc)	[M+H] ⁺ (exp)	Mass error [ppm]	Retention Time (min)	Assignment
M1	C ₂₀ H ₂₈ O ₃	317.2111	317.2112	-0.32	4.71	6 β OH-MD
M2	C ₂₀ H ₂₈ O ₃	317.2111	317.2100	-3.47	5.22	18OH-MD*
M3	C ₂₀ H ₂₈ O ₃	317.2111	317.2105	-1.89	5.34	16OH-MD*
M4	C ₂₀ H ₃₀ O ₂	303.2319	303.2318	0.33	6.97	5 β -DHMD

* Tentative assignment.

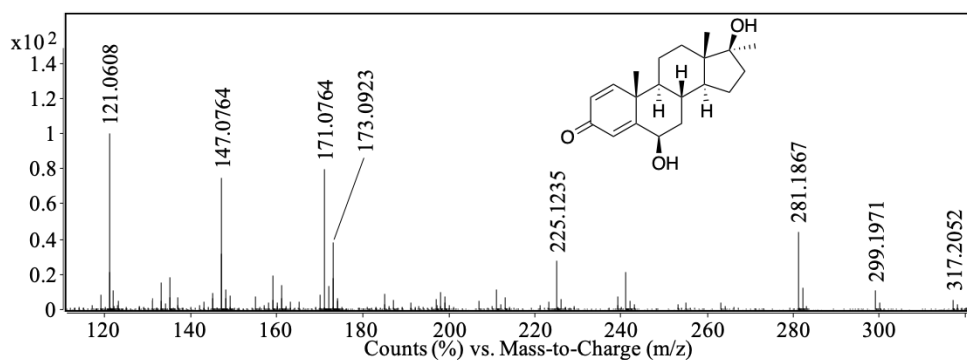


Figure 52: Product ion spectra (LC-ESI-MS/MS) of reference compound 6 β OH-MD, [M+H]⁺=317.2077, mass error -10.72 ppm, RT 4.78 min, collision energy 23.1 eV

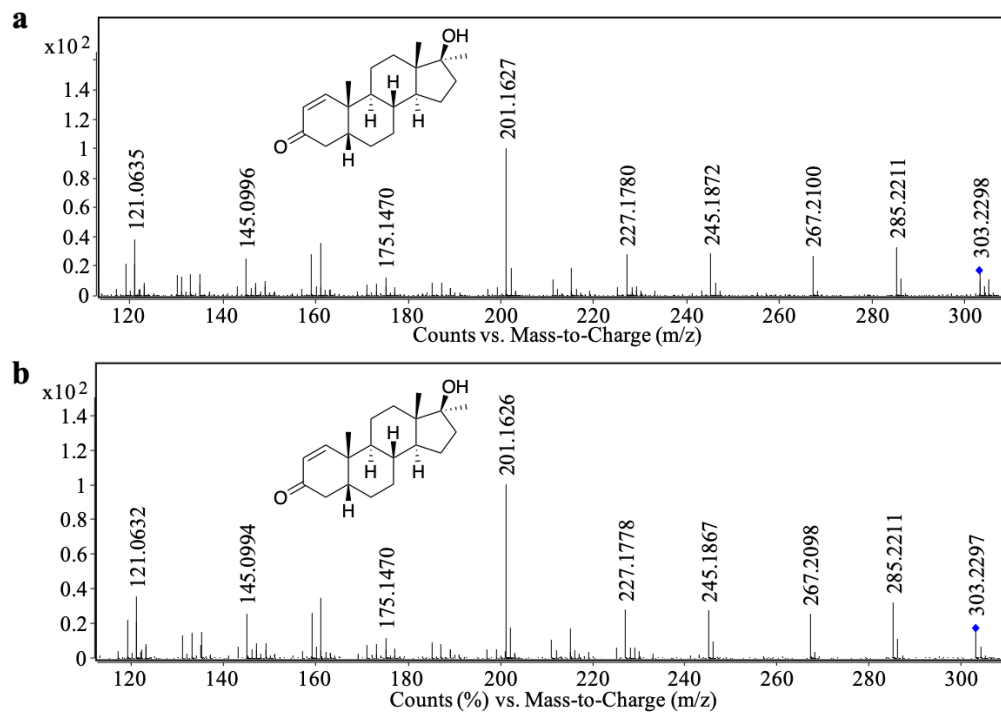


Figure 53: Product ion spectra (LC-ESI-MS/MS) of (a) 5 β -DHMD (**M4**) formed by medaka embryos incubated with 10 μ M MD, $[M+H]^+ = 303.2318$, mass error 0.33 ppm, RT 6.97 min, collision energy 22.3 eV, and (b) reference compound 5 β -DHMD, $[M+H]^+ = 303.2303$, mass error -5.28 ppm, RT 6.96 min, collision energy 22.3 eV

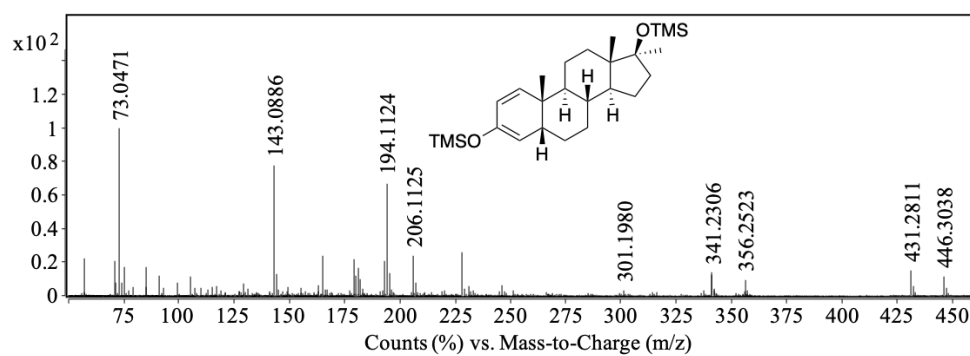
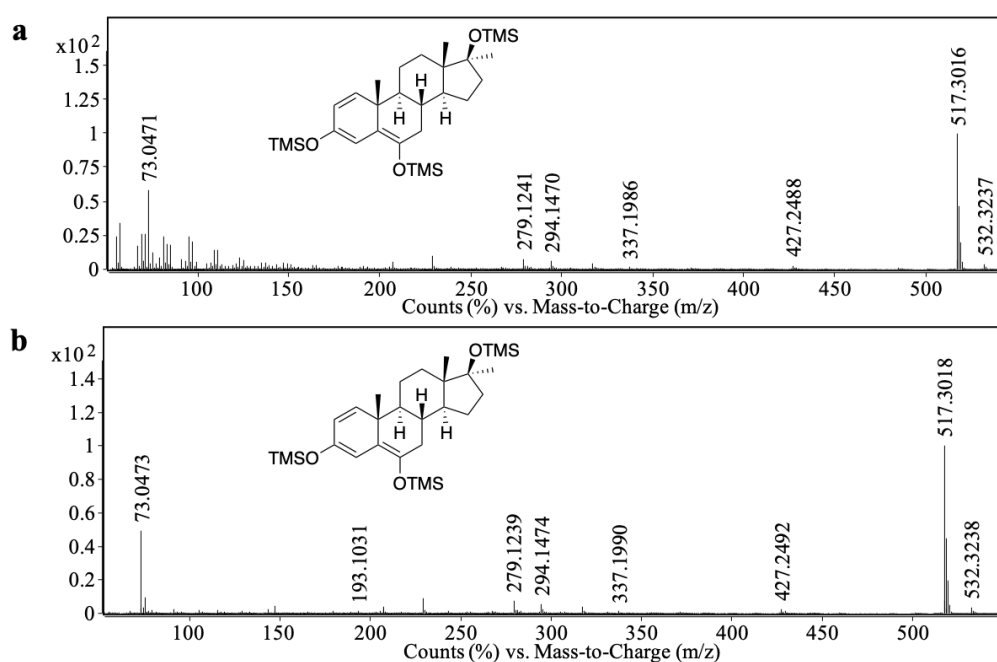


Figure 54: Normalized EI mass spectrum (GC-QTOF-MS) of TMS derivative of 5 β -DHMD (**M4**) formed by medaka embryos incubated with 10 μ M MD, $[M]^+ = 446.3038$, mass error 1.57 ppm, RT 3.99 min, at 70 eV. This figure is adapted from my published paper [168]

Table 39: Postulated fragments, exact masses, accurate masses, mass errors ($\Delta m/z$) for TMS-derivative of **M4**, GC-EI-QTOF-MS

Postulated fragment	Exact mass [m/z]	Accurate mass [m/z]	$\Delta m/z$ [ppm]
$[M]^+$	446.3031	446.3038	1.57
$[M-CH_3]^+$	431.2796	431.2811	3.48
$[M-TMSOH]^+$	356.2530	356.2523	-1.96
$[M-CH_3-TMSOH]^+$	341.2295	341.2306	3.22
$[M-2xTMSOH]^+$	266.2029	266.2012	-6.39
$[C_7H_{15}OSi]^+$	143.0887	143.0886	-0.70
$[TMS]^+$	73.0468	73.0471	4.11

**Figure 55:** Normalized EI mass spectra (GC-QTOF-MS) of TMS derivatives of (a) 6 β OH-MD (**M1**) formed by medaka embryos incubated with 10 μ M MD, $[M]^+$ =532.3237, mass error 3.38 ppm, RT 6.45 min, and (b) reference compound 6 β OH-MD, $[M]^+$ =532.3238, mass error 3.57 ppm, RT 6.45 min, at 70 eV. This figure is adapted from my published paper [168]**Table 40:** Postulated fragments, exact masses, accurate masses, mass errors ($\Delta m/z$) for TMS-derivative of **M1**, GC-EI-QTOF-MS. This table is adapted from my published paper [168]

Postulated fragment	Exact mass [m/z]	Accurate mass [m/z]	Mass error [ppm]
$[M]^+$	532.3219	532.3237	3.38
$[M-CH_3]^+$	517.2984	517.3016	6.19
$[M-CH_3-TMSOH]^+$	427.2483	427.2488	1.17
$[M-CH_3-2xTMSOH]^+$	337.1982	337.1986	1.19
$[TMS]^+$	73.0468	73.0471	4.11

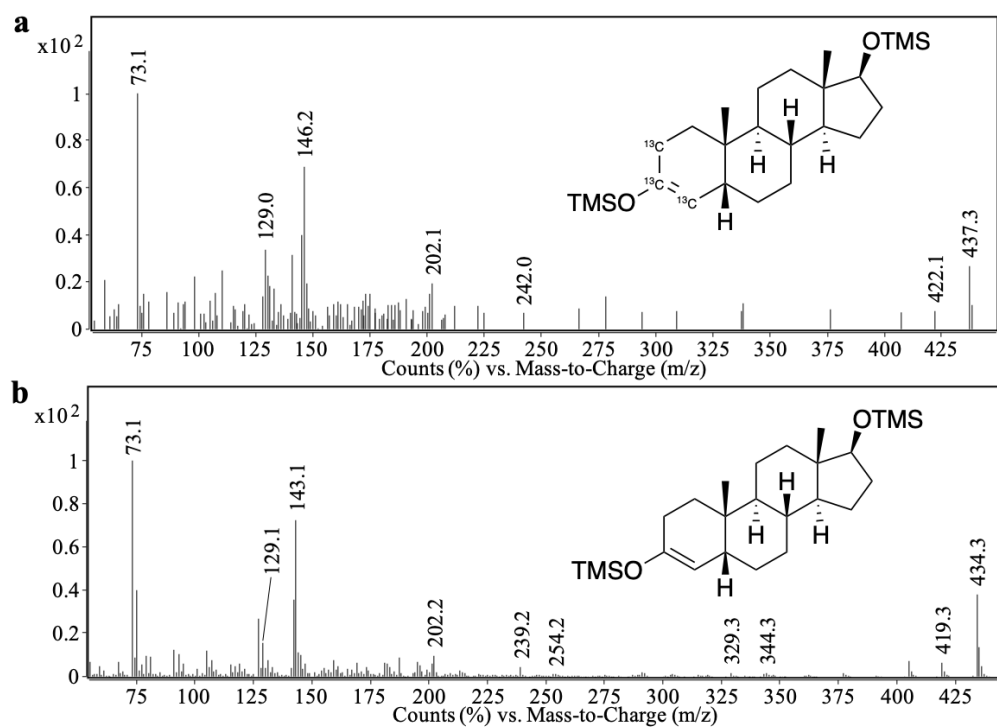


Figure 56: Normalized mass spectra (GC-EI-MS) of TMS derivatives of (a) [¹³C₃]-5β-DHT ($[M]^{+}=437$, RT 9.80 min), formed by medaka embryos incubated with [¹³C₃]-T, and (b) reference compound 5β-DHT ($[M]^{+}=434$, RT 9.87 min), at 70 eV

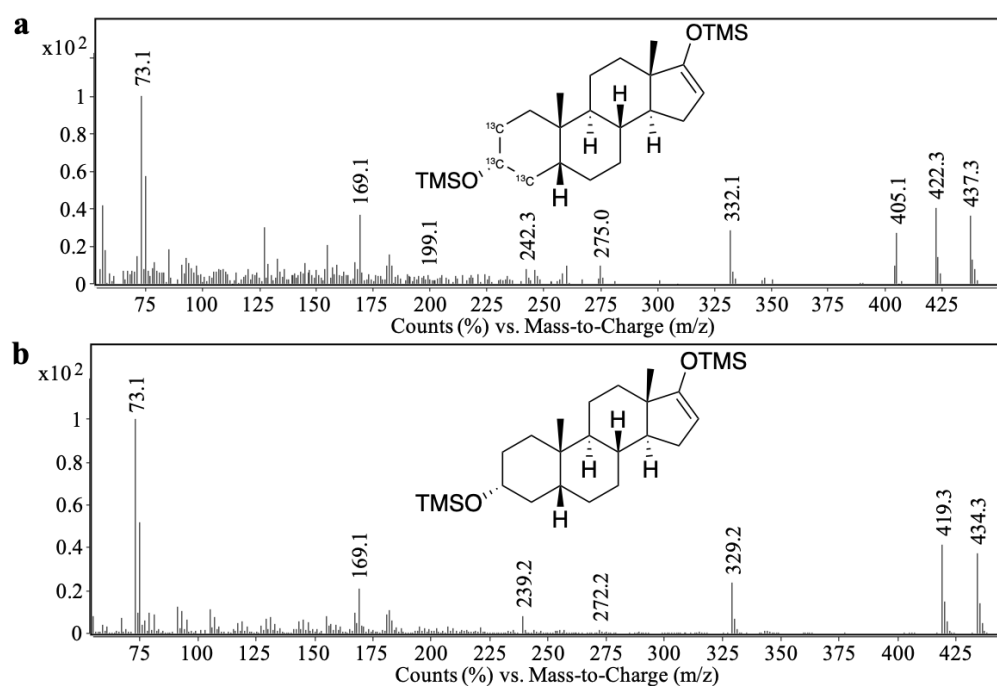


Figure 57: Normalized mass spectra (GC-EI-MS) of TMS derivatives of (a) [¹³C₃]-Etio ($[M]^{+}=437$, RT 11.03 min), formed by medaka embryos incubated with [¹³C₃]-T, and (b) reference compound Etio ($[M]^{+}=434$, RT 11.08 min), at 70 eV

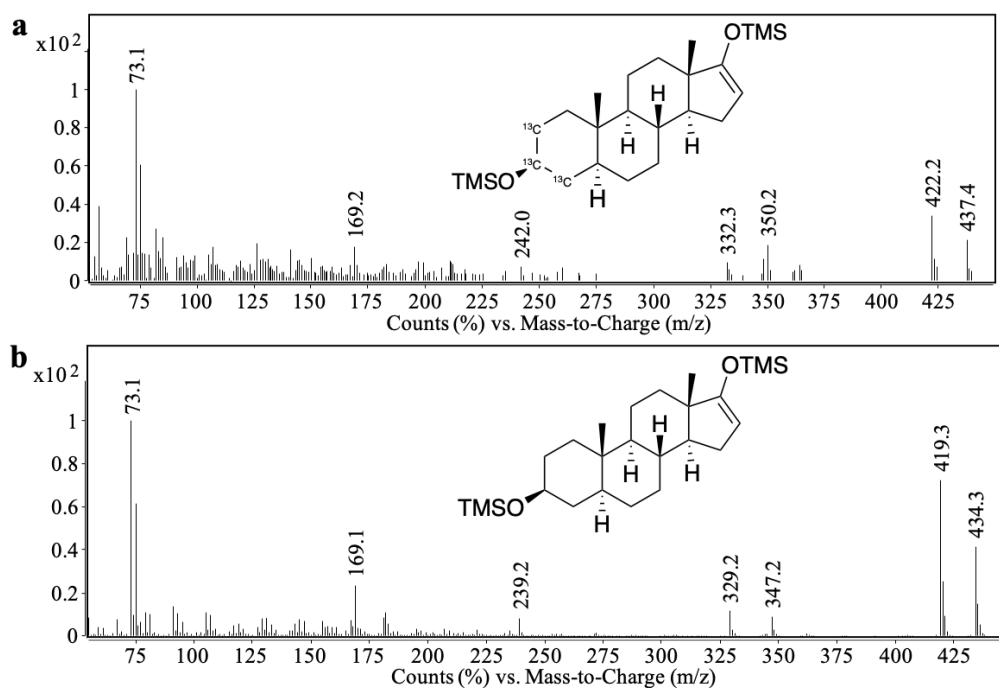


Figure 58: Normalized mass spectra (GC-EI-MS) of TMS derivatives of (a) $[^{13}\text{C}_3]$ -EA ($[M]^{++}=437$, RT 12.35 min), formed by medaka embryos incubated with $[^{13}\text{C}_3]$ -T, and (b) reference compound EA ($[M]^{++}=434$, RT 12.36 min), at 70 eV

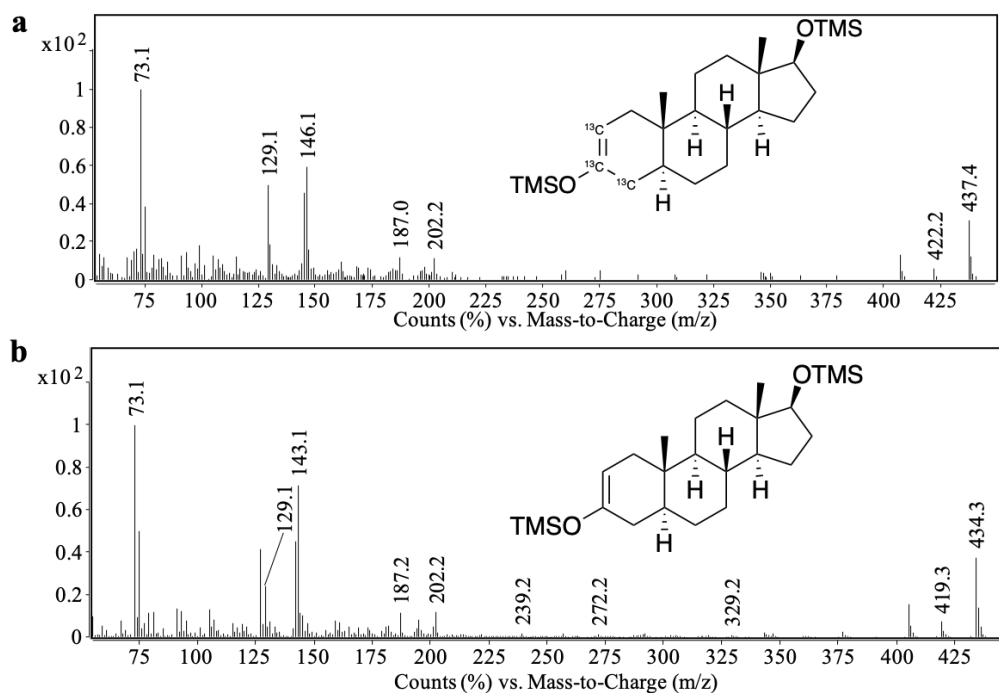


Figure 59: Normalized mass spectra (GC-EI-MS) of TMS derivatives of (a) $[^{13}\text{C}_3]$ -5 α -DHT ($[M]^{++}=437$, RT 12.99 min), formed by medaka embryos incubated with $[^{13}\text{C}_3]$ -T, and (b) reference compound 5 α -DHT ($[M]^{++}=434$, RT 13.03 min), at 70 eV

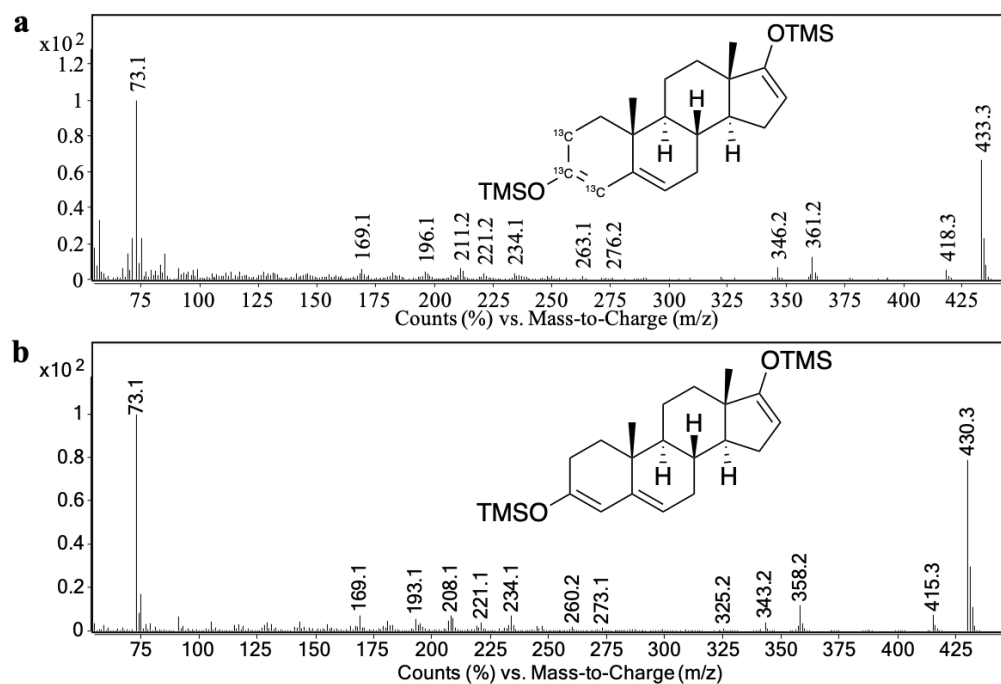


Figure 60: Normalized mass spectra (GC-EI-MS) of TMS derivatives of (a) $[^{13}\text{C}_3]$ -AED ($[M]^{+}=433$, RT 13.26 min), formed by medaka embryos incubated with $[^{13}\text{C}_3]$ -T, and (b) reference compound AED ($[M]^{+}=430$, RT 13.26 min), at 70 eV

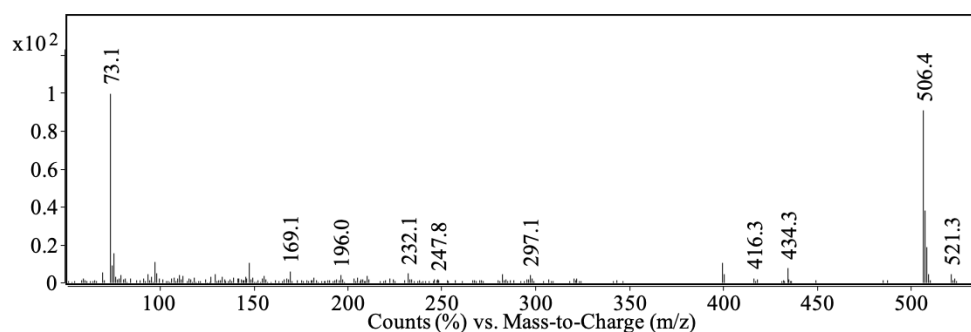


Figure 61: Normalized mass spectra (GC-EI-MS) of TMS derivative of an unidentified hydroxylated metabolite of $[^{13}\text{C}_3]$ -T ($[M]^{+}=521$, RT 16.54 min), at 70 eV

Table 41: Per-TMS derivatives of metabolites detected in samples obtained after incubation of medaka embryos with $[^{13}\text{C}_3]$ -T by GC-EI-MS

Analyte	Elemental Composition	$[M]^{+}$	Retention Time (min)
$[^{13}\text{C}_3]$ -5 α -DHT	$[^{13}\text{C}_3\text{C}_{22}\text{H}_{46}\text{O}_2\text{Si}_2]^{+}$	437	12.99
$[^{13}\text{C}_3]$ -5 β -DHT	$[^{13}\text{C}_3\text{C}_{22}\text{H}_{46}\text{O}_2\text{Si}_2]^{+}$	437	9.80
$[^{13}\text{C}_3]$ -Etio	$[^{13}\text{C}_3\text{C}_{22}\text{H}_{46}\text{O}_2\text{Si}_2]^{+}$	437	11.03
$[^{13}\text{C}_3]$ -EA	$[^{13}\text{C}_3\text{C}_{22}\text{H}_{46}\text{O}_2\text{Si}_2]^{+}$	437	12.35
$[^{13}\text{C}_3]$ -AED	$[^{13}\text{C}_3\text{C}_{22}\text{H}_{42}\text{O}_2\text{Si}_2]^{+}$	433	13.26
Unidentified metabolite	$[^{13}\text{C}_3\text{C}_{25}\text{H}_{50}\text{O}_3\text{Si}_3]^{+}$	521	16.54

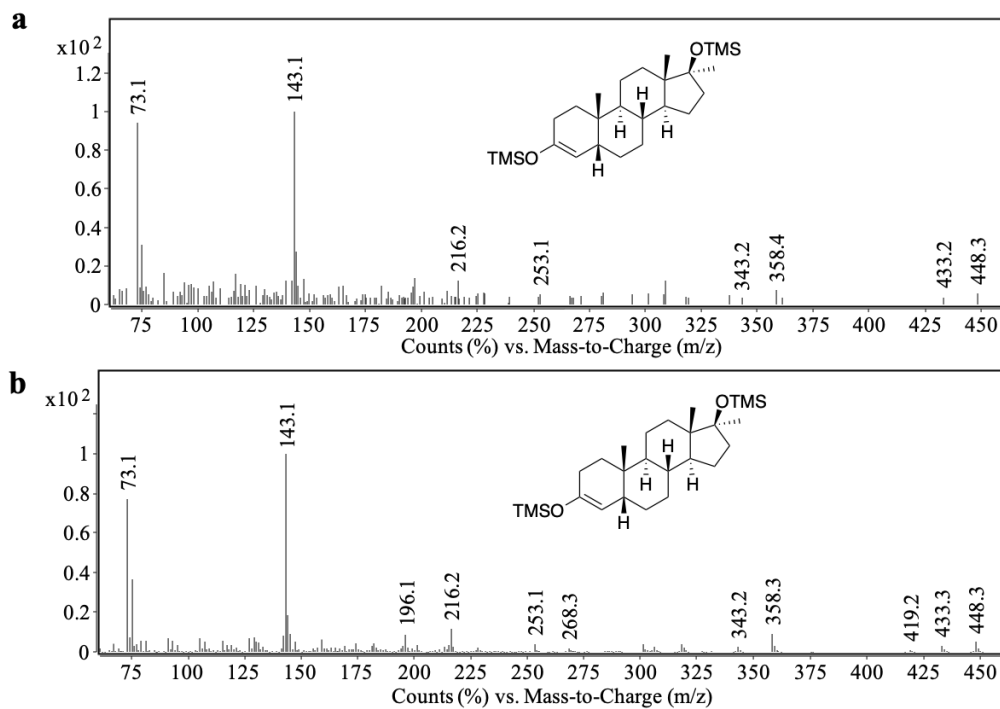


Figure 62: Normalized mass spectra (GC-EI-MS) of TMS derivatives of (a) 5β-MSL ($[M]^{+}=448$, RT 11.60 min), formed by medaka embryos incubated with MT, and (b) reference compound at 5β-MSL ($[M]^{+}=448$, RT 11.58 min), 70 eV

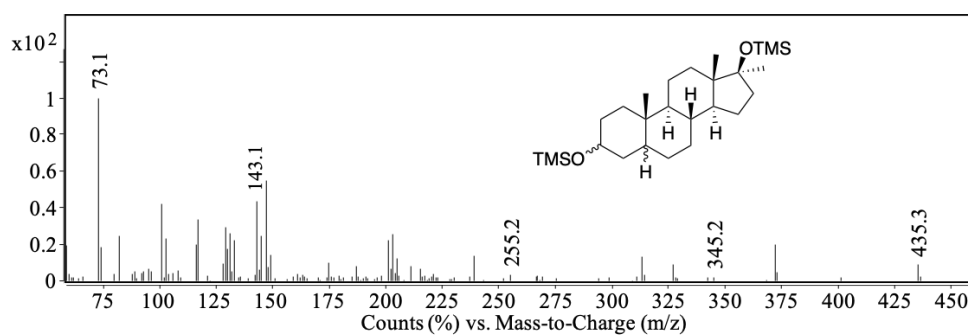


Figure 63: Normalized mass spectra (GC-EI-MS) of TMS derivative of 3ξ,5ξ-THMT ($[M-CH_3]^{+}=435$, RT 12.58 min), formed by medaka embryos incubated with MT, at 70 eV

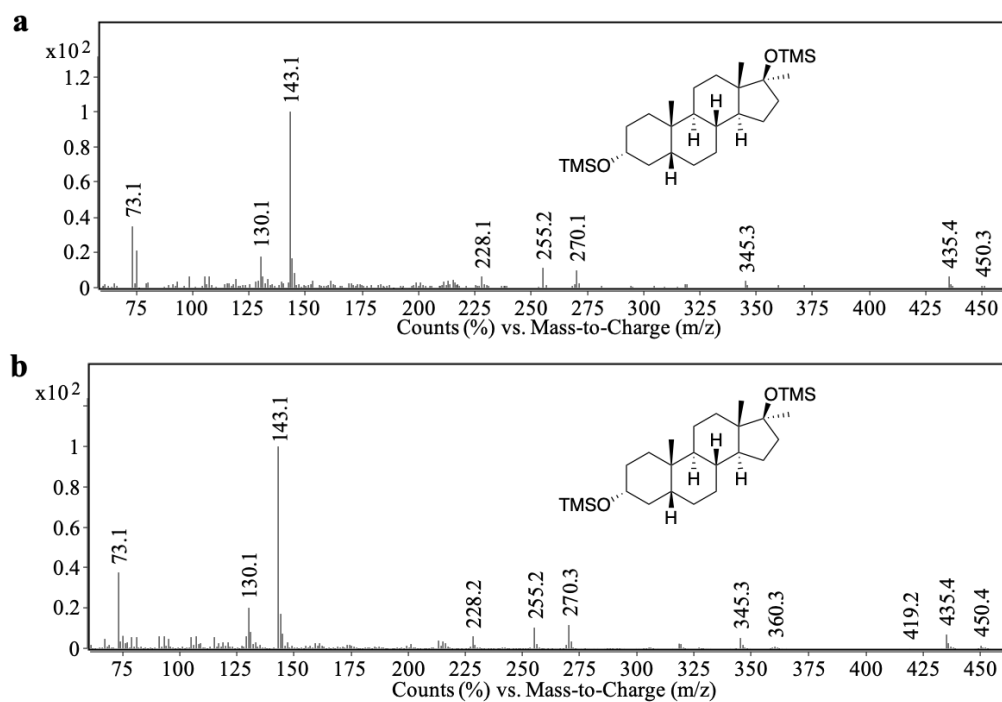


Figure 64: Normalized mass spectra (GC-EI-MS) of TMS derivatives of (a) $3\alpha,5\beta$ -THMT ($[M]^{+}=450$, RT 12.76 min), formed by medaka embryos incubated with MT, and (b) reference compound $3\alpha,5\beta$ -THMT ($[M]^{+}=450$, RT 12.87 min), at 70 eV

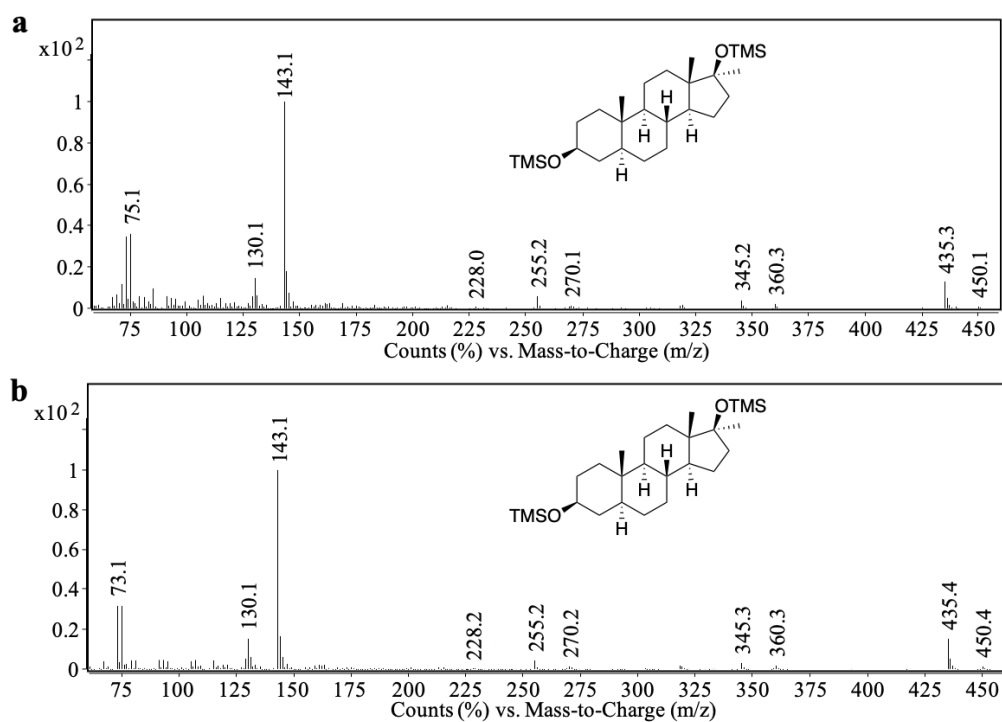


Figure 65: Normalized mass spectra (GC-EI-MS) TMS derivatives of (a) $3\beta,5\alpha$ -THMT ($[M]^{+}=450$, RT 14.52 min), formed by medaka embryos incubated with MT, and (b) reference compound $3\beta,5\alpha$ -THMT ($[M]^{+}=450$, RT 14.57 min) at 70 eV

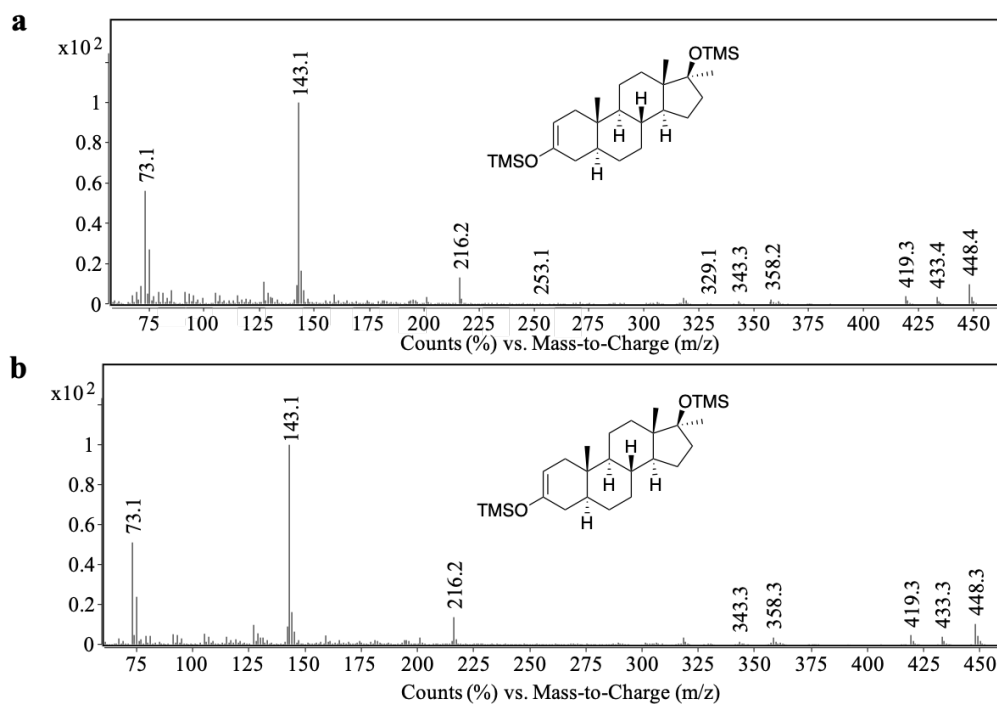
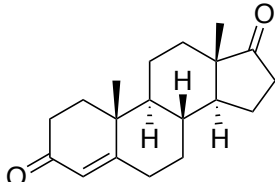
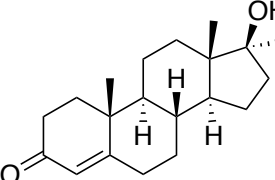
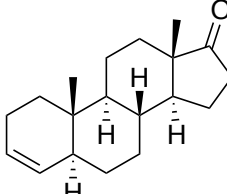
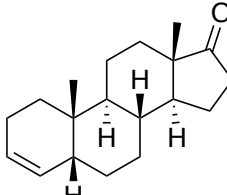
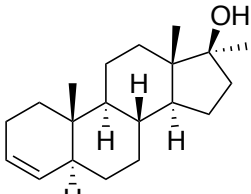
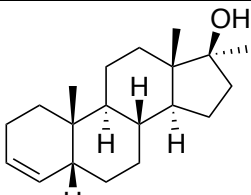
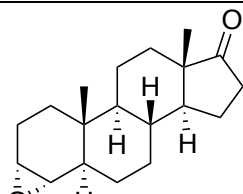
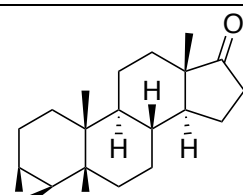


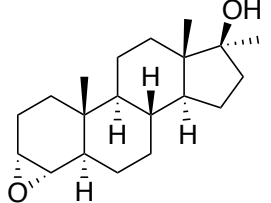
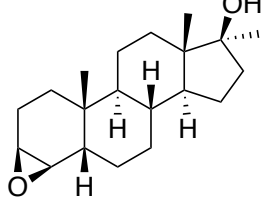
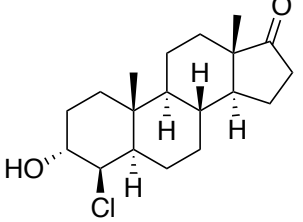
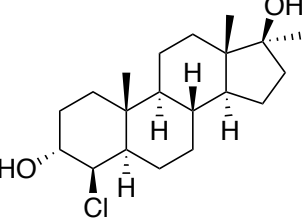
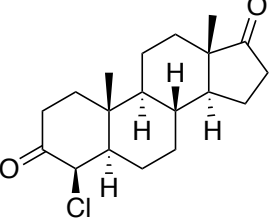
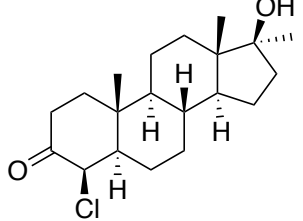
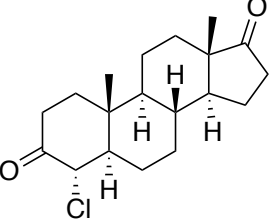
Figure 66: Normalized mass spectra (GC-EI-MS) of TMS derivatives of (a) MSL ($[M]^{+}=448$, RT 14.78 min), formed by medaka embryos incubated with MT, and (b) reference compound MSL ($[M]^{+}=448$, RT 14.88 min), at 70 eV

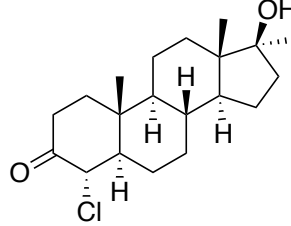
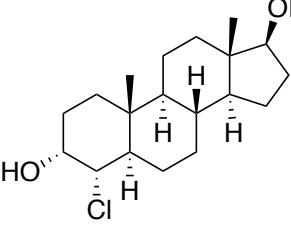
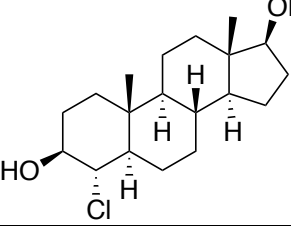
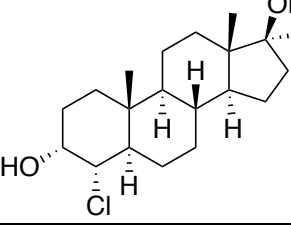
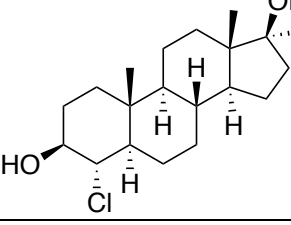
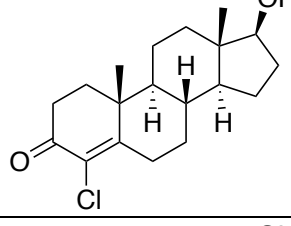
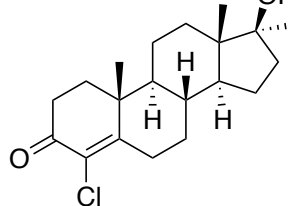
Table 42: Per-TMS derivatives of metabolites detected in samples obtained after incubation of medaka embryos with MT by GC-EI-MS

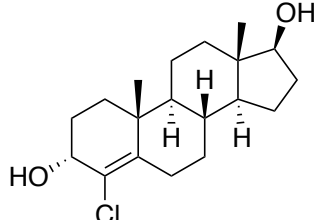
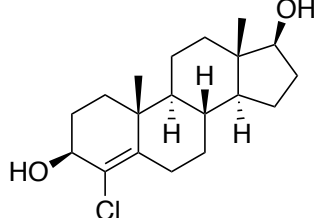
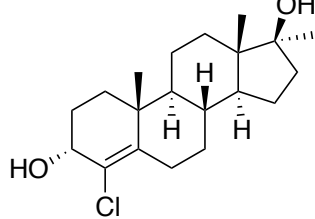
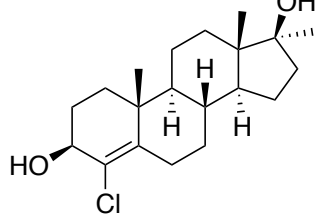
Analyte	Elemental Composition	$[M]^{+}$	Retention Time (min)
MSL	$[C_{26}H_{48}O_2Si_2]^{+}$	448	14.78
5 β -MSL	$[C_{26}H_{48}O_2Si_2]^{+}$	448	11.60
3 β ,5 α -THMT	$[C_{26}H_{50}O_2Si_2]^{+}$	450	14.52
3 α ,5 β -THMT	$[C_{26}H_{50}O_2Si_2]^{+}$	450	12.76
3 ξ ,5 ξ -THMT	$[C_{26}H_{50}O_2Si_2]^{+}$	450	12.58

Table 43: List of anabolic-androgenic steroids, metabolites, and derivatives involved the synthesis of reference materials in chapter 3.2.1

No.	Systematic Name	Structure
1	Androst-4-ene-3,17-dione	
2	17 β -Hydroxy-17 α -methyl-androst-4-ene-3-one	
3a	5 α -Androst-3-ene-17-one	
3b	5 β -Androst-3-ene-17-one	
4a	17 α -Methyl-5 α -androst-3-ene-17 β -ol	
4b	17 α -Methyl-5 β -androst-3-ene-17 β -ol	
5a	3 α ,4 α -Epoxy-5 α -androstan-17-one	
5b	3 β ,4 β -Epoxy-5 β -androstan-17-one	

No.	Systematic Name	Structure
6a	3 α ,4 α -Epoxy-17 α -methyl-5 α -androstan-17 β -ol	
6b	3 β ,4 β -Epoxy-17 α -methyl-5 β -androstan-17 β -ol	
7	4 β -Chloro-3 α -hydroxy-5 α -androstan-17-one	
8	4 β -Chloro-17 α -methyl-5 α -androstan-3 α ,17 β -diol	
9	4 β -Chloro-5 α -androstan-3,17-dione	
10	4 β -Chloro-17 β -hydroxy-17 α -methyl-5 α -androstan-3-one	
11	4 α -Chloro-5 α -androstan-3,17-dione	

No.	Systematic Name	Structure
12	4 α -Chloro-17 β -hydroxy-17 α -methyl-5 α -androstan-3-one	 <p>The structure shows a steroid nucleus with a ketone group at C-3, a chlorine atom at C-4, a methyl group at C-13, and a hydroxyl group at C-17. The stereochemistry is 5α, 13α, and 17β.</p>
13a	4 α -Chloro-5 α -androstan-3 α ,17 β -diol	 <p>The structure shows a steroid nucleus with hydroxyl groups at C-3 and C-17, and a chlorine atom at C-4. The stereochemistry is 5α, 13α, and 17β.</p>
13b	4 α -Chloro-5 α -androstan-3 β ,17 β -diol	 <p>The structure shows a steroid nucleus with hydroxyl groups at C-3 and C-17, and a chlorine atom at C-4. The stereochemistry is 5α, 13α, and 17β.</p>
14a	4 α -Chloro-17 α -methyl-5 α -androstan-3 α ,17 β -diol	 <p>The structure shows a steroid nucleus with hydroxyl groups at C-3 and C-17, a methyl group at C-13, and a chlorine atom at C-4. The stereochemistry is 5α, 13α, and 17β.</p>
14b	4 α -Chloro-17 α -methyl-5 α -androstan-3 β ,17 β -diol	 <p>The structure shows a steroid nucleus with hydroxyl groups at C-3 and C-17, a methyl group at C-13, and a chlorine atom at C-4. The stereochemistry is 5α, 13α, and 17β.</p>
15	4-Chloro-17 β -hydroxyandrost-4-ene-3-one	 <p>The structure shows a steroid nucleus with a ketone group at C-3, a double bond between C-4 and C-5, a chlorine atom at C-4, and a hydroxyl group at C-17. The stereochemistry is 13α and 17β.</p>
16	4-Chloro-17 β -hydroxy-17 α -methylandrost-4-ene-3-one	 <p>The structure shows a steroid nucleus with a ketone group at C-3, a double bond between C-4 and C-5, a methyl group at C-13, a chlorine atom at C-4, and a hydroxyl group at C-17. The stereochemistry is 13α and 17β.</p>

No.	Systematic Name	Structure
17a	4-Chloroandrost-4-ene-3 α ,17 β -diol	
17b	4-Chloroandrost-4-ene-3 β ,17 β -diol	
18a	4-Chloro-17 α -methylandro-4-ene-3 α ,17 β -diol	
18b	4-Chloro-17 α -methylandro-4-ene-3 β ,17 β -diol	

11 Independence Declaration

Herewith I certify that I have prepared and written my thesis independently and that I have not used any sources and aids other than those indicated by me.

A doctoral procedure has never been completed at any other university or applied to another department.

Lingyu Liu